

# Covariate-dependent hierarchical Dirichlet process

**Huizi Zhang**

*School of Mathematics  
University of Edinburgh  
Edinburgh, EH9 3FD, UK*

H.ZHANG-144@SMS.ED.AC.UK

**Sara Wade**

*School of Mathematics  
University of Edinburgh  
Edinburgh, EH9 3FD, UK*

SARA.WADE@ED.AC.UK

**Natalia Bochkina**

*School of Mathematics  
University of Edinburgh  
Edinburgh, EH9 3FD, UK*

N.BOCHKINA@ED.AC.UK

## Abstract

The intricacies inherent in contemporary real datasets demand more advanced statistical models to effectively address complex challenges. In this article we delve into problems related to identifying clusters across related groups, when additional covariate information is available. We formulate a novel Bayesian nonparametric approach based on mixture models, integrating ideas from the hierarchical Dirichlet process and “single-atoms” dependent Dirichlet process. The proposed method exhibits exceptional generality and flexibility, accommodating both continuous and discrete covariates through the utilization of appropriate kernel functions. We construct a robust and efficient Markov chain Monte Carlo (MCMC) algorithm involving data augmentation to tackle the intractable normalized weights. The versatility of the proposed model extends our capability to discern the relationship between covariates and clusters. Through testing on both simulated and real-world datasets, our model demonstrates its capacity to identify meaningful clusters across groups, providing valuable insights for a spectrum of applications.

**Keywords:** clustering, hierarchical model, dependent mixture model, nonparametric Bayesian statistics, Markov chain Monte Carlo

## 1 Introduction

The escalating volume and complexity of real datasets have posed formidable challenges in statistical analysis. Unstructured data is widespread across various domains, including biological applications such as single-cell RNA sequencing (scRNA-seq), and information retrieval scenarios dealing with raw documents from multiple corpora. Typically, a recurring and important objective in handling unstructured data is to uncover its inherent structure through clustering observations into groups, also known as unsupervised learning.

Mixture models are widely adopted approaches for clustering, due to their interpretability and flexibility. These generative models usually assume a common distribution family for each data point, and observations from the same cluster share the same parameters in the likelihood. In contrast to parametric mixture models, Bayesian nonparametric (BNP)

methods are gaining popularity as BNP allows for an infinite-dimensional parameter space, requiring fewer assumptions, thereby retaining greater flexibility.

The Dirichlet process (DP) by Ferguson (1973) is a typical example of BNP priors, allowing the number of clusters to grow as the data size increases. Numerous DP-based extensions have been proposed to address challenges in various contexts. The dependent Dirichlet process (DDP) of MacEachern (1999) facilitates the incorporation of exogenous covariates into clustering. The hierarchical Dirichlet process (HDP) by Teh et al. (2006) concentrates exclusively on categorical covariates, enabling clustering across related groups. There has been recent research on leveraging predictors in HDP. Dai and Storkey (2014) develops supervised HDP for topic modelling that can predict continuous or categorical response associated with each document (group) using generalized linear models. The hierarchical Dirichlet scaling process (Kim and Oh, 2014) considers documents with observed labels, and topic proportions are modelled dependent on the distance between the latent locations of labels and topics. Ren et al. (2008) extends HDP to dynamic HDP for time-evolving data, assuming that adjacent groups collected closer in time are more likely to share components, and new components can be added over time. Ren et al. (2011) incorporates spatial/temporal information using a kernel logistic regression, based on the stick-breaking representation (Sethuraman, 1994). Similarly, Coppola (2016) develops covariate-augmented nonparametric latent Dirichlet allocation, where covariates are included through a logistic stick-breaking process. Diana et al. (2020) proposes hierarchical dependent Dirichlet process (HDDP), combining HDP and “single-weights” DDP.

In this article, we propose a covariate-dependent hierarchical Dirichlet process (C-HDP), combining both hierarchical Dirichlet process and the “single-atoms” dependent Dirichlet process. External covariates can be flexibly incorporated to facilitate clustering across groups through the use of various kernel functions. The proposed method holds utility in various settings. For instance, biological researchers may be keen to understand how cellular latent time, an indicator of cell position in the developmental path, influences the identification of cell sub-populations from different experiment conditions (Figure 1). For efficient inference, we construct a novel Markov Chain Monte Carlo (MCMC) algorithm that employs latent variables to cope with the intractable normalized weights. We demonstrate that our model can capture the relationship between clusters and covariates, and identify reasonable clusters across groups in both simulated and real data.

The paper is organized as follows. We commence by providing a review of DP and its extensions DDP and HDP in Section 2. Section 3 outlines the definition of the covariate-dependent HDP, examples of common likelihood and kernel functions. The details of inference are presented in Section 4. In Section 5, we showcase the application of C-HDP to a real dataset on scRNA-seq. Section 6 concludes the paper and discusses potential future directions. The complete MCMC algorithm and simulation study are provided in the Appendix.

## 2 Review

To formally define our proposed model, we first provide introduction to existing standard approaches in the Bayesian nonparametric literature.

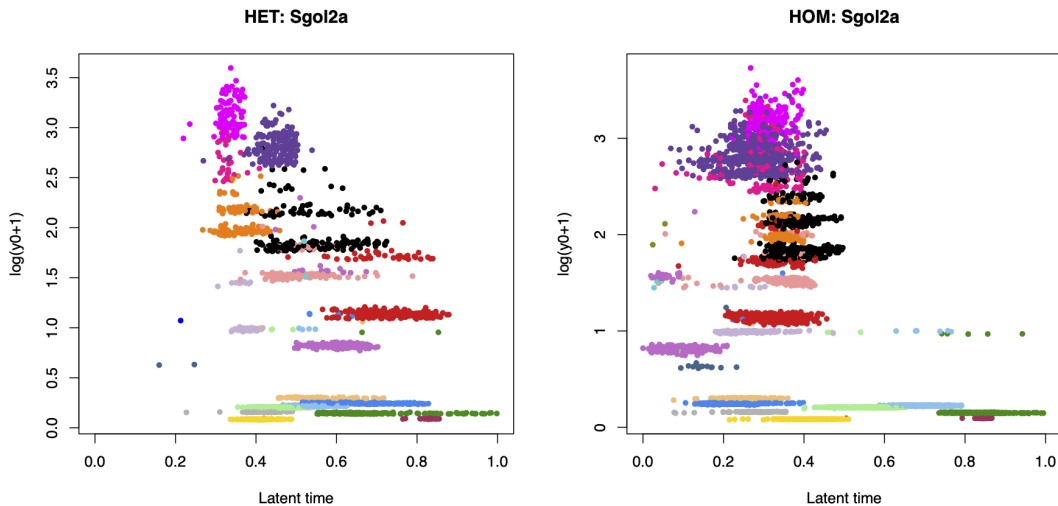


Figure 1: Latent counts versus latent time for scRNA-seq data (Manuel et al., 2022) collected under two conditions (HET and HOM). Observations are colored by cluster membership from Liu et al. (2024) without information of latent time.

**Dirichlet process** A random probability measure  $P$  on a space  $\Theta$  is said to follow a DP prior with baseline probability measure  $P_0$  and concentration parameter  $\alpha$ , denoted by  $P \sim \text{DP}(\alpha, P_0)$ , if for any finite partition  $\{A_1, \dots, A_k\}$  of  $\Theta$ ,

$$(P(A_1), P(A_2), \dots, P(A_k)) \sim \text{Dir}(\alpha P_0(A_1), \alpha P_0(A_2), \dots, \alpha P_0(A_k)),$$

where  $\text{Dir}(\alpha')$  denotes the Dirichlet distribution with concentration parameters  $\alpha'$ .

An important property of DP is the discrete nature of  $P$ . A random probability measure  $P \sim \text{DP}(\alpha, P_0)$  can be written as a combination of weights and point mass,  $P(\cdot) = \sum_{j=1}^{\infty} w_j \delta_{\theta_j^*}(\cdot)$ , where  $w_j$  are probability weights and  $\delta_{\theta_j^*}$  is the Dirac measure at  $\theta_j^*$ . Sethuraman (1994) derives the stick-breaking construction as follows.

$$P(\cdot) = \sum_{j=1}^{\infty} w_j \delta_{\theta_j^*}(\cdot), \tag{1}$$

$$w_1 = v_1, \quad w_j = v_j \prod_{l < j} (1 - v_l) \quad \text{for } j > 1, \quad v_j \stackrel{i.i.d.}{\sim} \text{Beta}(1, \alpha),$$

where  $\theta_j^* \stackrel{i.i.d.}{\sim} P_0$ , and  $v_j$  is independent of  $\theta_j^*$ . It can be shown that  $\sum_{j=1}^{\infty} w_j = 1$  almost surely (Ishwaran and James, 2001).

The discreteness of  $P$  implies there are ties among  $\theta_1, \dots, \theta_n$ , making DP a suitable prior in Bayesian mixture modelling. Moreover, it does not require the specification of the number of clusters  $k$ . Instead,  $k$  is data-driven and increases as the sample size gets large.

**Dependent Dirichlet process** The random probability measure  $P_x$  is constructed following a similar stick-breaking representation to Eq (1), with  $v_j(x), \theta_j^*(x)$  and  $\alpha(x)$ . DP can be considered as a special case where weights and atoms are independent of the covariate.

A common simplified DDP model is the “single-weights” DDP where the weights do not depend on  $x$  and are the same as in DP, whereas the atoms depend on the covariates,  $P_x(\cdot) = \sum_{j=1}^{\infty} w_j \delta_{\theta_j^*(x)}(\cdot)$ . Similarly there is a “single-atoms” DDP for covariate-dependent weights only,  $P_x(\cdot) = \sum_{j=1}^{\infty} w_j(x) \delta_{\theta_j^*}(\cdot)$ .

**Hierarchical Dirichlet process** Hierarchical Dirichlet process (Teh et al., 2006) focuses exclusively on categorical covariates, allowing for clustering across related groups. For observations  $y_{i,d}$  for the  $i$ -th subject in the  $d$ -th dataset, and a density  $f$  parameterised by subject-specific parameter  $\theta_{i,d}$ , HDP assumes the following hierarchical structure

$$\begin{aligned} y_{i,d} | \theta_{i,d} &\stackrel{i.i.d.}{\sim} f(y_{i,d} | \theta_{i,d}), & \theta_{i,d} | P_d &\stackrel{i.i.d.}{\sim} P_d, \\ P_d | \alpha, P &\stackrel{i.i.d.}{\sim} \text{DP}(\alpha, P), & P | \alpha_0, P_0 &\sim \text{DP}(\alpha_0, P_0), \end{aligned}$$

where another layer of DP prior is given to the global random probability measure  $P$ . Shared clusters are ensured by noticing that  $P$  is discrete with atoms given by the base measure  $P_0$ , and these atoms are also shared in  $P_d$  for each  $d$ . Teh et al. (2006) provide the stick-breaking construction

$$\begin{aligned} P_d &= \sum_{j=1}^{\infty} p_{j,d} \delta_{\theta_j^*}, & P &= \sum_{j=1}^{\infty} p_j \delta_{\theta_j^*}, \\ p_{j,d} &= v_{j,d} \prod_{l < j} (1 - v_{l,d}), & v_{j,d} &\sim \text{Beta} \left( \alpha p_j, \alpha \left( 1 - \sum_{l=1}^j p_l \right) \right), \\ p_j &= v_j \prod_{l < j} (1 - v_l), & v_j &\stackrel{i.i.d.}{\sim} \text{Beta}(1, \alpha_0), \end{aligned} \tag{2}$$

where  $\theta_j^* \stackrel{i.i.d.}{\sim} P_0$  are cluster-specific parameters. This construction also shows that different measures  $P_d$  share the same atoms  $\theta_j^*$  but with different cluster proportions  $p_{j,d}$ . Teh et al. (2006) show that HDP can be approximated by the finite-dimensional HDP as

$$\begin{aligned} P_d^J &= \sum_{j=1}^J p_{j,d}^J \delta_{\theta_j^*}, & P^J &= \sum_{j=1}^J p_j^J \delta_{\theta_j^*}, \\ p_{1,d}^J, \dots, p_{J,d}^J | \alpha, p_1^J, \dots, p_J^J &\sim \text{Dir}(\alpha p_1^J, \dots, \alpha p_J^J), \\ p_1^J, \dots, p_J^J | \alpha_0 &\sim \text{Dir} \left( \frac{\alpha_0}{J}, \dots, \frac{\alpha_0}{J} \right), \end{aligned} \tag{3}$$

and  $J$  is the truncation level. By introducing the latent allocation variables  $z_{i,d}$ , the finite HDP mixture model is

$$\begin{aligned} y_{i,d} | z_{i,d}, \{\theta_j^*\}_{j=1}^J &\stackrel{i.i.d.}{\sim} f(y_{i,d} | \theta_{z_{i,d}}^*), \\ z_{i,d} | p_{1,d}^J, \dots, p_{J,d}^J &\stackrel{i.i.d.}{\sim} \text{Cat}(p_{1,d}^J, \dots, p_{J,d}^J), \end{aligned}$$

where  $\theta_j^* \stackrel{i.i.d.}{\sim} P_0$ , and  $\text{Cat}(p_{1,d}^J, \dots, p_{J,d}^J)$  denotes the categorical distribution.

### 3 Methodology

Real-world datasets often encompass various types of covariates for statistical modelling. In order to achieve clustering with information from external predictors, we construct a covariate-dependent HDP that borrows ideas from the “single-atoms” DDP and HDP. In HDP, it is shown that  $\theta_{i,d} = \theta_j^*$  with probability  $p_{j,d}$ , i.e., the probability of belonging to the  $j$ -th cluster is the same for all observations in dataset  $d$ . We propose to introduce dependence by defining the probability as a function of the covariate  $x_{i,d}$ , leading to

$$P_d(x_{i,d}) = \sum_{j=1}^{\infty} p_{j,d}(x_{i,d}) \delta_{\theta_j^*},$$

in place of  $P_d$  in Eq (2). Specifically, the covariate-dependent probabilities are defined as

$$p_{j,d}(x_{i,d}) = \frac{p_{j,d} K(x_{i,d} | \psi_{j,d}^*)}{\sum_{k=1}^{\infty} p_{k,d} K(x_{i,d} | \psi_{k,d}^*)}, \quad (4)$$

where  $p_{j,d}$  is the same as the stick-breaking construction (Eq (2)), and  $K(x_{i,d} | \psi_{j,d}^*)$  is a kernel function relying on kernel parameters  $\psi_{j,d}^*$  and satisfies  $0 < K(x_{i,d} | \psi_{j,d}^*) < 1$ .

This formulation of covariate-dependent probabilities is motivated by Foti and Williamson (2012) where the dependent weights are provided for the normalized gamma process representation of the DP. A similar construction is given in Antoniano-Villalobos et al. (2014) in the context of nonparametric regression problem, where  $p_{j,d}$  can be considered as the probability that an observation belongs to cluster  $j$  regardless of the covariate value, and the kernel represents how likely an observation from cluster  $j$  will take the value  $x_{i,d}$ .

We remark that our C-HDP prior differs from the hierarchical dependent Dirichlet process prior in Diana et al. (2020) which combines the “single-weights” DDP and HDP instead. In particular, the covariate  $x$  is introduced in the global measure  $P$  instead of dataset-specific DPs  $P_d$ , and therefore the influence of the covariate is the same across datasets, whilst the effect is allowed to be different in our C-HDP model.

Similar to HDP, the finite-dimensional truncation for C-HDP is

$$P_d^J(x_{i,d}) = \sum_{j=1}^J p_{j,d}^J(x_{i,d}) \delta_{\theta_j^*}, \quad P^J = \sum_{j=1}^J p_j^J \delta_{\theta_j^*}, \quad (5)$$

where  $J$  is the truncation level and

$$\begin{aligned} p_{j,d}^J(x_{i,d}) &= \frac{q_{j,d} K(x_{i,d} | \psi_{j,d}^*)}{\sum_{k=1}^J q_{k,d} K(x_{i,d} | \psi_{k,d}^*)}, \\ q_{j,d} &\sim \text{Gamma}(\alpha p_j^J, 1), \\ p_1^J, \dots, p_J^J &\sim \text{Dir}\left(\frac{\alpha_0}{J}, \dots, \frac{\alpha_0}{J}\right). \end{aligned} \quad (6)$$

Note that  $q_{j,d}$  is not identifiable in this formulation. In fact, define  $w_{j,d} = \frac{q_{j,d}}{\sum_{k=1}^J q_{k,d}}$ , an alternative formulation of  $p_{j,d}^J(x_{i,d})$  is

$$\begin{aligned} p_{j,d}^J(x_{i,d}) &= \frac{w_{j,d} K(x_{i,d} | \psi_{j,d}^*)}{\sum_{k=1}^J w_{k,d} K(x_{i,d} | \psi_{k,d}^*)}, \\ w_{1,d}, \dots, w_{J,d} &\sim \text{Dir}(\alpha p_1^J, \dots, \alpha p_J^J). \end{aligned}$$

We provide this definition and relate it to the finite-dimensional HDP discussed in Eq (3). It will be shown later that parametrization in terms of  $q_{j,d}$  is preferred due to the standard full conditional distribution in the case of Gibbs sampling. From Teh et al. (2006) and Kingman (1975), it follows that  $p_{j,d}^J(x_{i,d}) \rightarrow p_{j,d}(x_{i,d})$  and  $P^J \rightarrow P$ .

### 3.1 Likelihood examples in mixture models

Depending on the type of the data, different distributions can be selected for the likelihood. Below are some examples for commonly employed likelihood:

**Gaussian likelihood** For a continuous response  $\mathbf{y}_{i,d} = (y_{i,1,d}, \dots, y_{i,G,d})^T \in \mathbb{R}^G$ , a normal likelihood with cluster-specific mean  $\boldsymbol{\mu}_j^*$  and covariance  $\boldsymbol{\Sigma}_j^*$ :

$$\mathbf{y}_{i,d} | z_{i,d} = j, \boldsymbol{\mu}_j^*, \boldsymbol{\Sigma}_j^* \sim \text{N}(\boldsymbol{\mu}_j^*, \boldsymbol{\Sigma}_j^*).$$

**Vector autoregressive (VAR) model** An extension of the normal likelihood to time-series data, based on a VAR model with lag 1 in the mean:

$$\mathbf{y}_{i,d} | \mathbf{y}_{i-1,d}, z_{i,d} = j, \mathbf{a}_j^*, \mathbf{B}_j^*, \boldsymbol{\Sigma}_j^* \sim \text{N}(\mathbf{a}_j^* + \mathbf{B}_j^* \mathbf{y}_{i-1,d}, \boldsymbol{\Sigma}_j^*), \quad (7)$$

where  $\mathbf{a}_j \in \mathbb{R}^G$  denotes the intercept, and  $\mathbf{B}_j$  is a  $G \times G$  matrix of the coefficients in VAR, both being cluster-specific.

**Negative-binomial likelihood** For count data, a negative binomial likelihood with cluster-specific mean  $\mu_{j,g}^*$  and dispersion  $\phi_{j,g}^*$  in each dimension  $g$ :

$$y_{i,g,d} | z_{i,d} = j, \mu_{j,g}^*, \phi_{j,g}^* \sim \text{NB}(\mu_{j,g}^*, \phi_{j,g}^*), \quad (8)$$

In all cases, we have  $z_{i,d} \stackrel{\text{ind}}{\sim} \text{Cat}(p_{1,d}^J(x_{i,d}), \dots, p_{J,d}^J(x_{i,d}))$ .

### 3.2 Examples of kernels for dependent weights

Below we provide a few examples of the kernel functions that will be used in the paper.

**Gaussian kernel**  $K(x_{i,d} | \boldsymbol{\psi}_{j,d}^*) = \exp\left(-\frac{(x_{i,d} - x_{j,d}^*)^2}{2\sigma_{j,d}^{*2}}\right)$  where  $\boldsymbol{\psi}_{j,d}^* = (x_{j,d}^*, \sigma_{j,d}^{*2})$ . The parameters  $x_{j,d}^*$  and  $\sigma_{j,d}^{*2}$  can be interpreted as the centre and dispersion of the covariate in each cluster  $j$ .

**Periodic kernel**  $K(x_{i,d} | \boldsymbol{\psi}_{j,d}^*) = \exp\left(-\frac{2}{\sigma_{j,d}^{*2}} \sin^2\left(\frac{x_{i,d} - x_{j,d}^*}{\lambda_{j,d}^*}\right)\right)$  where  $\boldsymbol{\psi}_{j,d}^* = (x_{j,d}^*, \sigma_{j,d}^{*2}, \lambda_{j,d}^*)$ .

Figure 2 shows the periodic kernel under different parameter values. The parameter  $x_{j,d}^*$  represents the value that maximizes the kernel and changing  $x_{j,d}^*$  will shift the kernel. The period is determined by  $\lambda_{j,d}^*$  and  $\sigma_{j,d}^{*2}$  is related to the minimum value of the kernel. In addition, the kernel becomes more spiky as  $\sigma_{j,d}^{*2}$  decreases. For Gaussian and periodic kernels, as  $\sigma_{j,d}^{*2} \rightarrow \infty$ , the C-HDP reduces to HDP.

**Categorical kernel**  $K(x_{i,d} | \boldsymbol{\psi}_{j,d}^*) = \prod_{l=1}^L (\rho_{j,d,l}^*)^{\mathbb{I}(x_{i,d}=l)}$  for  $x_{i,d} \in \{1, \dots, L\}$  where  $\boldsymbol{\psi}_{j,d}^* = (\rho_{j,d,1}^*, \dots, \rho_{j,d,L}^*)$  and the probabilities  $\rho_{j,d,l}^*$  sum to 1.

The choice of these kernels makes the denominator in Eq (4) finite, ensuring  $P_d(x_{i,d})$  is a valid probability measure.

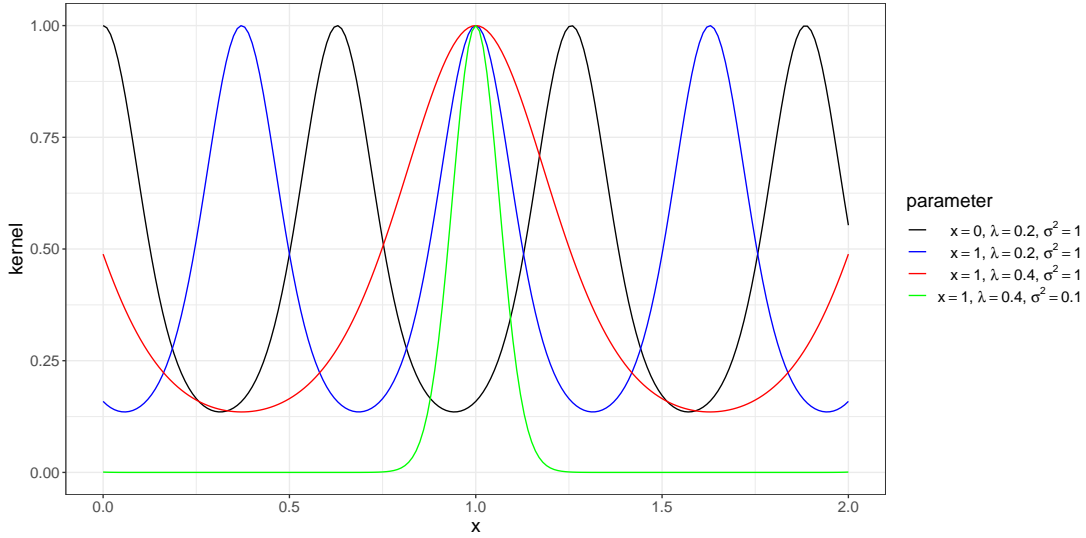


Figure 2: Example of periodic kernel for varying parameter values.

### 3.3 Suggested priors for kernel parameters in C-HDP

For efficient MCMC sampling as demonstrated later, a hierarchical prior for  $x_{j,d}^*$  and  $\sigma_{j,d}^{*2}$  is suggested for a Gaussian kernel:

$$\begin{aligned} x_{j,d}^* &\stackrel{i.i.d}{\sim} \text{N}(r_j, s^2), & r_j &\stackrel{i.i.d}{\sim} \text{N}(\mu_r, \sigma_r^2), & s^2 &\sim \text{IG}(\eta_1, \eta_2), \\ \sigma_{j,d}^{*2} &\stackrel{i.i.d}{\sim} \log\text{-N}(h_j, m^2), & h_j &\stackrel{i.i.d}{\sim} \text{N}(\mu_h, \sigma_h^2), & m^2 &\sim \text{IG}(\kappa_1, \kappa_2), \end{aligned} \quad (9)$$

where IG is the inverse-gamma distribution, and log-N denotes the log-normal distribution. The prior means  $(r_j, h_j)$  for  $x_{j,d}^*$  and  $\sigma_{j,d}^{*2}$  are chosen to be cluster-specific, and  $(r_j, h_j)$  are given normal hyper-priors with global means  $(\mu_r, \mu_h)$  to allow for borrowing information, which is similar to the hierarchical prior for  $q_{j,d}$  in Eq (6).

Regarding a periodic kernel, the following priors are recommended:

$$\begin{aligned} x_{j,d}^* &\stackrel{i.i.d}{\sim} \text{Unif}\left(-\frac{\pi\lambda_{j,d}^*}{2}, \frac{\pi\lambda_{j,d}^*}{2}\right), & \lambda_{j,d}^* &\stackrel{i.i.d}{\sim} \log\text{-N}(r_j, s^2), \\ \sigma_{j,d}^{*2} &\stackrel{i.i.d}{\sim} \text{IG}(a_j, b_j), & a_j &= 2 + \frac{h_j^2}{m^2}, & b_j &= h_j^2 + \frac{h_j^3}{m^2}, & h_j &\stackrel{i.i.d}{\sim} \log\text{-N}(\mu_h, \sigma_h^2), \end{aligned} \quad (10)$$

where the shape  $a_j$  and scale  $b_j$  are modelled as functions of the mean  $h_j$  and variance  $m^2$  of the inverse-gamma prior. The hyper-priors for  $r_j, s^2, m^2$  are of the same form as Eq (9). Note that  $x_{j,d}^*$  is restricted within one period  $(\pi\lambda_{j,d}^*)$  for identifiability.

## 4 Inference

In this section we describe a Gibbs sampling scheme for C-HDP mixture model. Gibbs sampling can be applied to draw posterior samples for parameters with full conditionals of a standard form. For non-standard full conditional densities, adaptive Metropolis-Hastings

(AMH) can be used (Griffin and Stephens, 2013, Chapter 7). Below we highlight the key steps in constructing the Gibbs sampler.

#### 4.1 A data augmentation trick

For mixture models, the complete data likelihood is widely employed to allow for efficient inference, which is usually of the form

$$f(\mathbf{y}_{i,d}, z_{i,d} = j | \mathbf{q}_{1:J,d}, \boldsymbol{\theta}_j^*, \boldsymbol{\psi}_{1:J,d}^*, x_{i,d}) = \frac{q_{j,d} K(x_{i,d} | \boldsymbol{\psi}_{j,d}^*)}{\sum_{k=1}^J q_{k,d} K(x_{i,d} | \boldsymbol{\psi}_{k,d}^*)} \times f(\mathbf{y}_{i,d} | \boldsymbol{\theta}_j^*).$$

However, the intractable sum in the denominator makes it difficult to obtain standard full conditional densities for  $q_{j,d}$  and kernel parameters. We propose to use a data augmentation trick, introducing a latent variable  $\xi_{i,d} \in (0, +\infty)$ , and the augmented data likelihood is

$$f(\mathbf{y}_{i,d}, \xi_{i,d}, z_{i,d} = j | \mathbf{q}_{1:J,d}, \boldsymbol{\theta}_j^*, \boldsymbol{\psi}_{1:J,d}^*, x_{i,d}) = \exp\left(-\xi_{i,d} \sum_{j=1}^J q_{j,d} K(x_{i,d} | \boldsymbol{\psi}_{j,d}^*)\right) \times q_{j,d} K(x_{i,d} | \boldsymbol{\psi}_{j,d}^*) \times f(\mathbf{y}_{i,d} | \boldsymbol{\theta}_j^*). \quad (11)$$

Using the fact that  $\int_0^\infty \exp(-\xi\lambda) d\xi = \frac{1}{\lambda}$ , we can restore the above complete data likelihood by integrating out  $\xi_{i,d}$ . It is worth noticing that  $\xi_{i,d}$  does not have a physical interpretation, unlike  $z_{i,d}$ . Define  $N_{j,d}$  as the number of observations in component  $j$  in dataset  $d$  and  $C_d$  the size of data  $d$ . The augmented data likelihood yields standard full conditional distributions to enable sampling both  $q_{j,d}$  and  $\xi_{i,d}$  effectively:

$$\begin{aligned} \pi(q_{j,d} | \dots) &\propto (q_{j,d})^{N_{j,d}} \times \exp\left(-q_{j,d} \sum_{i=1}^{C_d} \xi_{i,d} K(x_{i,d} | \boldsymbol{\psi}_{j,d}^*)\right) \times (q_{j,d})^{\alpha p_j^J - 1} \exp(-q_{j,d}) \\ &\propto (q_{j,d})^{N_{j,d} + \alpha p_j^J - 1} \times \exp\left(-q_{j,d} \left[1 + \sum_{i=1}^{C_d} \xi_{i,d} K(x_{i,d} | \boldsymbol{\psi}_{j,d}^*)\right]\right), \\ \Rightarrow q_{j,d} | \dots &\sim \text{Gamma}\left(N_{j,d} + \alpha p_j^J, 1 + \sum_{i=1}^{C_d} \xi_{i,d} K(x_{i,d} | \boldsymbol{\psi}_{j,d}^*)\right). \\ \pi(\xi_{i,d} | \dots) &\propto \exp\left(-\xi_{i,d} \sum_{j=1}^J q_{j,d} K(x_{i,d} | \boldsymbol{\psi}_{j,d}^*)\right). \\ \Rightarrow \xi_{i,d} | \dots &\sim \text{Gamma}\left(1, \sum_{j=1}^J q_{j,d} K(x_{i,d} | \boldsymbol{\psi}_{j,d}^*)\right). \end{aligned}$$

In addition to the intricate denominator, the presence of the kernel parameters inside the exponential term in Eq (11) also poses challenges. For kernel parameters, we introduce another latent variable  $u_{i,j,d} \in (0, 1)$  to facilitate MCMC sampling. The update of  $\boldsymbol{\psi}_{j,d}^*$  and  $\boldsymbol{\theta}_j^*$  depends on the choice of the kernel and likelihood. If conjugate priors are chosen, the full conditional densities of  $\boldsymbol{\psi}_{j,d}^*$  and  $\boldsymbol{\theta}_j^*$  will have a closed form.



Consider the Gaussian kernel with priors given in Eq (9). The full conditional distribution for  $x_{j,d}^*$  is

$$\pi(x_{j,d}^* | \dots) \propto \prod_{i:z_{i,d}=j} K(x_{i,d} | \boldsymbol{\psi}_{j,d}^*) \times \prod_{i=1}^{C_d} \exp(-\xi_{i,d} q_{j,d} K(x_{i,d} | \boldsymbol{\psi}_{j,d}^*)) \times \text{N}(x_{j,d}^* | r_j, s^2).$$

With the introduction of  $u_{i,j,d} \in (0, 1)$ , the above can be written as

$$\pi(x_{j,d}^* | \dots) \propto \prod_{i:z_{i,d}=j} K(x_{i,d} | \boldsymbol{\psi}_{j,d}^*) \times \prod_{i=1}^{C_d} \mathbb{I}(u_{i,j,d} < M_{i,j,d}) \times \text{N}(x_{j,d}^* | r_j, s^2),$$

where  $M_{i,j,d} = \exp(-\xi_{i,d} q_{j,d} K(x_{i,d} | \boldsymbol{\psi}_{j,d}^*))$ . It can be shown that the full conditional of the latent variable is  $u_{i,j,d} | \dots \sim \text{Unif}(0, M_{i,j,d})$ , and for the kernel parameter  $x_{j,d}^*$  it is a truncated normal distribution:

$$\pi(x_{j,d}^* | \dots) \propto \text{N}(x_{j,d}^* | \hat{r}_{j,d}, \hat{s}_{j,d}^2) \times \mathbb{I}(x_{j,d}^* \in A_{j,d}),$$

where

$$\hat{s}_{j,d}^2 = \left( \frac{1}{s^2} + \frac{N_{j,d}}{\sigma_{j,d}^{*2}} \right)^{-1}, \quad \hat{r}_{j,d} = \frac{r_j/s^2 + \sum_{i:z_{i,d}=j} x_{i,d}/\sigma_{j,d}^{*2}}{1/s^2 + N_{j,d}/\sigma_{j,d}^{*2}},$$

and the truncation region is of the form

$$A_{j,d} = \bigcap_{i: -\log u_{i,j,d} < \xi_{i,d} q_{j,d}} A_{i,j,d},$$

where

$$A_{i,j,d} = \left( -\infty, x_{i,d} - \sqrt{-2\sigma_{j,d}^{*2} \log \left[ -\frac{\log u_{i,j,d}}{\xi_{i,d} q_{j,d}} \right]} \right) \cup \left( t_{i,d} + \sqrt{-2\sigma_{j,d}^{*2} \log \left[ -\frac{\log u_{i,j,d}}{\xi_{i,d} q_{j,d}} \right]}, +\infty \right).$$

The full derivation and details of the Gibbs sampling algorithm are presented in Appendix.

## 4.2 Clustering

Given posterior samples of the allocations  $z_{i,d}$ , an optimal clustering is obtained that minimizes the posterior expected variation of information (VI) (Wade and Ghahramani, 2018). Due to label switching (Stephens, 2000), the posterior inference of the other parameters is based on a post-processing step where allocations are fixed to the optimal one.

## 4.3 Covariate-dependent predictive quantities of interest

For likelihood associated with a mean parameter with clustering property, such as  $\mu_j^*$  in Section 3.1, the mean conditional on the covariate, kernel parameters,  $\boldsymbol{\mu}^*$  and  $\mathbf{q}$  is

$$\mathbb{E}(y|x, \mathbf{q}, \boldsymbol{\mu}^*, \boldsymbol{\psi}^*) = \sum_{j=1}^J p_{j,d}^J(x) \mu_j^*, \quad (12)$$

where  $\mathbf{q}, \boldsymbol{\mu}^*, \boldsymbol{\psi}^*$  denote a collection of variables for  $q_{j,d}, \mu_j^*$  and  $\psi_{j,d}^*$ , respectively. Therefore, we can obtain covariate-dependent mean of the posterior predictive distribution as

$$\begin{aligned} \mathbb{E}(\tilde{y}|\tilde{x}, \mathbf{X}, \mathbf{Y}) &= \int \tilde{y} \cdot \pi(\tilde{y}|\tilde{x}, \mathbf{Y}, \mathbf{X})d\tilde{y} = \int \tilde{y} \int \pi(\tilde{y}|\boldsymbol{\Theta}, \tilde{x})\pi(\boldsymbol{\Theta}|\mathbf{X}, \mathbf{Y})d\boldsymbol{\Theta}d\tilde{y} \\ &= \int \int \tilde{y} \cdot \pi(\tilde{y}|\boldsymbol{\Theta}, \tilde{x})d\tilde{y} \times \pi(\boldsymbol{\Theta}|\mathbf{X}, \mathbf{Y})d\boldsymbol{\Theta} \\ &= \int \mathbb{E}(\tilde{y}|\tilde{x}, \mathbf{q}, \boldsymbol{\mu}^*, \boldsymbol{\psi}^*) \times \pi(\boldsymbol{\Theta}|\mathbf{X}, \mathbf{Y})d\boldsymbol{\Theta}, \end{aligned}$$

where  $\tilde{x}$  and  $\tilde{y}$  denote the new data,  $\mathbf{Y}$  and  $\mathbf{X}$  denote the observed data, and  $\boldsymbol{\Theta}$  represents all the unknown parameters. The mean of the posterior predictive distribution can be approximated by the average of MCMC samples:

$$\mathbb{E}(\tilde{y}|\tilde{x}, \mathbf{X}, \mathbf{Y}) \approx \frac{1}{L} \sum_{l=1}^L \mathbb{E}(\tilde{y}|\tilde{x}, \mathbf{q}^{(l)}, \boldsymbol{\mu}^{*(l)}, \boldsymbol{\psi}^{*(l)}),$$

where  $\mathbf{q}^{(l)}, \boldsymbol{\mu}^{*(l)}, \boldsymbol{\psi}^{*(l)}$  denote the  $l$ -th MCMC sample.

## 5 Application to single-cell RNA sequencing data Pax6

We demonstrate the application of the C-HDP prior on single-cell RNA sequencing data, using a Gaussian kernel.

The experimental datasets Pax6 (Manuel et al., 2022) were obtained to study the influence of the transcription factor, Pax6, on the brain development in the embryonic cells from mice. Pax6 has been shown to affect a forebrain organizer and is involved in many regional gene expression pattern defects (Caballero et al., 2014).

There are two datasets of total mRNA counts for the control group (HET) and mutant group (HOM). Both groups have counts for the same set of genes. The control group has Pax6 knocked out in one strand of DNA, while the mutant group has Pax6 removed in both strands. Each data  $d$  ( $d = 1, 2$ ) contains the mRNA counts  $y_{c,g,d}$  for gene  $g$  ( $g = 1, \dots, G$ ) in cell  $c$  ( $c = 1, \dots, C_d$ ). After pre-processing in Liu et al. (2024), the HET and HOM datasets contain  $C_1 = 3096$  and  $C_2 = 5282$  cells, both with  $G = 2529$  genes. The covariate of interest is the cell-specific latent time  $t_{c,d} \in [0, 1]$  introduced below, and the goal is to find unique and shared clusters with similar expression patterns across two groups, based on the total mRNA count matrices, while incorporating the information of the latent time.

A typical drawback of scRNA-seq data is that the cells are killed during measurements being taken, and therefore the resulting scRNA-seq dataset only provides a static snapshot of cellular states. Recently, to study the dynamic information from cells, La Manno et al. (2018) proposed RNA velocity and latent time, derived from a per-gene model based on the amount of unspliced mRNAs and spliced mRNAs. The obtained latent time can imply the cellular position in the biological process, which may be informative to clustering the cells.

For each group, the abundance of unspliced and spliced counts are obtained from *velocity* pipeline (La Manno et al., 2018) and the latent time  $t_{c,d}$  is computed from a generalized RNA velocity model (Bergen et al., 2020).

### 5.1 The model for Pax6

The model for clustering the Pax6 data extends the work in Liu et al. (2024). Liu et al. (2024) employed the HDP prior to cluster the same Pax6 datasets, where the clustering model is built upon *bayNorm* (Tang et al., 2020) that addresses the problem of normalization, imputation and batch effect correction in an integrated manner.

The observed count  $y_{c,g,d}$  is assumed to follow a binomial distribution given the latent true count  $y_{c,g,d}^0$ , with cell-specific capture efficiency  $\beta_{c,d}$

$$y_{c,g,d}|y_{c,g,d}^0, \beta_{c,d} \sim \text{Bin}(y_{c,g,d}^0, \beta_{c,d}).$$

The binomial distribution accounts for the case where partial true counts are observed. The latent counts follow a negative-binomial distribution accounting for over-dispersion:

$$y_{c,g,d}^0|\mu_{c,g,d}, \phi_{c,g,d} \sim \text{NB}(\mu_{c,g,d}, \phi_{c,g,d}),$$

with mean expression  $\mu_{c,g,d}$  and dispersion  $\phi_{c,g,d}$  that are both specific to each gene and cell. The latent counts can be integrated out to obtain:

$$y_{c,g,d}|\mu_{c,g,d}, \phi_{c,g,d}, \beta_{c,d} \sim \text{NB}(\mu_{c,g,d}\beta_{c,d}, \phi_{c,g,d}),$$

where it is noticed that  $\mu$  and  $\beta$  are not identifiable while only their product is. An informative prior for  $\beta_{c,d}$  is applied to mitigate this problem (Liu et al., 2024).

#### 5.1.1 KERNEL

A Gaussian kernel is applied with kernel parameters  $\boldsymbol{\psi}_{j,d}^* = (t_{j,d}^*, \sigma_{j,d}^{*2})$ . The parameters  $t_{j,d}^*$  and  $\sigma_{j,d}^{*2}$  represent the centre and variability of the latent time in each cluster  $j$ . The priors are defined as in Eq (9).

#### 5.1.2 BASE MEASURE

The mean and dispersion are modelled from the C-HDP prior (Eq (5)),

$$(\boldsymbol{\mu}_{c,d}, \boldsymbol{\phi}_{c,d})|P_d^J(t_{c,d}) \sim P_d^J(t_{c,d}),$$

where  $\boldsymbol{\mu}_{c,d} = (\mu_{c,1,d}, \dots, \mu_{c,G,d})$  and  $\boldsymbol{\phi}_{c,d} = (\phi_{c,1,d}, \dots, \phi_{c,G,d})$  are the mean expression and dispersion for the  $c$ -th cell in dataset  $d$  across all genes. For the base measure  $P_0$ , Liu et al. (2024) choose to model the relationship between  $\mu_{j,g}^*$  and  $\phi_{j,g}^*$  (cluster-specific parameters for gene  $g$ ) as follows

$$\mu_{j,g}^* \stackrel{i.i.d}{\sim} \log\text{-N}(0, \alpha_\mu^2), \quad \phi_{j,g}^*|\mu_{j,g}^* \stackrel{ind}{\sim} \log\text{-N}(b_0 + b_1 \log(\mu_{j,g}^*), \alpha_\phi^2).$$

The linear relationship between the logarithmic mean expression and dispersion has been observed in Eling et al. (2018), Brennecke et al. (2013) and Vallejos et al. (2015). The value of  $\alpha_\mu^2$  can be set using the empirical estimates for the mean parameters from *bayNorm*. The mean-dispersion parameters  $\mathbf{b} = (b_0, b_1)^T$  and  $\alpha_\phi^2$  have hyper-priors as follows

$$\mathbf{b}|\alpha_\phi^2 \sim \text{N}(\mathbf{m}_b, \alpha_\phi^2 V_b), \quad \alpha_\phi^2 \sim \text{IG}(\nu_1, \nu_2),$$

where by default  $V_b = \mathbf{I}$ , and we use the estimated mean and dispersion parameters from *bayNorm* to determine  $\mathbf{m}_b, \nu_1$  and  $\nu_2$ .

### 5.1.3 CAPTURE EFFICIENCIES $\beta_{c,d}$

The prior for  $\beta_{c,d}$  is extended from Liu et al. (2024)

$$\beta_{c,d} \stackrel{ind}{\sim} \text{Beta}(a_d^\beta, b_d^\beta),$$

The values of  $a_d^\beta, b_d^\beta$  are based on the empirical estimates from *bayNorm*. To avoid bimodal and exponentially decaying (increasing) shape of Beta prior, we set  $a_d^\beta, b_d^\beta > 1$ . For identifiability of  $\beta_{c,d}$ , an informative prior is used, where the mean is specified to be an estimate of global mean capture efficiency across cells (0.06) (Tang et al., 2020).

### 5.1.4 CONCENTRATION PARAMETERS $\alpha, \alpha_0$

The weakly informative priors are

$$\alpha \sim \text{Gamma}(1, 1), \quad \alpha_0 \sim \text{Gamma}(1, 1).$$

If prior information on the number of clusters is available, we can use this information to set the hyper-parameters.

A simulation study for the model is given in the Appendix.

## 5.2 Results on the real data Pax6

In practice, it is common to run multiple chains with a large number of iterations to account for sensitivity to different initial values and to ensure convergence. Nevertheless, in the case of high dimensional data, chains can easily get stuck into local posterior modes even after sufficiently long time. To overcome such problems and reduce computational costs, Coleman et al. (2022) develop a general method to exploit posterior distribution of data partitions, based on an ensemble of Bayesian clustering results. The method does not require the chain to reach convergence and hence is expected to relieve computational burden.

Consensus clustering simply runs large numbers of chains with a small number of iterations. The key step is to choose a suitable number of chains  $W$  and the length of the chain  $D$ , such that the posterior similarity matrix (PSM) computed from the  $D$ -th iteration in  $W$  chains is stable enough. Coleman et al. (2022) propose a heuristic method making use of the elbow plot, by plotting the mean absolute difference (MAD) against candidate  $D$  or  $W$ , and lower MAD is favored (see Appendix).

### 5.2.1 CLUSTERING

With a truncation level of  $J = 15$ , tuning parameters  $W = 100$  and  $D = 1000$  (evidence in Figure 3), 10 clusters are identified from VI, shared in both HET and HOM. Figure 4 shows the posterior similarity matrix, where there is still some uncertainty to further split the clusters. The size of each cluster is provided in the left panel of Figure 5, with cluster 1 having the largest number of cells. We also show the proportions of HET and HOM cells in each cluster (right panel), and find under-represented/over-represented cluster if the proportion of HET (or HOM) is less/greater than the overall proportion. In this case, clusters 2, 4, 6, 8 are found to be over-represented in HOM, clusters 3, 7, 9 are under-represented in HOM, and the rest clusters show relatively stable proportions.

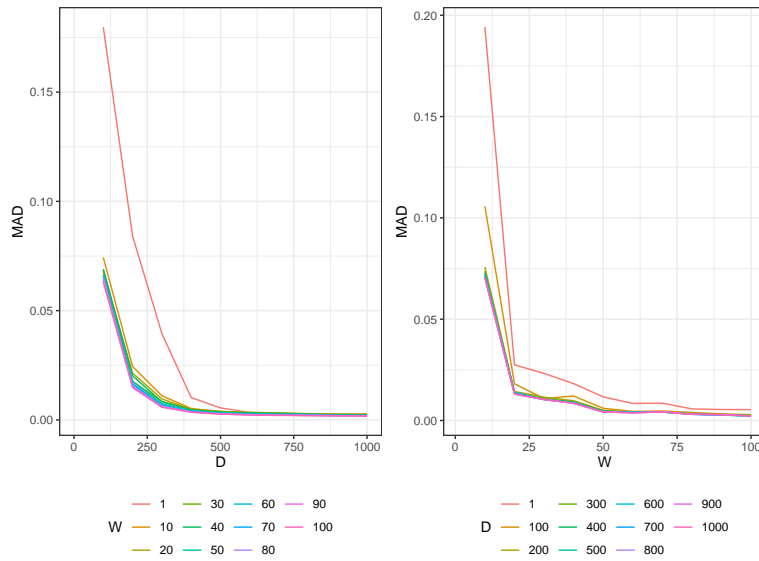
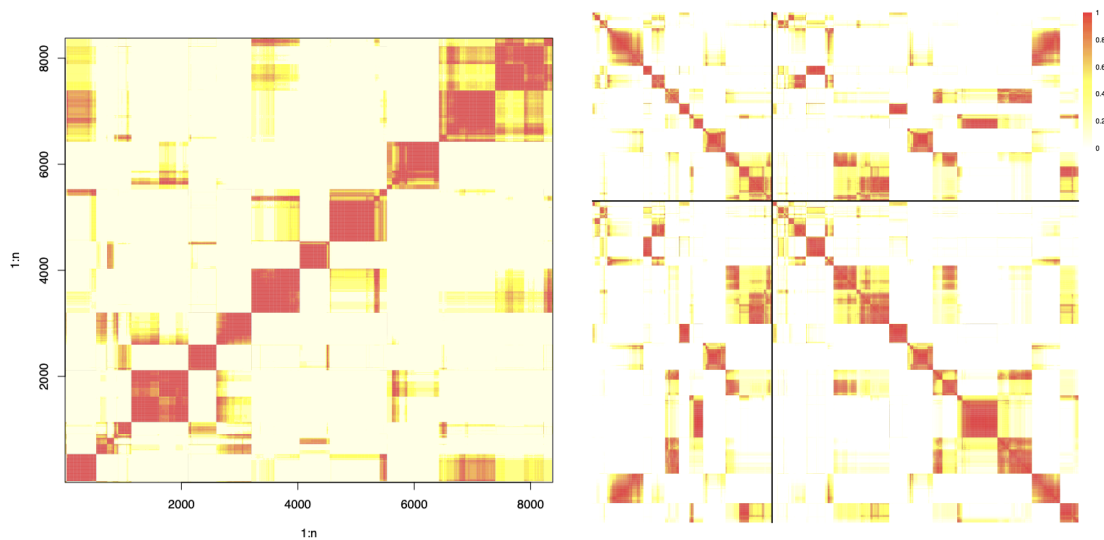
Figure 3: Choice of  $W$  and  $D$  in consensus clustering for Pax6.

Figure 4: Left: Posterior similarity matrix for all cells without distinguishing between datasets. Right: Posterior similarity matrix for cells within each dataset. The black solid line separates two datasets.

For the post-processing step, the total number of MCMC iteration is 28000. We use a burn-in of 20000 iterations and a thinning of 4, leading to 2000 samples in the end.

Figure 6 displays the first principal component computed from the observed gene expression matrix against latent time, with each cell colored by the posterior probability of belonging to a specific cluster. It is worth noting that some cells have posterior probabilities

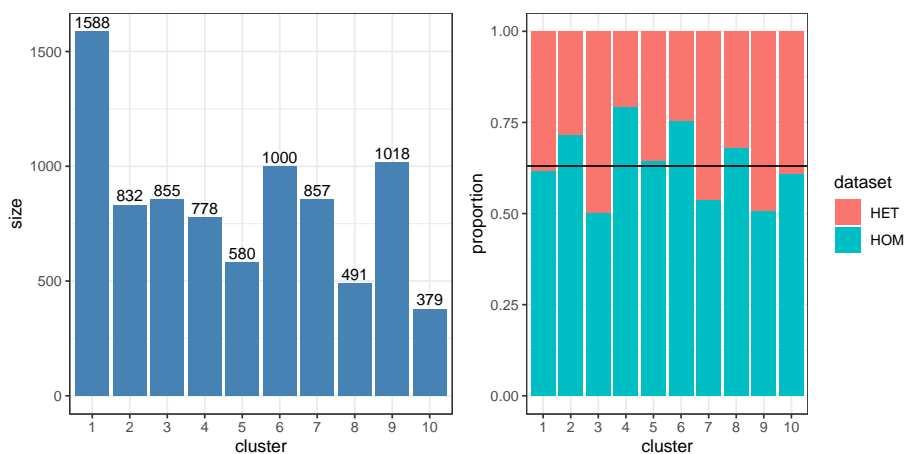


Figure 5: Left: Size of each cluster found in Pax6. Right: proportions of HET and HOM cells in each cluster. The black horizontal line represents the overall proportion.

between 0.25-0.75 (dark blue), suggesting uncertainty in cell allocations. Additionally, some clusters appear to be well-separated by the latent time, e.g. cluster 3 and 9 in HET.

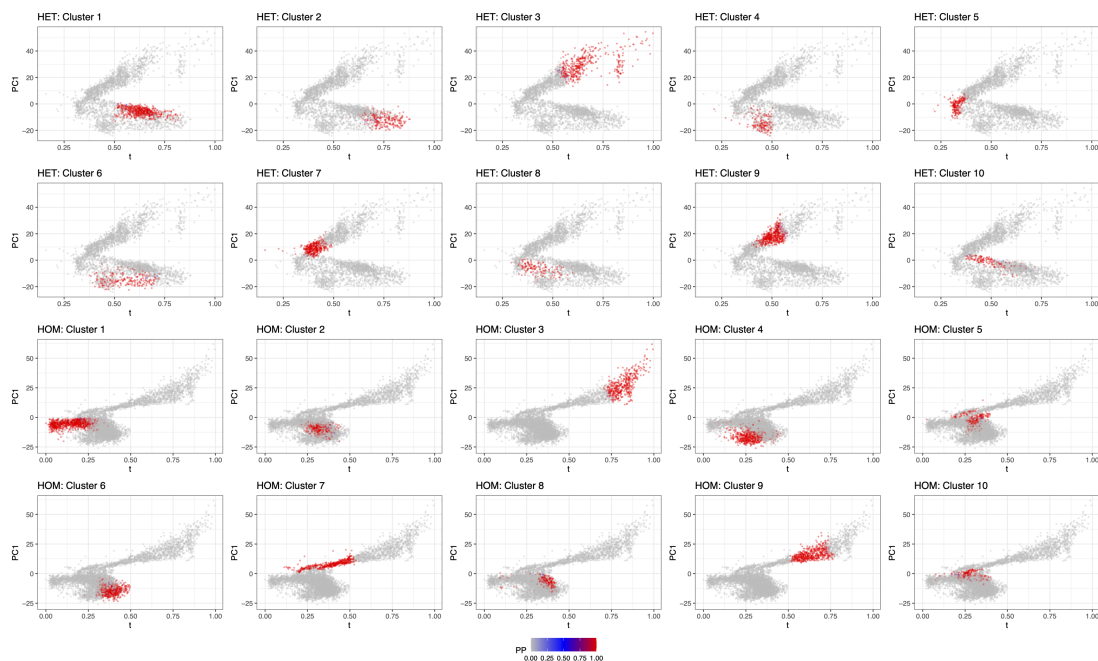


Figure 6: Plot of first principal component against latent time. In each panel, the color represents the posterior probability that the cell belongs to the specific cluster.

## 5.2.2 MARKER GENES

Using posterior samples from the post-processing step, we follow the definition in Liu et al. (2024) to identify globally differentially expressed genes (DE) based on mean parameters  $\mu_{j,g}^*$  and differentially dispersed genes (DD) based on dispersion parameters  $\phi_{j,g}^*$ . DE genes are detected based on the posterior tail probabilities that the absolute value of the log-fold change (LFC) of the mean expression between two clusters  $j$  and  $j'$  is greater than a threshold  $\tau_0$ . Formally, this probability is defined as

$$P_g(j, j') = \Pr \left( \left| \log \left( \frac{\mu_{j,g}^*}{\mu_{j',g}^*} \right) \right| > \tau_0 \mid \mathbf{Z}, \mathbf{Y} \right),$$

where  $\mathbf{Z} = \{z_{c,d}\}_{c=1,d=1}^{C_d,D}$ ,  $\mathbf{Y} = \{y_{c,g,d}\}_{c=1,g=1,d=1}^{C_d,G,D}$ .

Global DE genes are found by considering the maximum posterior tail probabilities across all pairwise clusters,

$$P_g^* = \max_{(j,j')} P_g(j, j').$$

Then genes with  $P_g^*$  greater than a threshold  $\alpha_M$  are identified as global DE genes. This threshold is set to control the expected false discovery rate (EFDR) to 0.05 (Vallejos et al., 2016). Intuitively, global DE genes have mean expressions that are different between at least two clusters. Global DD genes are detected in a similar way, based on the dispersion parameters to compute maximum tail probabilities  $L_g^*$ .

The thresholds for DE and for DD genes are both set to 2.5. There are 50.81% and 20.52% of the total genes classified as global DE and global DD genes. Figure 7 displays heatmaps of the estimated mean and dispersion parameters for marker genes in all 10 clusters. Cluster 3 exhibits distinct mean expression patterns compared to the other clusters, with global DE genes showing higher expression levels. On the other hand, global DD genes in cluster 7 have smaller dispersion levels.

## 5.2.3 LATENT COUNTS

Following from Section 4.3, we compute the mean of the latent count for a cell  $c$  with unknown cluster membership, conditional on time, mean expressions,  $\mathbf{q}$  and kernel parameters:

$$\mathbb{E}(y_{c,g,d}^0 \mid t_{c,d} = t, \mathbf{q}, \boldsymbol{\mu}^*, \boldsymbol{\psi}^*) = \sum_{j=1}^J p_{j,d}^J(t) \mu_{j,g}^*,$$

which produces an estimate of the mean expression as a function of time.

Figure 8 displays the posterior mean of the mean latent count against the latent time for the top 20 global DE genes (in terms of maximum tail probabilities) for each dataset, based on the post-processing step. It is evident that the means for the top global DE genes change over time, and some genes, such as *Rgs20* and *Mcm3*, share similar trends. The 95% highest posterior density (HPD) interval is relatively smaller in HOM.

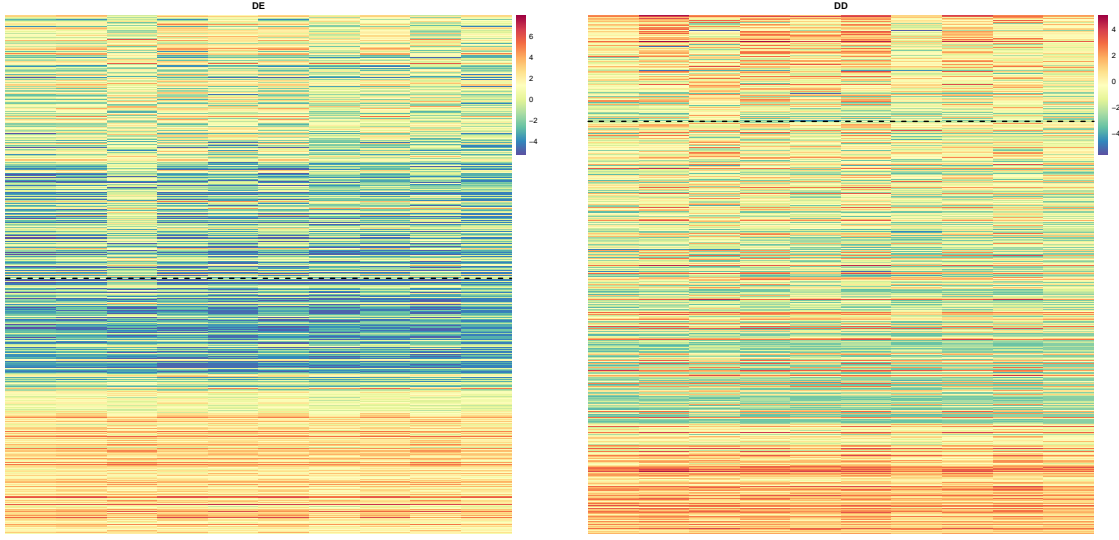


Figure 7: Global marker genes: Heatmaps of posterior mean of mean parameters  $\mu_{j,g}^*$  (left) and dispersion parameters  $\phi_{j,g}^*$  (right) on the log scale. Rows correspond to genes and columns correspond to clusters. Genes are ordered by decreasing maximum posterior tail probabilities  $P_g^*$  and  $L_g^*$  from top to bottom. Genes above the black dashed lines are global marker genes.

Additionally, Tang et al. (2020) and Liu et al. (2024) provide posterior mean of the latent counts given the allocation variables, capture efficiencies and unique parameters

$$\mathbb{E}[y_{c,g,d}^0 | y_{c,g,d}, z_{c,d} = j, \beta_{c,d}, \mu_{j,g}^*, \phi_{j,g}^*] = y_{c,g,d} \frac{\mu_{j,g}^* + \phi_{j,g}^*}{\mu_{j,g}^* \beta_{c,d} + \phi_{j,g}^*} + \mu_{j,g}^* \frac{\phi_{j,g}^* (1 - \beta_{c,d})}{\mu_{j,g}^* \beta_{c,d} + \phi_{j,g}^*},$$

which can be used to approximate the posterior mean of latent counts as

$$\mathbb{E}[y_{c,g,d}^0 | \mathbf{Y}] \approx \frac{1}{L} \sum_{l=1}^L \mathbb{E}[y_{c,g,d}^0 | y_{c,g,d}, z_{c,d}^{(l)} = j, \beta_{c,d}^{(l)}, \mu_{j,g}^{*(l)}, \phi_{j,g}^{*(l)}]. \quad (13)$$

Figure 9 shows the t-SNE (Van der Maaten and Hinton, 2008) plots for the observed counts and estimated latent counts from Eq (13) using samples in the post-processing step. From the observed counts, some clusters are already quite separated, such as the purple and dark green clusters. The separation is much more apparent in the latent counts.

#### 5.2.4 TIME-DEPENDENT PROBABILITIES

For time-dependent probabilities, due to label switching, our inference is based on the post-processing step. Figure 10 shows 100 posterior samples of  $p_{j,d}^J(t)$  for each cluster in each dataset. Compared to HOM, its uncertainty in HET is larger, which may be attributed to the smaller data size of HET. Additionally, for some clusters such as cluster 1 in HET, the probabilities appear to be bimodal, suggesting that cells with different latent time may still have relatively high probabilities of belonging to the same cluster. Notably, cluster 3 and



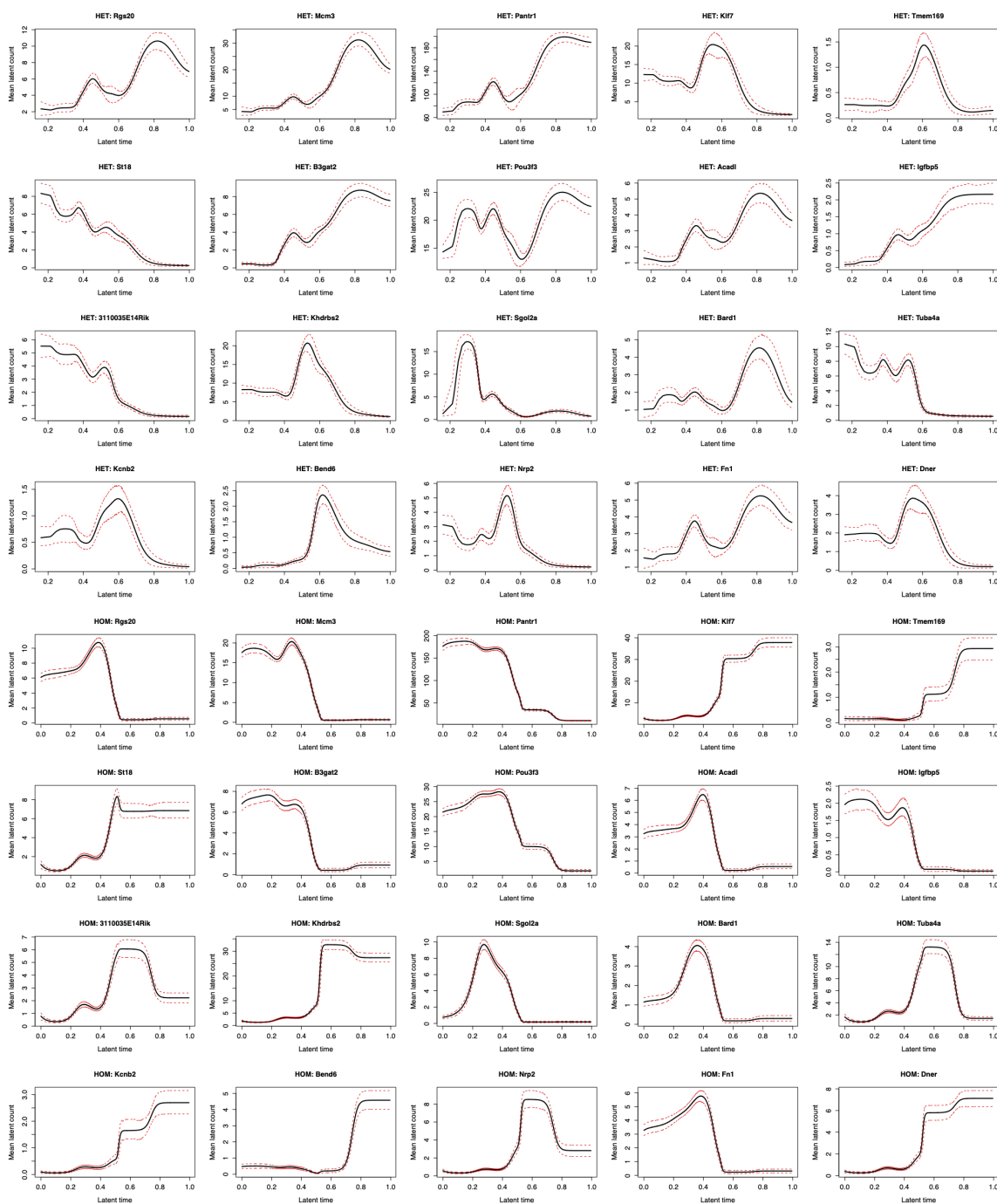


Figure 8: Posterior mean of mean latent counts against latent time for HET (top 4 rows) and HOM (bottom rows) for top 20 global DE genes. The 95% highest posterior density interval is given in dashed red line.

cluster 9 in HET have almost non-overlapping support for latent time, where probabilities are positive. This observation aligns with our previous discussion in Figure 6.

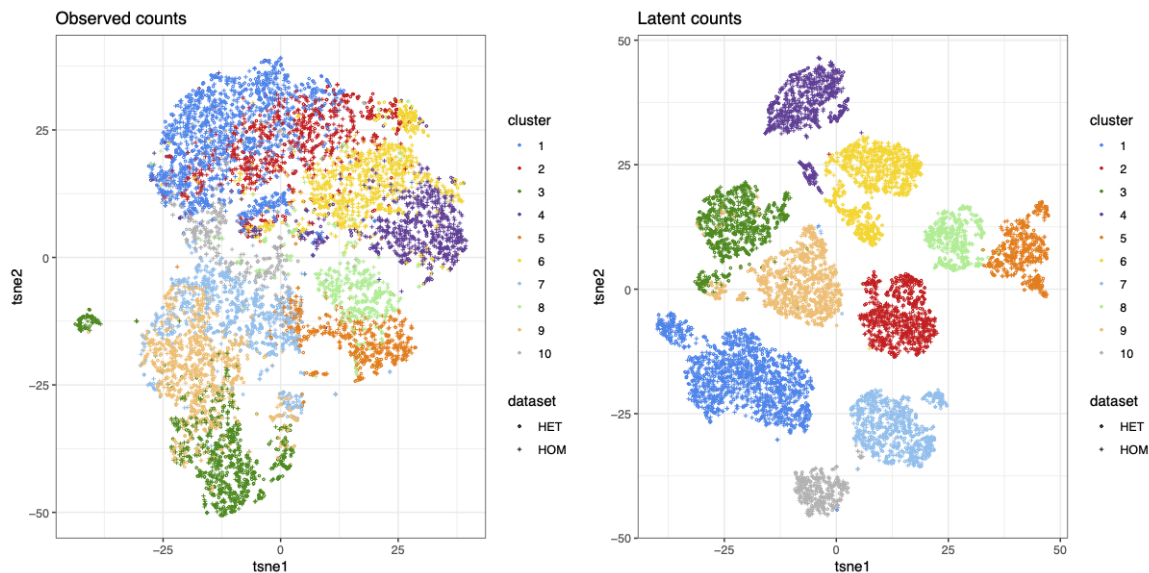


Figure 9: Observed counts (left) and latent counts (right) after t-SNE. Cells belonging to different clusters are set to different colors. Different symbols indicate different datasets.

Finally, posterior predictive checks have been conducted (Gelman et al., 1996) based on replicate data, and there is no strong disagreement between the data and model (see Appendix).

## 6 Conclusion

In this paper we have developed a covariate-dependent hierarchical Dirichlet process prior to flexibly integrate external covariates into clustering across related groups, combining the strengths from HDP and “single-atoms” DDP. The method has been applied to a real dataset on single-cell RNA sequencing with the use of a Gaussian kernel. The results demonstrate that our C-HDP prior yields meaningful clusters for both datasets. The identified clusters reveal separation in the lower dimensional embeddings of the scRNA-seq data. In particular, the covariate-dependent probabilities enhance our understanding of the influence of external covariates on clustering. Further, we provide estimation of the latent counts as a function of the covariate (time) in the scRNA-seq data.

However, while we have constructed an efficient Gibbs sampling algorithm for posterior inference, this algorithm may still face the dilemma of getting trapped in the local modes and a large number of iteration is needed to reach convergence. The problem is even more severe for high-dimensional scRNA-seq data. Alternative methods will be considered in the future, and one option is posterior bootstrap (Fong et al., 2019) suitable for multimodal posteriors. The method accounts for model misspecification and generates independent samples from the nonparametric posterior with exact inference. It admits parallel Monte Carlo sampling scheme for faster computation than conventional MCMC algorithm. Finally, it is worth extending the model to encompass covariate-dependent atoms as well, enhancing its applicability to more complex datasets.

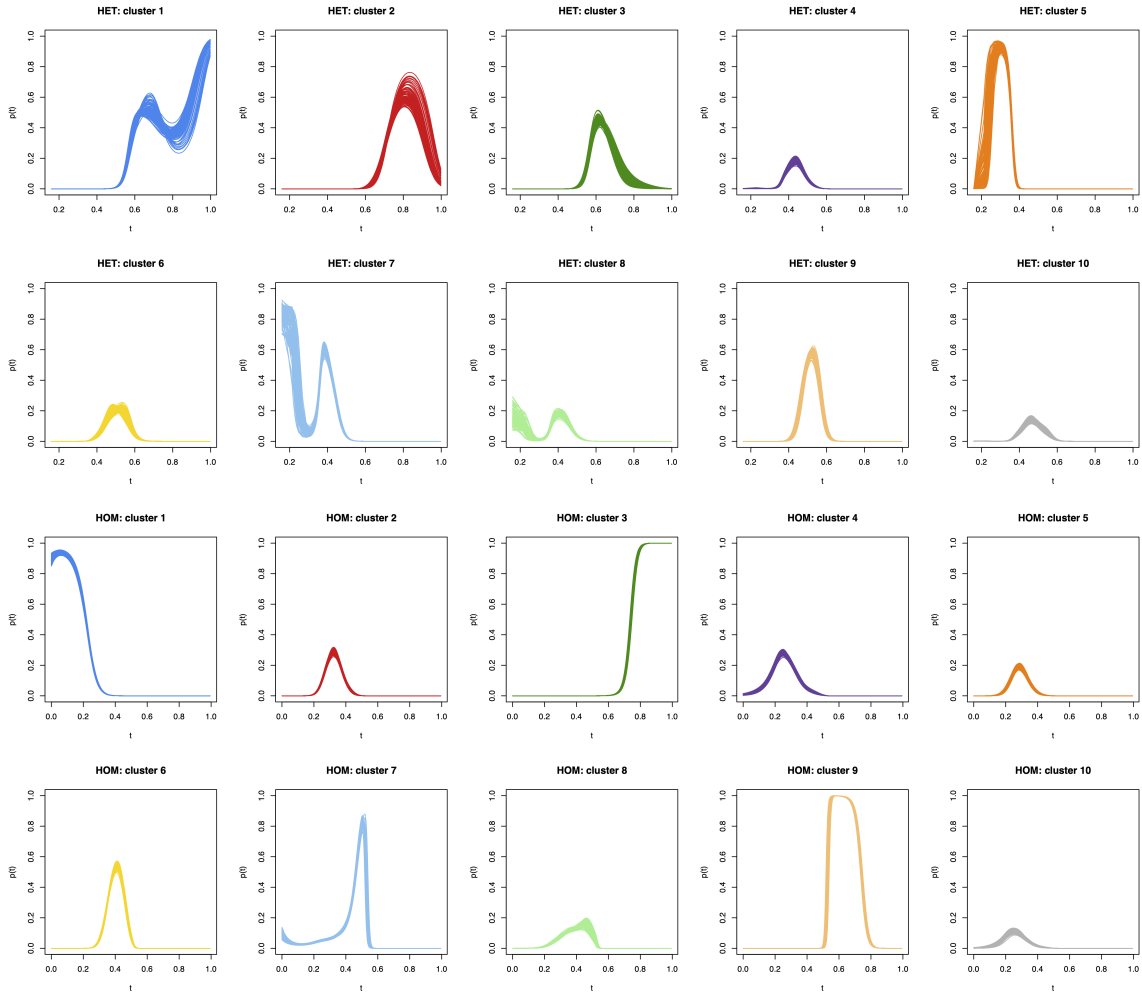


Figure 10: Time-dependent probabilities for each cluster in each dataset for Pax6.

## References

- Isadora Antoniano-Villalobos, Sara Wade, and Stephen G Walker. A Bayesian nonparametric regression model with normalized weights: A study of hippocampal atrophy in Alzheimer’s disease. *Journal of the American Statistical Association*, 109(506):477–490, 2014.
- Volker Bergen, Marius Lange, Stefan Peidli, F Alexander Wolf, and Fabian J Theis. Generalizing RNA velocity to transient cell states through dynamical modeling. *Nature Biotechnology*, 38(12):1408–1414, 2020.
- Philip Brennecke, Simon Anders, Jong Kyoung Kim, Aleksandra A Kołodziejczyk, Xiuwei Zhang, Valentina Proserpio, Bianka Baying, Vladimir Benes, Sarah A Teichmann, John C Marioni, et al. Accounting for technical noise in single-cell RNA-seq experiments. *Nature Methods*, 10(11):1093–1095, 2013.
- Isabel Martín Caballero, Martine N Manuel, Michael Molinek, Idoia Quintana-Urzainqui, Da Mi, Tomomi Shimogori, and David J Price. Cell-autonomous repression of Shh by transcription factor Pax6 regulates diencephalic patterning by controlling the central diencephalic organizer. *Cell Reports*, 8(5):1405–1418, 2014.
- Stephen Coleman, Paul D.W. Kirk, and Chris Wallace. Consensus clustering for Bayesian mixture models. *BMC Bioinformatics*, 23(1):290, 2022.
- Paul B Conn, Devin S Johnson, Perry J Williams, Sharon R Melin, and Mevin B Hooten. A guide to Bayesian model checking for ecologists. *Ecological Monographs*, 88(4):526–542, 2018.
- Antonio Coppola. *Covariate-Dependent Nonparametric Mixture Models*. PhD thesis, 2016.
- Andrew M Dai and Amos J Storkey. The supervised hierarchical Dirichlet process. *IEEE Transactions on Pattern Analysis and Machine Intelligence*, 37(2):243–255, 2014.
- Alex Diana, Eleni Matechou, Jim Griffin, and Alison Johnston. A hierarchical dependent Dirichlet process prior for modelling bird migration patterns in the UK. *The Annals of Applied Statistics*, 14(1):473–493, 2020.
- Nils Eling, Arianne C Richard, Sylvia Richardson, John C Marioni, and Catalina A Vallejos. Correcting the mean-variance dependency for differential variability testing using single-cell RNA sequencing data. *Cell Systems*, 7(3):284–294, 2018.
- Thomas S Ferguson. A Bayesian analysis of some nonparametric problems. *The Annals of Statistics*, pages 209–230, 1973.
- Edwin Fong, Simon Lyddon, and Chris Holmes. Scalable nonparametric sampling from multimodal posteriors with the posterior bootstrap. In *International Conference on Machine Learning*, pages 1952–1962. PMLR, 2019.
- Nick Foti and Sinead Williamson. Slice sampling normalized kernel-weighted completely random measure mixture models. In *Advances in Neural Information Processing Systems*, volume 25. Curran Associates, Inc., 2012.

- Andrew Gelman. Two simple examples for understanding posterior p-values whose distributions are far from uniform. *Electronic Journal of Statistics*, 7:2595 – 2602, 2013. doi: 10.1214/13-EJS854. URL <https://doi.org/10.1214/13-EJS854>.
- Andrew Gelman, Xiao-Li Meng, and Hal Stern. Posterior predictive assessment of model fitness via realized discrepancies. *Statistica Sinica*, pages 733–760, 1996.
- Andrew Gelman, John B Carlin, Hal S Stern, David B Dunson, Aki Vehtari, and Donald B Rubin. *Bayesian Data Analysis*. CRC press, 2013.
- Jim E. Griffin and David A. Stephens. *Advances in Markov chain Monte Carlo*. Bayesian Theory and Applications. Oxford University Press, Oxford, 2013.
- Nils Lid Hjort, Fredrik A Dahl, and Gunnhildur Högnadóttir Steinbakk. Post-processing posterior predictive p values. *Journal of the American Statistical Association*, 101(475): 1157–1174, 2006.
- Hemant Ishwaran and Lancelot F James. Gibbs sampling methods for stick-breaking priors. *Journal of the American Statistical Association*, 96(453):161–173, 2001.
- Marc Kery and J. Andrew Royle. *Applied Hierarchical Modeling in Ecology*. Elsevier, London, UK, 2015.
- Dongwoo Kim and Alice Oh. Hierarchical Dirichlet scaling process. In *International Conference on Machine Learning*, pages 973–981. PMLR, 2014.
- John FC Kingman. Random discrete distributions. *Journal of the Royal Statistical Society: Series B (Methodological)*, 37(1):1–15, 1975.
- Gioele La Manno et al. RNA velocity of single cells. *Nature*, 560:494–498, 2018.
- Alex Lewin, Natalia Bochkina, and Sylvia Richardson. Fully bayesian mixture model for differential gene expression: simulations and model checks. *Statistical Applications in Genetics and Molecular Biology*, 6(1), 2007.
- Jinlu Liu, Sara Wade, and Natalia Bochkina. Shared Differential Clustering across Single-cell RNA Sequencing Datasets with the Hierarchical Dirichlet Process. *Econometrics and Statistics*, 2024. ISSN 2452-3062.
- Stephen Neil MacEachern. Dependent nonparametric processes. In *ASA Proceedings of the Section on Bayesian Statistical Science*, pages 50–55, 1999.
- Martine Manuel, Kai Boon Tan, Zrinko Kozic, Michael Molinek, Tiago Sena Marcos, Maizatul Fazilah Abd Razak, Dániel Dobolyi, Ross Dobie, Beth E. P. Henderson, Neil C. Henderson, Wai Kit Chan, Michael I. Daw, John O. Mason, and David J. Price. Pax6 limits the competence of developing cerebral cortical cells to respond to inductive inter-cellular signals. *PLoS Biology*, 20(9):1–54, 09 2022.
- Lu Ren, David B Dunson, and Lawrence Carin. The dynamic hierarchical Dirichlet process. In *International Conference on Machine Learning*, pages 824–831, 2008.

- Lu Ren, Lan Du, Lawrence Carin, and David B Dunson. Logistic stick-breaking process. *Journal of Machine Learning Research*, 12(1), 2011.
- Jayaram Sethuraman. A constructive definition of Dirichlet priors. *Statistica Sinica*, pages 639–650, 1994.
- Sandip Sinharay and Hal S Stern. Posterior predictive model checking in hierarchical models. *Journal of Statistical Planning and Inference*, 111(1):209–221, 2003. ISSN 0378-3758. doi: [https://doi.org/10.1016/S0378-3758\(02\)00303-8](https://doi.org/10.1016/S0378-3758(02)00303-8). URL <https://www.sciencedirect.com/science/article/pii/S0378375802003038>. Special issue I: Model Selection, Model Diagnostics, Empirical Bayes and Hierarchical Bayes.
- Matthew Stephens. Dealing with label switching in mixture models. *Journal of the Royal Statistical Society: Series B (Statistical Methodology)*, 62(4):795–809, 2000.
- Wenhao Tang, François Bertaux, Philipp Thomas, Claire Stefanelli, Malika Saint, Samuel Marguerat, and Vahid Shahrezaei. baynorm: Bayesian gene expression recovery, imputation and normalization for single-cell RNA-sequencing data. *Bioinformatics*, 36(4):1174–1181, 2020.
- Yee Whye Teh, Michael I Jordan, Matthew J Beal, and David M Blei. Hierarchical Dirichlet Processes. *Journal of the American Statistical Association*, 101(476):1566–1581, 2006.
- Catalina A Vallejos, John C Marioni, and Sylvia Richardson. BASiCS: Bayesian analysis of single-cell sequencing data. *PLoS Computational Biology*, 11(6):e1004333, 2015.
- Catalina A. Vallejos, Sylvia Richardson, and John C. Marioni. Beyond comparisons of means: understanding changes in gene expression at the single-cell level. *Genome Biology*, 17(1):70, 2016.
- Laurens Van der Maaten and Geoffrey Hinton. Visualizing data using t-SNE. *Journal of Machine Learning Research*, 9(11), 2008.
- Sara Wade and Zoubin Ghahramani. Bayesian cluster analysis: Point estimation and credible balls (with discussion). *Bayesian Analysis*, 13(2):559–626, 2018.

## Appendix A. Posterior inference for Pax6

Let  $\boldsymbol{\psi}_{j,d}^* = (t_{j,d}^*, \sigma_{j,d}^{*2})$  denote the parameters in the Gaussian kernel. The complete model is as follows:

$$\begin{aligned}
 y_{c,g,d} | z_{c,d} = j, \mu_{j,g}^*, \phi_{j,g}^*, \beta_{c,d} &\stackrel{ind}{\sim} \text{NB}(\mu_{j,g}^* \beta_{c,d}, \phi_{j,g}^*), \\
 z_{c,d} | p_{1,d}^J(t_{c,d}), \dots, p_{J,d}^J(t_{c,d}) &\stackrel{ind}{\sim} \text{Cat}(p_{1,d}^J(t_{c,d}), \dots, p_{J,d}^J(t_{c,d})), \\
 p_{j,d}^J(t_{c,d}) &= \frac{q_{j,d} K(t_{c,d} | \boldsymbol{\psi}_{j,d}^*)}{\sum_{k=1}^J q_{k,d} K(t_{c,d} | \boldsymbol{\psi}_{k,d}^*)}, \\
 q_{j,d} &\stackrel{ind}{\sim} \text{Gamma}(\alpha p_j^J, 1), \\
 p_1^J, \dots, p_J^J &\sim \text{Dir}\left(\frac{\alpha_0}{J}, \dots, \frac{\alpha_0}{J}\right), \\
 t_{j,d}^* &\stackrel{ind}{\sim} \text{N}(r_j, s^2), \\
 r_j &\stackrel{i.i.d}{\sim} \text{N}(\mu_r, \sigma_r^2), \\
 s^2 &\sim \text{IG}(\eta_1, \eta_2), \\
 \sigma_{j,d}^{*2} &\stackrel{ind}{\sim} \text{log-N}(h_j, m^2), \\
 h_j &\stackrel{i.i.d}{\sim} \text{N}(\mu_h, \sigma_h^2), \\
 m^2 &\sim \text{IG}(\kappa_1, \kappa_2), \\
 \mu_{j,g}^* &\stackrel{i.i.d}{\sim} \text{log-N}(0, \alpha_\mu^2), \\
 \phi_{j,g}^* | \mu_{j,g}^* &\stackrel{ind}{\sim} \text{log-N}(b_0 + b_1 \log(\mu_{j,g}^*), \alpha_\phi^2), \\
 \beta_{c,d} &\stackrel{ind}{\sim} \text{Beta}(a_d^\beta, b_d^\beta), \\
 \mathbf{b} | \alpha_\phi^2 &\sim \text{N}(\mathbf{m}_b, \alpha_\phi^2 V_b), \\
 \alpha_\phi^2 &\sim \text{IG}(\nu_1, \nu_2), \\
 \alpha &\sim \text{Gamma}(1, 1), \\
 \alpha_0 &\sim \text{Gamma}(1, 1).
 \end{aligned}$$

Define  $\mathbf{Z} = \{z_{c,d}\}_{c=1,d=1}^{C_d,D}$ ,  $\mathbf{Y} = \{y_{c,g,d}\}_{c=1,g=1,d=1}^{C_d,G,D}$ ,  $\mathbf{t} = \{t_{c,d}\}_{c=1,d=1}^{C_d,D}$ ,  $\mathbf{q} = \{q_{j,d}\}_{j=1,d=1}^{J,D}$ ,  $\mathbf{p}^J = (p_1^J, \dots, p_J^J)$ ,  $\boldsymbol{\mu}_j^* = (\mu_{j,1}^*, \dots, \mu_{j,G}^*)$ ,  $\boldsymbol{\phi}_j^* = (\phi_{j,1}^*, \dots, \phi_{j,G}^*)$ ,  $\boldsymbol{\beta} = \{\beta_{c,d}\}_{c=1,d=1}^{C_d,D}$ ,  $\boldsymbol{\xi} = \{\xi_{c,d}\}_{c=1,d=1}^{C_d,D}$ ,  $\mathbf{b} = (b_0, b_1)^T$ ,  $\mathbf{t}^* = \{t_{j,d}^*\}_{j=1,d=1}^{J,D}$ ,  $\boldsymbol{\sigma}^{*2} = \{\sigma_{j,d}^{*2}\}_{j=1,d=1}^{J,D}$ ,  $\mathbf{r} = (r_1, \dots, r_J)$ ,  $\mathbf{h} = (h_1, \dots, h_J)$ . The posterior distribution is

$$\begin{aligned}
 & \pi(\mathbf{Z}, \mathbf{q}, \mathbf{p}^J, \boldsymbol{\mu}^*, \boldsymbol{\phi}^*, \boldsymbol{\beta}, \boldsymbol{\xi}, \alpha, \alpha_0, \mathbf{b}, \alpha_\phi^2, \mathbf{t}^*, \boldsymbol{\sigma}^{*2}, \mathbf{r}, s^2, \mathbf{h}, m^2 | \mathbf{Y}, \mathbf{t}) \\
 & \propto \prod_{j=1}^J \prod_{(c,d):z_{c,d}=j} \prod_{g=1}^G \text{NB}(y_{c,d,g} | \mu_{j,g}^* \beta_{c,d}, \phi_{j,g}^*) \\
 & \quad \times \prod_{j=1}^J \prod_{d=1}^D \prod_{c:z_{c,d}=j} K(t_{c,d} | \boldsymbol{\psi}_{j,d}^*) \times \prod_{j=1}^J \prod_{d=1}^D (q_{j,d})^{N_{j,d}} \\
 & \quad \times \prod_{j=1}^J \prod_{d=1}^D \prod_{c=1}^{C_d} \exp(-\xi_{c,d} q_{j,d} K(t_{c,d} | \boldsymbol{\psi}_{j,d}^*)) \\
 & \quad \times \prod_{j=1}^J \prod_{d=1}^D \text{Gamma}(q_{j,d} | \alpha p_j^J, 1) \times \text{Dir}\left(\mathbf{p}^J | \frac{\alpha_0}{J}, \dots, \frac{\alpha_0}{J}\right) \\
 & \quad \times \prod_{j=1}^J \prod_{g=1}^G [\log\text{-N}(\mu_{j,g}^* | 0, \alpha_\mu^2) \times \log\text{-N}(\phi_{j,g}^* | b_0 + b_1 \log(\mu_{j,g}^*), \alpha_\phi^2)] \\
 & \quad \times \prod_{d=1}^D \prod_{c=1}^{C_d} \text{Beta}(\beta_{c,d} | a_d^\beta, b_d^\beta) \times \text{Gamma}(\alpha | 1, 1) \times \text{Gamma}(\alpha_0 | 1, 1) \\
 & \quad \times \text{N}(\mathbf{b} | m_b, \alpha_\phi^2 V_b) \times \text{IG}(\alpha_\phi^2 | \nu_1, \nu_2) \\
 & \quad \times \prod_{j=1}^J \prod_{d=1}^D [\text{N}(t_{j,d}^* | r_j, s^2) \times \log\text{-N}(\sigma_{j,d}^{*2} | h_j, m^2)] \times \prod_{j=1}^J [\text{N}(r_j | \mu_r, \sigma_r^2) \times \text{N}(h_j | \mu_h, \sigma_h^2)] \\
 & \quad \times \text{IG}(s^2 | \eta_1, \eta_2) \times \text{IG}(m^2 | \kappa_1, \kappa_2),
 \end{aligned} \tag{14}$$

where  $N_{j,d} = \sum_{c=1}^{C_d} \mathbb{I}(z_{c,d} = j)$  is the number of cells in component  $j$  in dataset  $d$ ,  $\mathbb{I}(\cdot)$  is the indicator function that takes the value 1 if the condition inside the bracket holds, and is 0 otherwise. The first three lines come from the augmented data likelihood. The MCMC algorithm (Gibbs sampling) iteratively samples from the full conditional distributions of (blocked) parameters. For standard full conditional densities, we can draw samples directly, while adaptive Metropolis-Hastings (AMH) is used for non-standard forms. Denote  $\mathbf{C} = (C_1, \dots, C_D)$ . The time complexity for each parameter is provided below.

- dataset-specific parameters for cluster likelihood  $\mathbf{q}$ :  $\mathcal{O}(\text{sum}(\mathbf{C})J)$ .
- latent cell-specific parameters  $\boldsymbol{\xi}$ :  $\mathcal{O}(\text{sum}(\mathbf{C})J)$ .
- latent parameters  $\{u_{c,j,d}\}_{c=1,j=1,d=1}^{C_d,J,D}$  to aid sampling kernel parameters:  $\mathcal{O}(\text{sum}(\mathbf{C})J)$ .
- kernel parameters (mean)  $\mathbf{t}^*$ :  $\mathcal{O}(\text{sum}(\mathbf{C})J)$ .



- kernel parameters (variance)  $\sigma^{*2}$ :  $\mathcal{O}(\text{sum}(\mathbf{C})J)$ .
- concentration parameter  $\alpha$ :  $\mathcal{O}(JD)$ .
- concentration parameter  $\alpha_0$ :  $\mathcal{O}(J)$ .
- allocation variables  $\mathbf{Z}$ :  $\mathcal{O}(\text{sum}(\mathbf{C})JG)$ .
- component probabilities  $\mathbf{p}^J$ :  $\mathcal{O}(JD)$ .
- mean-dispersion parameters  $\mathbf{b}, \alpha_\phi^2$ :  $\mathcal{O}(JG)$ .
- cluster-specific parameters  $\boldsymbol{\mu}_{1:J,1:G}^*, \boldsymbol{\phi}_{1:J,1:G}^*$ :  $\mathcal{O}(\text{sum}(\mathbf{C})JG)$ .
- capture efficiencies  $\boldsymbol{\beta}$ :  $\mathcal{O}(\text{sum}(\mathbf{C})J)$ .
- hyper-parameters  $\mathbf{r}, s^2, \mathbf{h}, m^2$  for the kernel parameters:  $\mathcal{O}(JD)$ .

### A.1 Dataset-specific parameters for cluster likelihood $q_{j,d}$

For each  $j$  and  $d$ , the full conditional distribution is

$$\begin{aligned} & \pi(q_{j,d} | \{z_{c,d}\}_{c=1}^{C_d}, \alpha, p_j^J, \{\xi_{c,d}\}_{c=1}^{C_d}, \{t_{c,d}\}_{c=1}^{C_d}, t_{j,d}^*, \sigma_{j,d}^{*2}) \\ & \propto (q_{j,d})^{N_{j,d}} \times \exp\left(-q_{j,d} \sum_{c=1}^{C_d} \xi_{c,d} K(t_{c,d} | \boldsymbol{\psi}_{j,d}^*)\right) \\ & \quad \times (q_{j,d})^{\alpha p_j^J - 1} \exp(-q_{j,d}) \\ & \propto (q_{j,d})^{N_{j,d} + \alpha p_j^J - 1} \times \exp\left(-q_{j,d} \left[1 + \sum_{c=1}^{C_d} \xi_{c,d} K(t_{c,d} | \boldsymbol{\psi}_{j,d}^*)\right]\right), \end{aligned}$$

i.e.,

$$q_{j,d} | \dots \sim \text{Gamma}\left(N_{j,d} + \alpha p_j^J, 1 + \sum_{c=1}^{C_d} \xi_{c,d} K(t_{c,d} | \boldsymbol{\psi}_{j,d}^*)\right).$$

### A.2 Latent cell-specific parameters $\xi_{c,d}$

For each  $c$  and  $d$ , the full conditional distribution is

$$\pi(\xi_{c,d} | \mathbf{q}_{1:J,d}, t_{c,d}, \mathbf{t}_{1:J,d}^*, \boldsymbol{\sigma}_{1:J,d}^{*2}) \propto \exp\left(-\xi_{c,d} \sum_{j=1}^J q_{j,d} K(t_{c,d} | \boldsymbol{\psi}_{j,d}^*)\right),$$

i.e.,

$$\xi_{c,d} | \dots \sim \text{Gamma}\left(1, \sum_{j=1}^J q_{j,d} K(t_{c,d} | \boldsymbol{\psi}_{j,d}^*)\right).$$

### A.3 Kernel parameters $t_{j,d}^*$ and $\sigma_{j,d}^{*2}$

The joint full conditional distribution for  $\mathbf{t}^*$  and  $\boldsymbol{\sigma}^{*2}$  is

$$\begin{aligned} & \pi(\mathbf{t}^*, \boldsymbol{\sigma}^{*2} | \mathbf{Z}, \mathbf{t}, \boldsymbol{\xi}, \mathbf{q}, \mathbf{r}, s^2, \mathbf{h}, m^2) \\ & \propto \prod_{j=1}^J \prod_{d=1}^D \prod_{c:z_{c,d}=j} K(t_{c,d} | \boldsymbol{\psi}_{j,d}^*) \times \prod_{j=1}^J \prod_{d=1}^D \prod_{c=1}^{C_d} \exp(-\xi_{c,d} q_{j,d} K(t_{c,d} | \boldsymbol{\psi}_{j,d}^*)) \\ & \quad \times \prod_{j=1}^J \prod_{d=1}^D \left[ \text{N}(t_{j,d}^* | r_j, s^2) \times \log\text{-N}(\sigma_{j,d}^{*2} | h_j, m^2) \right]. \end{aligned}$$

Due to the presence of the exponential term, it is impossible to obtain standard distributions. We introduce latent variables  $\mathbf{u} = \{u_{c,j,d}\}_{c=1, j=1, d=1}^{C_d, J, D} \in (0, 1)$ . Furthermore, for simplicity, we write  $M_{c,j,d} = \exp(-\xi_{c,d} q_{j,d} K(t_{c,d} | \boldsymbol{\psi}_{j,d}^*))$  and the joint full conditional distribution becomes

$$\begin{aligned} \pi(\mathbf{t}^*, \boldsymbol{\sigma}^{*2}, \mathbf{u} | \dots) & \propto \prod_{j=1}^J \prod_{d=1}^D \prod_{c:z_{c,d}=j} K(t_{c,d} | \boldsymbol{\psi}_{j,d}^*) \times \prod_{j=1}^J \prod_{d=1}^D \prod_{c=1}^{C_d} \mathbb{I}(u_{c,j,d} < M_{c,j,d}) \\ & \quad \times \prod_{j=1}^J \prod_{d=1}^D \left[ \text{N}(t_{j,d}^* | r_j, s^2) \times \log\text{-N}(\sigma_{j,d}^{*2} | h_j, m^2) \right]. \end{aligned} \tag{15}$$

By integrating over  $u_{c,j,d}$  on  $(0, 1)$ , we can obtain the previous joint full conditional distribution. Now we also need to sample  $u_{c,j,d}$  in addition to  $t_{j,d}^*$  and  $\sigma_{j,d}^{*2}$ .

#### A.3.1 LATENT PARAMETERS $u_{c,j,d}$

For each  $c, j$  and  $d$ , the full conditional distribution is

$$\pi(u_{c,j,d} | \xi_{c,d}, q_{j,d}, t_{c,d}, t_{j,d}^*, \sigma_{j,d}^{*2}) \propto \mathbb{I}(u_{c,j,d} < M_{c,j,d}),$$

i.e.,

$$u_{c,j,d} | \dots \sim \text{Unif}(0, \exp(-\xi_{c,d} q_{j,d} K(t_{c,d} | \boldsymbol{\psi}_{j,d}^*))).$$

#### A.3.2 MEAN PARAMETERS $t_{j,d}^*$

For each  $j$  and  $d$ , the full conditional distribution is

$$\begin{aligned} & \pi(t_{j,d}^* | r_j, s^2, \{z_{c,d}\}_{c=1}^{C_d}, \{\xi_{c,d}\}_{c=1}^{C_d}, \{u_{c,j,d}\}_{c=1}^{C_d}, \{t_{c,d}\}_{c=1}^{C_d}, q_{j,d}, \sigma_{j,d}^{*2}) \\ & \propto \prod_{c:z_{c,d}=j} K(t_{c,d} | \boldsymbol{\psi}_{j,d}^*) \times \text{N}(t_{j,d}^* | r_j, s^2) \times \mathbb{I}(t_{j,d}^* \in A_{j,d}). \end{aligned}$$

Let  $I_{j,d} = \{c : z_{c,d} = j\}$ . The first two terms are proportional to

$$\begin{aligned}
 & \exp \left[ -\frac{1}{2\sigma_{j,d}^{*2}} \sum_{I_{j,d}} (t_{j,d}^* - t_{c,d})^2 \right] \times \exp \left[ -\frac{1}{2s^2} (t_{j,d}^* - r_j)^2 \right] \\
 & \propto \exp \left[ -\frac{1}{2\sigma_{j,d}^{*2}} \left( N_{j,d} t_{j,d}^{*2} - 2t_{j,d}^* \sum_{I_{j,d}} t_{c,d} \right) - \frac{1}{2s^2} (t_{j,d}^{*2} - 2t_{j,d}^* r_j) \right] \\
 & \propto \exp \left( -\frac{1}{2\sigma_{j,d}^{*2} s^2} \left[ (\sigma_{j,d}^{*2} + N_{j,d} s^2) t_{j,d}^{*2} - 2t_{j,d}^* \left( r_j \sigma_{j,d}^{*2} + s^2 \sum_{I_{j,d}} t_{c,d} \right) \right] \right) \\
 & \propto \mathbb{N}(t_{j,d}^* | \hat{r}_{j,d}, \hat{s}_{j,d}^2),
 \end{aligned}$$

where

$$\begin{aligned}
 \hat{s}_{j,d}^2 &= \left( \frac{1}{s^2} + \frac{N_{j,d}}{\sigma_{j,d}^{*2}} \right)^{-1}, \\
 \hat{r}_{j,d} &= \frac{r_j/s^2 + \sum_{I_{j,d}} t_{c,d}/\sigma_{j,d}^{*2}}{1/s^2 + N_{j,d}/\sigma_{j,d}^{*2}}.
 \end{aligned}$$

The indicator function  $\mathbb{I}(t_{j,d}^* \in A_{j,d})$  truncates this normal distribution for  $t_{j,d}^*$ , which results from the indicator function in Eq (15). The region  $A_{j,d}$  is

$$\begin{aligned}
 A_{j,d} &= \bigcap_{c=1}^{C_d} A_{c,j,d} = \bigcap_{c=1}^{C_d} \{t_{j,d}^* : u_{c,j,d} < \exp(-\xi_{c,d} q_{j,d} K(t_{c,d} | \psi_{j,d}^*))\} \\
 &= \bigcap_{c=1}^{C_d} \left\{ t_{j,d}^* : -\frac{\log u_{c,j,d}}{\xi_{c,d} q_{j,d}} > \exp \left( -\frac{1}{2\sigma_{j,d}^{*2}} (t_{c,d} - t_{j,d}^*)^2 \right) \right\} \\
 &= \bigcap_{c=1}^{C_d} \left\{ t_{j,d}^* : \log \left[ -\frac{\log u_{c,j,d}}{\xi_{c,d} q_{j,d}} \right] > -\frac{1}{2\sigma_{j,d}^{*2}} (t_{c,d} - t_{j,d}^*)^2 \right\}.
 \end{aligned}$$

Since the right-hand side is always negative, if  $-\frac{\log u_{c,j,d}}{\xi_{c,d} q_{j,d}} \geq 1 \Rightarrow -\log u_{c,j,d} \geq \xi_{c,d} q_{j,d}$ , we have  $A_{c,j,d} = \mathbb{R}$  and hence there is no truncation. Otherwise,

$$A_{c,j,d} = \left( -\infty, t_{c,d} - \sqrt{-2\sigma_{j,d}^{*2} \log \left[ -\frac{\log u_{c,j,d}}{\xi_{c,d} q_{j,d}} \right]} \right) \cup \left( t_{c,d} + \sqrt{-2\sigma_{j,d}^{*2} \log \left[ -\frac{\log u_{c,j,d}}{\xi_{c,d} q_{j,d}} \right]}, +\infty \right).$$

Hence the region  $A_{j,d}$  is given by

$$A_{j,d} = \bigcap_{c: -\log u_{c,j,d} < \xi_{c,d} q_{j,d}} A_{c,j,d}.$$

Combining all terms together, the full conditional distribution of  $t_{j,d}^*$  is a truncated normal distribution

$$t_{j,d}^* | \dots \sim \mathbb{N}(\hat{r}_{j,d}, \hat{s}_{j,d}^2).$$

with truncation region  $A_{j,d}$ . Note that if there is no cell in dataset  $d$  that belongs to component  $j$ , we will sample  $t_{j,d}^*$  from the prior truncated to  $A_{j,d}$ . Furthermore, if it satisfies that  $\{c : -\log u_{c,j,d} < \xi_{c,d} q_{j,d}\} = \emptyset$ , there is no truncation. Therefore, there are actually four possible cases, based on truncation or not and whether or not the component  $j$  is empty in dataset  $d$ .

### A.3.3 VARIANCE PARAMETERS $\sigma_{j,d}^{*2}$

For each  $j$  and  $d$ , the full conditional distribution is

$$\begin{aligned} & \pi(\sigma_{j,d}^{*2} | h_j, m^2, \{z_{c,d}\}_{c=1}^{C_d}, \{\xi_{c,d}\}_{c=1}^{C_d}, \{u_{c,j,d}\}_{c=1}^{C_d}, \{t_{c,d}\}_{c=1}^{C_d}, q_{j,d}, t_{j,d}^*) \\ & \propto \prod_{c: z_{c,d}=j} K(t_{c,d} | \psi_{j,d}^*) \times \log\text{-N}(\sigma_{j,d}^{*2} | h_j, m^2) \times \mathbb{I}(\sigma_{j,d}^{*2} \in B_{j,d}). \end{aligned}$$

The first two terms are proportional to

$$\exp \left[ -\frac{1}{2\sigma_{j,d}^{*2}} \sum_{I_{j,d}} (t_{j,d}^* - t_{c,d})^2 \right] \times \frac{1}{\sigma_{j,d}^{*2}} \exp \left[ -\frac{1}{2m^2} \left( \log(\sigma_{j,d}^{*2}) - h_j \right)^2 \right], \quad (16)$$

which is not a standard form and hence we will apply adaptive Metropolis-Hastings. The region  $B_{j,d}$  is given by

$$\begin{aligned} B_{j,d} &= \bigcap_{c=1}^{C_d} B_{c,j,d} = \bigcap_{c=1}^{C_d} \left\{ \sigma_{j,d}^{*2} : u_{c,j,d} < \exp(-\xi_{c,d} q_{j,d} K(t_{c,d} | \psi_{j,d}^*)) \right\} \\ &= \bigcap_{c=1}^{C_d} \left\{ \sigma_{j,d}^{*2} : -\frac{\log u_{c,j,d}}{\xi_{c,d} q_{j,d}} > \exp \left( -\frac{1}{2\sigma_{j,d}^{*2}} (t_{c,d} - t_{j,d}^*)^2 \right) \right\} \\ &= \bigcap_{c=1}^{C_d} \left\{ \sigma_{j,d}^{*2} : \log \left[ -\frac{\log u_{c,j,d}}{\xi_{c,d} q_{j,d}} \right] > -\frac{1}{2\sigma_{j,d}^{*2}} (t_{c,d} - t_{j,d}^*)^2 \right\}. \end{aligned}$$

Similar to  $t_{j,d}^*$ , if  $-\frac{\log u_{c,j,d}}{\xi_{c,d} q_{j,d}} \geq 1 \Rightarrow -\log u_{c,j,d} \geq \xi_{c,d} q_{j,d}$ , we have  $B_{c,j,d} = \mathbb{R}^+$  and hence there is no truncation. Otherwise,

$$B_{c,j,d} = \left( 0, -\frac{(t_{c,d} - t_{j,d}^*)^2}{2 \log \left[ -\frac{\log u_{c,j,d}}{\xi_{c,d} q_{j,d}} \right]} \right).$$

Hence the region  $B_{j,d}$  is

$$B_{j,d} = \bigcap_{c: -\log u_{c,j,d} < \xi_{c,d} q_{j,d}} B_{c,j,d} = \left( 0, \sigma_{j,d}^+ \right),$$

where

$$\sigma_{j,d}^+ = \min_{c: -\log u_{c,j,d} < \xi_{c,d} q_{j,d}} -\frac{(t_{c,d} - t_{j,d}^*)^2}{2 \log \left[ -\frac{\log u_{c,j,d}}{\xi_{c,d} q_{j,d}} \right]}.$$

Below we will describe the AMH for  $\sigma_{j,d}^{*2}$ .

**AMH for  $\sigma_{j,d}^{*2}$**  The adaptive Metropolis-Hastings algorithm we adopt is based on Algorithm 4 of Chapter 7 in Griffin and Stephens (2013). The AMH is the same for each  $j$  and  $d$ , and hence for simplicity, we will drop the subscript  $j, d$  in this section.

1. Apply the following transformation to  $\sigma^{*2}$ :

$$X = g(\sigma^{*2}) = -\log\left(\frac{1}{\sigma^{*2}} - \frac{1}{\sigma^+}\right) \in \mathbb{R}.$$

The Jacobian term is

$$J_x = \frac{dX}{d\sigma^{*2}} = \frac{\sigma^+}{\sigma^{*2}(\sigma^+ - \sigma^{*2})}.$$

The inverse transformation is

$$\sigma^{*2} = \frac{1}{\exp(-x) + 1/\sigma^+} \in (0, \sigma^+).$$

2. Let  $d$  denote the dimension of  $X$  ( $d = 1$  for the case of  $\sigma_{j,d}^{*2}$ ). Suppose the current iteration is  $n$  and the sampled  $\sigma^{*2}$  from iteration  $n - 1$  is  $\sigma_{old}^{*2}$ . Conditional on  $\sigma^+$  at the current iteration, we define  $X_{old} = g(\sigma_{old}^{*2})$ .

We use random walk to sample  $X_{new}$ . For  $n \leq 100$ , we sample  $X_{new}$  from  $N(X_{old}, 0.01 \times \mathbf{I}_d)$ . For  $n > 100$ , denote  $s_d = 2.4^2/d$ , then we propose  $X_{new} \sim N(X_{old}, s_d \times (\Sigma_{n-1} + \epsilon \mathbf{I}_d))$ , and  $\sigma_{new}^{*2}$  is obtained using the inverse transformation. For the rest of this supplement, we will use  $Q_n$  to denote the proposal distribution at step  $n$ .

For all the AMH we perform, we use  $\epsilon = 0.01$ , and  $\Sigma_{n-1}$  is the sample covariance (or variance) based on the past  $n - 1$  sampled  $X$ , which needs to be computed at every iteration. To avoid large-matrix computation, Liu et al. (2024) use a recursive formulae to update  $\Sigma_n$  after the  $n$ -th iteration. The details are provided later.

3. Since this is a Metropolis-Hastings step, we need to compute the acceptance probability to decide to accept  $\sigma_{new}^{*2}$  or not. Let  $\pi(\sigma^{*2})$  denote the posterior distribution. The acceptance probability is

$$\begin{aligned} \alpha(\sigma_{new}^{*2}, \sigma_{old}^{*2}) &= \min\left(1, \frac{\pi(\sigma_{new}^{*2})Q_n(\sigma_{old}^{*2}|\sigma_{new}^{*2})}{\pi(\sigma_{old}^{*2})Q_n(\sigma_{new}^{*2}|\sigma_{old}^{*2})}\right) \\ &= \min\left(1, \frac{\pi(\sigma_{new}^{*2})|J_{x_{old}}|}{\pi(\sigma_{old}^{*2})|J_{x_{new}}|}\right), \end{aligned}$$

where  $\pi(\sigma_{new}^{*2})/\pi(\sigma_{old}^{*2})$  is given by Eq (16) evaluated at the new and old  $\sigma^{*2}$ , and the determinant of the Jacobian  $|J_x|$  is provided in step 1, conditional on  $\sigma^+$  in the current iteration:

$$\frac{|J_{x_{old}}|}{|J_{x_{new}}|} = \frac{\sigma_{new}^{*2}(\sigma^+ - \sigma_{new}^{*2})}{\sigma_{old}^{*2}(\sigma^+ - \sigma_{old}^{*2})}. \quad (17)$$

In practice, the log acceptance probability is used. Taking the logarithm of Eq (16) and Eq (17) yields

$$l_{post} = -\frac{1}{2\sigma^{*2}} \sum_{I_{j,d}} (t^* - t_{c,d})^2 - \log(\sigma^{*2}) - \frac{1}{2m^2} (\log(\sigma^{*2}) - h_j)^2,$$

$$\log\left(\frac{|J_{x_{old}}|}{|J_{x_{new}}|}\right) = \log(\sigma_{new}^{*2}) + \log(\sigma^+ - \sigma_{new}^{*2}) - \log(\sigma_{old}^{*2}) - \log(\sigma^+ - \sigma_{old}^{*2}),$$

where  $l_{post}$  denotes the posterior distribution on the log scale.

4. After making the decision to accept the proposed value or not, we will compute the sample covariance/variance  $\Sigma_n$ .

For  $d = 1$ , the variance  $\Sigma_n$  is computed based on 2 statistics:  $M_2(n-1)$  and  $\bar{X}_{n-1}$  from the previous  $n-1$  samples, and the new value  $x_n$ . The definition of the two statistics are

$$M_2(n) = \sum_{i=1}^n (x_i - \bar{x}_n)^2,$$

$$\bar{x}_n = \frac{1}{n} \sum_{i=1}^n x_i.$$

The following relationship is observed between  $\bar{X}_n$  and  $\bar{X}_{n-1}$ , and between  $M_2(n)$  and  $M_2(n-1)$ :

$$\bar{x}_n = \left(1 - \frac{1}{n}\right) \bar{x}_{n-1} + \frac{x_n}{n},$$

and

$$\begin{aligned} \Sigma_n &= \frac{1}{n-1} \sum_{i=1}^n (x_i - \bar{x}_n)^2 = \frac{1}{n-1} M_2(n) \\ &= \frac{1}{n-1} [M_2(n-1) + (x_n - \bar{x}_{n-1})(x_n - \bar{x}_n)]. \end{aligned} \quad (18)$$

The proof of Eq (18) is as follows:

$$\begin{aligned} (n-1)\Sigma_n - (n-2)\Sigma_{n-1} &= \sum_{i=1}^n (x_i - \bar{x}_n)^2 - \sum_{i=1}^{n-1} (x_i - \bar{x}_{n-1})^2 \\ &= (x_n - \bar{x}_n)^2 + \sum_{i=1}^{n-1} ((x_i - \bar{x}_n)^2 - (x_i - \bar{x}_{n-1})^2) \\ &= (x_n - \bar{x}_n)^2 + \sum_{i=1}^{n-1} (x_i - \bar{x}_n + x_i - \bar{x}_{n-1})(\bar{x}_{n-1} - \bar{x}_n) \\ &= (x_n - \bar{x}_n)^2 + (\bar{x}_n - x_n)(\bar{x}_{n-1} - \bar{x}_n) \\ &= (x_n - \bar{x}_n)(x_n - \bar{x}_n - \bar{x}_{n-1} + \bar{x}_n) \\ &= (x_n - \bar{x}_n)(x_n - \bar{x}_{n-1}). \end{aligned}$$

Hence we first compute  $\bar{x}_n$  from  $\bar{x}_{n-1}$  and  $x_n$ . Then  $\bar{x}_n, \bar{x}_{n-1}, x_n$  and  $M_2(n-1)$  are used for the calculation of  $\Sigma_n$ .

For  $d > 1$ , we will compute  $\Sigma_n$  based on 2 statistics:  $\tilde{S}(n-1)$  and  $\mathbf{m}(n-1)$  given by the previous  $n-1$  simulations, and the new sample  $\mathbf{x}_n = (x_{n,1}, \dots, x_{n,d})$ .  $\tilde{S}(n-1)$  is a symmetric matrix of dimension  $d \times d$ , defined by the following:

$$\tilde{S}(n-1) = \begin{bmatrix} \sum_{i=1}^{n-1} (x_{i,1})^2 & \sum_{i=1}^{n-1} x_{i,1}x_{i,2} & \cdots & \sum_{i=1}^{n-1} x_{i,1}x_{i,d} \\ \vdots & \vdots & \ddots & \vdots \\ \sum_{i=1}^{n-1} x_{i,d}x_{i,1} & \sum_{i=1}^{n-1} x_{i,d}x_{i,2} & \cdots & \sum_{i=1}^{n-1} x_{i,d}x_{i,d} \end{bmatrix},$$

where  $\mathbf{m}(n-1)$  is a  $d$ -dimension vector, with each component  $m_{d'}(n-1)$  denoting the mean of  $x_{d'}$  from the first  $(n-1)$  samples:

$$\mathbf{m}(n-1) = (m_1(n-1), \dots, m_d(n-1)).$$

The element in the covariance matrix of  $X$  after  $n$  iterations ( $\Sigma_n$ ) is given by

$$\begin{aligned} \Sigma_n(u, v) &= \frac{1}{n-1} \sum_{i=1}^n (x_{i,u} - m_u(n))(x_{i,v} - m_v(n)) \\ &= \frac{1}{n-1} \left[ \sum_{i=1}^n x_{i,u}x_{i,v} - m_v(n) \sum_{i=1}^n x_{i,u} - m_u(n) \sum_{i=1}^n x_{i,v} + n \times m_v(n)m_u(n) \right] \\ &= \frac{1}{n-1} \left[ \sum_{i=1}^n x_{i,u}x_{i,v} - n \times m_v(n)m_u(n) \right] \\ &= \frac{1}{n-1} \sum_{i=1}^n x_{i,u}x_{i,v} - \frac{n}{n-1} m_v(n)m_u(n). \end{aligned}$$

Hence the covariance matrix could be written in the following form:

$$\Sigma_n = \frac{1}{n-1} \tilde{S}(n) - \frac{n}{n-1} (\mathbf{m}(n)^T \mathbf{m}(n)),$$

and we note the following relationship:

$$\begin{aligned} \tilde{S}(n) &= \tilde{S}(n-1) + \mathbf{x}_n^T \mathbf{x}_n, \\ \mathbf{m}(n) &= \left(1 - \frac{1}{n}\right) \mathbf{m}(n-1) + \frac{1}{n} \mathbf{x}_n. \end{aligned}$$

Therefore, we first compute  $\tilde{S}(n)$  and  $\mathbf{m}(n)$  based on  $\tilde{S}(n-1), \mathbf{m}(n-1)$  and the new value  $\mathbf{x}_n$ . Then the covariance matrix can be calculated from  $\tilde{S}(n)$  and  $\mathbf{m}(n)$ .

Finally, we remark that the full conditional density of  $\sigma_{j,d}^{*2}$  also has four possible forms, depending on truncation or not, and whether component  $j$  in dataset  $d$  is empty or not. The above AMH will be applied when the component  $j$  is occupied. Besides, in this case, if there is no truncation (the upper bound  $\sigma_{j,d}^+ = \infty$ ), the transformation defined in step 1 will reduce to a simple log-transformation, and the Jacobian is simply  $1/\sigma_{j,d}^{*2}$ . When component  $j$  is empty in some MCMC iterations, we will draw samples from the log-normal prior (may or may not be truncated). For such iterations, all the samples are accepted with probability 1, and are transformed to  $X$  to update the covariance/variance.

#### A.4 Concentration parameters $\alpha$ and $\alpha_0$

##### A.4.1 CONCENTRATION PARAMETER $\alpha$

The full conditional distribution of  $\alpha$  is

$$\begin{aligned} \pi(\alpha|\mathbf{q}, \mathbf{p}^J) &\propto \prod_{j=1}^J \prod_{d=1}^D \text{Gamma}(q_{j,d}|\alpha p_j^J, 1) \times \text{Gamma}(\alpha|1, 1) \\ &\propto \prod_{j=1}^J \prod_{d=1}^D \left[ \frac{1}{\Gamma(\alpha p_j^J)} (q_{j,d})^{\alpha p_j^J} \right] \times \exp(-\alpha). \end{aligned}$$

The distribution is not of a standard form and we apply the AMH as described in section A.3.3. Specifically, we use the log-transformation

$$X = \log(\alpha) \in \mathbb{R}.$$

The Jacobian is

$$J_x = \frac{dX}{d\alpha} = \frac{1}{\alpha}.$$

and the inverse transformation is  $\alpha = \exp(x)$ . We use the random walk to sample a new  $X$  as stated before.

The logarithm of the full conditional density is

$$lpost = -\alpha + \sum_{j=1}^J \sum_{d=1}^D [\alpha p_j^J \log(q_{j,d}) - \log(\Gamma(\alpha p_j^J))].$$

Hence the acceptance probability of the new sample is

$$\begin{aligned} \alpha(\alpha_{new}, \alpha_{old}) &= \min \left( 1, \frac{\pi(\alpha_{new}) Q_n(\alpha_{old}|\alpha_{new})}{\pi(\alpha_{old}) Q_n(\alpha_{new}|\alpha_{old})} \right) \\ &= \min \left( 1, \frac{\pi(\alpha_{new}) \alpha_{new}}{\pi(\alpha_{old}) \alpha_{old}} \right) \\ &= \min(1, \exp[lpost_{new} - lpost_{old} + \log(\alpha_{new}) - \log(\alpha_{old})]). \end{aligned}$$

After the decision of rejection or acceptance, we update the sample variance following step 4 of section A.3.3 ( $d = 1$ ).

##### A.4.2 CONCENTRATION PARAMETER $\alpha_0$

The full conditional distribution of  $\alpha$  is

$$\begin{aligned} \pi(\alpha_0|\mathbf{p}^J) &\propto \text{Gamma}(\alpha_0|1, 1) \times \text{Dir} \left( \mathbf{p}^J \mid \frac{\alpha_0}{J}, \dots, \frac{\alpha_0}{J} \right) \\ &\propto \exp(-\alpha_0) \times \frac{\Gamma(\alpha_0)}{[\Gamma(\frac{\alpha_0}{J})]^J} \prod_{j=1}^J (p_j^J)^{\frac{\alpha_0}{J}}. \end{aligned}$$

Same log-transformation is applied

$$X = \log(\alpha_0) \in \mathbb{R},$$



with Jacobian

$$J_x = \frac{dX}{d\alpha_0} = \frac{1}{\alpha_0},$$

and the inverse transformation is  $\alpha_0 = \exp(x)$ .

The logarithm of the full conditional distribution is

$$lpost = -\alpha_0 + \log(\Gamma(\alpha_0)) - J \log\left(\Gamma\left(\frac{\alpha_0}{J}\right)\right) + \frac{\alpha_0}{J} \sum_{j=1}^J \log(p_j^J).$$

The acceptance probability is

$$\begin{aligned} \alpha(\alpha_{0,new}, \alpha_{0,old}) &= \min\left(1, \frac{\pi(\alpha_{0,new})Q_n(\alpha_{0,old}|\alpha_{0,new})}{\pi(\alpha_{0,old})Q_n(\alpha_{0,new}|\alpha_{0,old})}\right) \\ &= \min\left(1, \frac{\pi(\alpha_{0,new})\alpha_{0,new}}{\pi(\alpha_{0,old})\alpha_{0,old}}\right) \\ &= \min(1, \exp[lpost_{new} - lpost_{old} + \log(\alpha_{0,new}) - \log(\alpha_{0,old})]). \end{aligned}$$

The variance is updated similarly to  $\alpha$ .

### A.5 Allocation variables $z_{c,d}$

We notice that  $z_{c,d}$  only plays a role though the augmented data likelihood for every  $c$  and  $d$ . Hence  $z_{c,d}$  is independent across  $c, d$ , yielding

$$\pi(z_{c,d} = j | \boldsymbol{\mu}_{1:J,1:G}^*, \boldsymbol{\phi}_{1:J,1:G}^*, \boldsymbol{\beta}, \mathbf{Y}, \mathbf{t}, \mathbf{q}) \propto \prod_{g=1}^G \text{NB}(y_{c,g,d} | \mu_{j,g}^* \beta_{c,d}, \phi_{j,g}^*) \times q_{j,d} K(t_{c,d} | \psi_{j,d}^*).$$

Denote

$$\tilde{p}(z_{c,d} = j | \boldsymbol{\mu}_{1:J,1:G}^*, \boldsymbol{\phi}_{1:J,1:G}^*, \boldsymbol{\beta}, \mathbf{Y}, \mathbf{t}, \mathbf{q}) = \prod_{g=1}^G \text{NB}(y_{c,g,d} | \mu_{j,g}^* \beta_{c,d}, \phi_{j,g}^*) \times q_{j,d} K(t_{c,d} | \psi_{j,d}^*).$$

The full conditional distribution is then

$$\pi(z_{c,d} = j | \boldsymbol{\mu}_{1:J,1:G}^*, \boldsymbol{\phi}_{1:J,1:G}^*, \boldsymbol{\beta}, \mathbf{Y}, \mathbf{t}, \mathbf{q}) = \frac{\tilde{K} \tilde{p}(z_{c,d} = j | \boldsymbol{\mu}_{1:J,1:G}^*, \boldsymbol{\phi}_{1:J,1:G}^*, \boldsymbol{\beta}, \mathbf{Y}, \mathbf{t}, \mathbf{q})}{\tilde{K} \sum_{l=1}^J \tilde{p}(z_{c,d} = l | \boldsymbol{\mu}_{1:J,1:G}^*, \boldsymbol{\phi}_{1:J,1:G}^*, \boldsymbol{\beta}, \mathbf{Y}, \mathbf{t}, \mathbf{q})}. \quad (19)$$

It is possible that the sum in the denominator can be very small. To avoid computational problem, we remove the most extreme probability

$$\log(\tilde{K}) = -\max_j \log(\tilde{p}(z_{c,d} = j | \boldsymbol{\mu}_{1:J,1:G}^*, \boldsymbol{\phi}_{1:J,1:G}^*, \boldsymbol{\beta}, \mathbf{Y}, \mathbf{t}, \mathbf{q})).$$

In all, we sample  $z_{c,d}$  from  $\{1, \dots, J\}$  according to  $\pi(z_{c,d} = j | \boldsymbol{\mu}_{1:J,1:G}^*, \boldsymbol{\phi}_{1:J,1:G}^*, \boldsymbol{\beta}, \mathbf{Y}, \mathbf{t}, \mathbf{q})$ . This is repeated for every  $c$  and  $d$ .

### A.6 Component probabilities $p_j^J$

The full conditional distribution is

$$\begin{aligned} \pi(p_1^J, \dots, p_J^J | \mathbf{q}, \alpha, \alpha_0) &\propto \prod_{j=1}^J \prod_{d=1}^D \text{Gamma}(q_{j,d} | \alpha p_j^J, 1) \times \text{Dir}\left(p_1^J, \dots, p_J^J | \frac{\alpha_0}{J}, \dots, \frac{\alpha_0}{J}\right) \\ &\propto \prod_{j=1}^J \prod_{d=1}^D \left[ \frac{1}{\Gamma(\alpha p_j^J)} (q_{j,d})^{\alpha p_j^J} \right] \times \prod_{j=1}^J (p_j^J)^{\frac{\alpha_0}{J} - 1}, \end{aligned}$$

where  $p_j^J$  cannot be separated with each other and the distribution is also non-standard. Therefore, we apply AMH as in ?. Because  $p_j^J$  ( $j = 1, \dots, J$ ) sum to one, the following transformation is made to obtain  $\mathbf{X} \in \mathbb{R}^{J-1}$ :

$$X_j = \log\left(\frac{P_j}{P_J}\right), \quad j = 1, \dots, J-1.$$

The inverse transformation is given by

$$\begin{aligned} p_j^J &= \frac{\exp(x_j)}{1 + \sum_{j=1}^{J-1} \exp(x_j)}, \quad j = 1, \dots, J-1, \\ p_J^J &= 1 - \sum_{j=1}^{J-1} p_j^J = \frac{1}{1 + \sum_{j=1}^{J-1} \exp(x_j)}. \end{aligned}$$

As for the Jacobian matrix, it is given by:

$$\begin{aligned} J_{\mathbf{x}} &= \begin{pmatrix} \frac{dx_1}{dp_1} & \frac{dx_2}{dp_1} & \dots & \frac{dx_{J-1}}{dp_1} \\ \vdots & \vdots & \ddots & \vdots \\ \frac{dx_1}{dp_{J-1}} & \frac{dx_2}{dp_{J-1}} & \dots & \frac{dx_{J-1}}{dp_{J-1}} \end{pmatrix} \\ &= \begin{pmatrix} \frac{1}{p_1} + \frac{1}{p_J} & \dots & \frac{1}{p_J} \\ \vdots & \ddots & \vdots \\ \frac{1}{p_J} & \dots & \frac{1}{p_{J-1}} + \frac{1}{p_J} \end{pmatrix} \\ &= \begin{pmatrix} \frac{1}{p_J} & \dots & \frac{1}{p_J} \\ \vdots & \ddots & \vdots \\ \frac{1}{p_J} & \dots & \frac{1}{p_J} \end{pmatrix} + \begin{pmatrix} \frac{1}{p_1} & 0 & \dots & 0 \\ 0 & \frac{1}{p_2} & \vdots & 0 \\ \vdots & \vdots & \ddots & 0 \\ 0 & 0 & \dots & \frac{1}{p_{J-1}} \end{pmatrix} \\ &= B + A. \end{aligned}$$

Because  $\det(A+B) = \det(A) + \det(B) + \text{Tr}(A^{-1}B) \det(A)$ ,  $\det(B) = 0$  and  $\det(A) = \prod_{j=1}^{J-1} \frac{1}{p_j}$ , it follows that  $\det(A+B) = \prod_{j=1}^{J-1} \frac{1}{p_j} + (1-p_J) \prod_{j=1}^J \frac{1}{p_j} = \prod_{j=1}^J \frac{1}{p_j}$ . Therefore,

$$\log |J_{\mathbf{x}}| = \log \left[ \prod_{j=1}^J \frac{1}{p_j} \right] = - \sum_{j=1}^J \log(p_j).$$

The log full conditional distribution is

$$lpost = \sum_{j=1}^J \sum_{d=1}^D [\alpha p_j^J \log(q_{j,d}) - \log \Gamma(\alpha p_j^J)] + \sum_{j=1}^J \left[ \left( \frac{\alpha_0}{J} - 1 \right) \log(p_j^J) \right].$$

Combining all terms together, the acceptance probability is

$$\begin{aligned} \alpha(\mathbf{p}_{new}^J, \mathbf{p}_{old}^J) &= \min \left( 1, \frac{\pi(\mathbf{p}_{new}^J) Q_n(\mathbf{p}_{old}^J | \mathbf{p}_{new}^J)}{\pi(\mathbf{p}_{old}^J) Q_n(\mathbf{p}_{new}^J | \mathbf{p}_{old}^J)} \right) \\ &= \min \left( 1, \frac{\pi(\mathbf{p}_{new}^J) |J_{\mathbf{x}_{old}}|}{\pi(\mathbf{p}_{old}^J) |J_{\mathbf{x}_{new}}|} \right) \\ &= \min \left( 1, \exp \left[ lpost_{new} - lpost_{old} + \sum_{j=1}^J (\log(p_{j,new}^J) - \log(p_{j,old}^J)) \right] \right). \end{aligned}$$

We mention that the sampling of a new transformed variable  $\mathbf{X}_{new}$  is slightly different from step 2 in section A.3.3. Instead of a fixed scale parameter  $s_d = 2.4^2/d$  ( $d = J - 1$  for the case of  $\mathbf{p}^J$ ),  $s_d$  is also updated at each iteration. The idea is to adapt  $s_d$  to achieve an average acceptance probability of 0.234 (Algorithm 6 of Chapter 7 in Griffin and Stephens (2013)), which is designed for multivariate target distribution.

Let the initial value  $s_d^{(1)} = 0.001$ . Suppose the current iteration is  $n$ , and  $\mathbf{X}_{new}$  is the new sample after the decision of rejection or not. Define

$$\lambda^{(n)} = \exp \left( \log(s_d^{(n)}) + n^{-0.7} \times (\alpha(\mathbf{p}_{new}^J, \mathbf{p}_{old}^J) - 0.234) \right),$$

then

$$s_d^{(n+1)} = \begin{cases} \lambda^-, & \text{if } \lambda^{(n)} < \lambda^-, \\ \lambda^{(n)}, & \text{if } \lambda^{(n)} \in [\lambda^-, \lambda^+], \\ \lambda^+, & \text{if } \lambda^{(n)} > \lambda^+, \end{cases}$$

where  $\lambda^- = \exp(-50)$  and  $\lambda^+ = \exp(50)$ . The update of the covariance matrix follows from step 4 (multivariate case) in section A.3.3.

## A.7 Mean-dispersion parameters $\mathbf{b}$ and $\alpha_\phi^2$

The joint distribution of  $\mathbf{b} = (b_0, b_1)^T$  and  $\alpha_\phi^2$  is

$$\begin{aligned} \pi(\mathbf{b}, \alpha_\phi^2 | \boldsymbol{\mu}_{1:J,1:G}^*, \boldsymbol{\phi}_{1:J,1:G}^*) &\propto \mathcal{N}(\mathbf{b} | \mathbf{m}_b, \alpha_\phi^2 V_b) \times \text{IG}(\alpha_\phi^2 | v_1, v_2) \times \prod_{j=1}^J \prod_{g=1}^G \text{log-N}(\phi_{j,g}^* | b_0 + b_1 \log(\mu_{j,g}^*), \alpha_\phi^2) \\ &\propto (\alpha_\phi^2)^{-(v_1+2+\frac{JG}{2})} \\ &\quad \times \exp \left( -\frac{1}{\alpha_\phi^2} \left[ \frac{1}{2} \sum_{j=1}^J \sum_{g=1}^G (\log(\phi_{j,g}^*) - b_0 - b_1 \log(\mu_{j,g}^*))^2 + \frac{1}{2} (b_0^2 + b_1^2) \right. \right. \\ &\quad \left. \left. - \mathbf{b}^T \mathbf{m}_b + \frac{1}{2} \mathbf{m}_b^T \mathbf{m}_b + v_2 \right] \right). \end{aligned}$$

For  $\mathbf{b}$ , we have

$$\pi(\mathbf{b}|\boldsymbol{\mu}^*, \boldsymbol{\phi}^*, \alpha_\phi^2) \propto \exp\left(-\frac{1}{2\alpha_\phi^2} \left[ \sum_{j=1}^J \sum_{g=1}^G (\log(\phi_{j,g}^*) - b_0 - b_1 \log(\mu_{j,g}^*))^2 + (b_0^2 + b_1^2) - 2\mathbf{b}^T \mathbf{m}_b \right]\right), \quad (20)$$

which can be written in terms of matrix notation as

$$\sum_{j=1}^J \sum_{g=1}^G (\log(\phi_{j,g}^*) - b_0 - b_1 \log(\mu_{j,g}^*))^2 = \sum_{j=1}^J (\log(\boldsymbol{\phi}_j^*) - \tilde{\boldsymbol{\mu}}_j \mathbf{b})^T (\log(\boldsymbol{\phi}_j^*) - \tilde{\boldsymbol{\mu}}_j \mathbf{b}),$$

where  $\log(\boldsymbol{\phi}_j^*)$  has dimension  $G \times 1$ ,  $\tilde{\boldsymbol{\mu}}_j$  has dimension  $G \times 2$  and  $\mathbf{b}$  has dimension  $2 \times 1$ :

$$\log(\boldsymbol{\phi}_j^*) = \begin{bmatrix} \log(\phi_{j,1}^*) \\ \vdots \\ \log(\phi_{j,G}^*) \end{bmatrix}, \quad \tilde{\boldsymbol{\mu}}_j = \begin{bmatrix} 1 & \log(\mu_{j,1}^*) \\ \vdots & \vdots \\ 1 & \log(\mu_{j,G}^*) \end{bmatrix}, \quad \mathbf{b} = \begin{bmatrix} b_0 \\ b_1 \end{bmatrix}.$$

The above equation is equivalent to

$$\begin{aligned} & \sum_{j=1}^J \left[ \log(\boldsymbol{\phi}_j^*)^T \log(\boldsymbol{\phi}_j^*) - 2\mathbf{b}^T \tilde{\boldsymbol{\mu}}_j^T \log(\boldsymbol{\phi}_j^*) + \mathbf{b}^T \tilde{\boldsymbol{\mu}}_j^T \tilde{\boldsymbol{\mu}}_j \mathbf{b} \right] \\ &= \sum_{j=1}^J \left[ \log(\boldsymbol{\phi}_j^*)^T \log(\boldsymbol{\phi}_j^*) \right] - 2\mathbf{b}^T \sum_{j=1}^J \tilde{\boldsymbol{\mu}}_j^T \log(\boldsymbol{\phi}_j^*) + \mathbf{b}^T \left( \sum_{j=1}^J \tilde{\boldsymbol{\mu}}_j^T \tilde{\boldsymbol{\mu}}_j \right) \mathbf{b}. \end{aligned}$$

Therefore,

$$\begin{aligned} \pi(\mathbf{b}|\boldsymbol{\mu}^*, \boldsymbol{\phi}^*, \alpha_\phi^2) &\propto \exp\left(-\frac{1}{2\alpha_\phi^2} \left[ \mathbf{b}^T \left( \sum_{j=1}^J \tilde{\boldsymbol{\mu}}_j^T \tilde{\boldsymbol{\mu}}_j + \mathbf{I} \right) \mathbf{b} - 2\mathbf{b}^T \left( \sum_{j=1}^J \tilde{\boldsymbol{\mu}}_j^T \log(\boldsymbol{\phi}_j^*) + \mathbf{m}_b \right) \right. \right. \\ &\quad \left. \left. + \sum_{j=1}^J \left[ \log(\boldsymbol{\phi}_j^*)^T \log(\boldsymbol{\phi}_j^*) \right] \right]\right), \end{aligned}$$

i.e.,

$$\mathbf{b} | \dots \sim N(\tilde{\mathbf{m}}_b, \alpha_\phi^2 \tilde{V}_b),$$

where

$$\begin{aligned} \tilde{\mathbf{m}}_b &= \left( \sum_{j=1}^J \tilde{\boldsymbol{\mu}}_j^T \tilde{\boldsymbol{\mu}}_j + \mathbf{I} \right)^{-1} \left( \sum_{j=1}^J \tilde{\boldsymbol{\mu}}_j^T \log(\boldsymbol{\phi}_j^*) + \mathbf{m}_b \right), \\ \tilde{V}_b &= \left( \sum_{j=1}^J \tilde{\boldsymbol{\mu}}_j^T \tilde{\boldsymbol{\mu}}_j + \mathbf{I} \right)^{-1}. \end{aligned}$$

As for  $\alpha_\phi^2 | \boldsymbol{\mu}^*, \boldsymbol{\phi}^*$ , a closed form can be obtained by integrating out  $\mathbf{b}$  in the joint distribution as shown below.

$$\begin{aligned} \pi(\alpha_\phi^2 | \boldsymbol{\mu}^*, \boldsymbol{\phi}^*) &= \int \pi(\mathbf{b}, \alpha_\phi^2 | \boldsymbol{\mu}^*, \boldsymbol{\phi}^*) d\mathbf{b} \\ &\propto \int \left( \frac{1}{\alpha_\phi^2} \right)^{v_1+1} \exp\left(-\frac{v_2}{\alpha_\phi^2}\right) \left( \frac{1}{\alpha_\phi^2} \right)^{JG/2} \left( \frac{1}{\alpha_\phi^2} \right) \\ &\quad \times \exp\left(-\frac{1}{2\alpha_\phi^2} \left[ (\mathbf{b} - \tilde{\mathbf{m}}_b)^T \tilde{V}_b^{-1} (\mathbf{b} - \tilde{\mathbf{m}}_b) - \tilde{\mathbf{m}}_b^T \tilde{V}_b^{-1} \tilde{\mathbf{m}}_b \right. \right. \\ &\quad \left. \left. + \sum_{j=1}^J \log(\phi_j^*)^T \log(\phi_j^*) + \mathbf{m}_b^T \mathbf{m}_b \right] \right) d\mathbf{b}. \end{aligned}$$

Now since

$$\int \frac{1}{\alpha_\phi^2} \exp\left(-\frac{1}{2\alpha_\phi^2} (\mathbf{b} - \tilde{\mathbf{m}}_b)^T \tilde{V}_b^{-1} (\mathbf{b} - \tilde{\mathbf{m}}_b)\right) d\mathbf{b} = \text{Constant},$$

it follows that

$$\begin{aligned} \pi(\alpha_\phi^2 | \boldsymbol{\mu}^*, \boldsymbol{\phi}^*) &\propto \left( \frac{1}{\alpha_\phi^2} \right)^{v_1+1} \exp\left(-\frac{v_2}{\alpha_\phi^2}\right) \left( \frac{1}{\alpha_\phi^2} \right)^{JG/2} \\ &\quad \times \exp\left(-\frac{1}{2\alpha_\phi^2} \left[ -\tilde{\mathbf{m}}_b^T \tilde{V}_b^{-1} \tilde{\mathbf{m}}_b + \sum_{j=1}^J \log(\phi_j^*)^T \log(\phi_j^*) + \mathbf{m}_b^T \mathbf{m}_b \right] \right) \\ &\propto \left( \frac{1}{\alpha_\phi^2} \right)^{v_1+1+JG/2} \\ &\quad \times \exp\left(-\frac{1}{\alpha_\phi^2} \left[ v_2 + \frac{1}{2} \left( \sum_{j=1}^J \log(\phi_j^*)^T \log(\phi_j^*) - \tilde{\mathbf{m}}_b^T \tilde{V}_b^{-1} \tilde{\mathbf{m}}_b + \mathbf{m}_b^T \mathbf{m}_b \right) \right] \right). \end{aligned}$$

Therefore,

$$\alpha_\phi^2 | \boldsymbol{\mu}^*, \boldsymbol{\phi}^* \sim \text{IG}(\tilde{v}_1, \tilde{v}_2),$$

where

$$\begin{aligned} \tilde{v}_1 &= v_1 + JG/2, \\ \tilde{v}_2 &= v_2 + \frac{1}{2} \left( \sum_{j=1}^J \log(\phi_j^*)^T \log(\phi_j^*) - \tilde{\mathbf{m}}_b^T \tilde{V}_b^{-1} \tilde{\mathbf{m}}_b + \mathbf{m}_b^T \mathbf{m}_b \right). \end{aligned}$$

### A.8 Cluster-specific parameters $\mu_{j,g}^*$ and $\phi_{j,g}^*$

From the overall posterior distribution (Eq (14)), we notice that, for each  $j$  and  $g$ ,

$$\begin{aligned} \pi(\mu_{j,g}^*, \phi_{j,g}^* | \mathbf{Z}, \mathbf{b}, \alpha_\phi^2, \mathbf{Y}, \beta) &\propto \text{log-N}(\mu_{j,g}^* | 0, \alpha_\mu^2) \times \text{log-N}(\phi_{j,g}^* | b_0 + b_1 \log(\mu_{j,g}^*), \alpha_\phi^2) \\ &\times \prod_{(c,d):z_{c,d}=j} \text{NB}(y_{c,d,g} | \mu_{j,g}^* \beta_{c,d}, \phi_{j,g}^*) \\ &\propto \left( \frac{1}{\mu_{j,g}^* \phi_{j,g}^*} \right) \exp \left( -\frac{1}{2\alpha_\mu^2} (\log \mu_{j,g}^*)^2 - \frac{1}{2\alpha_\phi^2} (\log \phi_{j,g}^* - (b_0 + b_1 \log \mu_{j,g}^*))^2 \right) \times \\ &\prod_{(c,d):z_{c,d}=j} \binom{y_{c,g,d} + \phi_{j,g}^* - 1}{\phi_{j,g}^* - 1} \left( \frac{\phi_{j,g}^*}{\mu_{j,g}^* \beta_{c,d} + \phi_{j,g}^*} \right)^{\phi_{j,g}^*} \left( \frac{\mu_{j,g}^*}{\mu_{j,g}^* \beta_{c,d} + \phi_{j,g}^*} \right)^{y_{c,g,d}}. \end{aligned}$$

This is not a standard distribution and hence we will apply AMH to sample for  $(\mu_{j,g}^*, \phi_{j,g}^*)$ . For clarity, we will drop the subscript  $j$  and  $g$  here. The transformation is

$$\mathbf{X} = (X_1, X_2) = (\log(\mu^*), \log(\phi^*)) \in \mathbb{R}^2,$$

with inverse transformation

$$\mu^* = \exp(x_1), \quad \phi^* = \exp(x_2).$$

The Jacobian is

$$J_{\mathbf{X}} = \begin{pmatrix} \frac{dx_1}{d\mu^*} & \frac{dx_1}{d\phi^*} \\ \frac{dx_2}{d\mu^*} & \frac{dx_2}{d\phi^*} \end{pmatrix} = \begin{pmatrix} \frac{1}{\mu^*} & 0 \\ 0 & \frac{1}{\phi^*} \end{pmatrix},$$

so  $|J_{\mathbf{X}}| = \frac{1}{\mu^* \phi^*}$ .

The logarithm of the full conditional distribution is

$$\begin{aligned} lpost &= -\log(\mu_{j,g}^* \phi_{j,g}^*) - \frac{1}{2\alpha_\mu^2} (\log \mu_{j,g}^*)^2 - \frac{1}{2\alpha_\phi^2} (\log \phi_{j,g}^* - (b_0 + b_1 \log \mu_{j,g}^*))^2 \\ &+ \sum_{(c,d):z_{c,d}=j} \log \binom{y_{c,g,d} + \phi_{j,g}^* - 1}{\phi_{j,g}^* - 1} + \phi_{j,g}^* \log \left( \frac{\phi_{j,g}^*}{\mu_{j,g}^* \beta_{c,d} + \phi_{j,g}^*} \right) + y_{c,g,d} \log \left( \frac{\mu_{j,g}^*}{\mu_{j,g}^* \beta_{c,d} + \phi_{j,g}^*} \right). \end{aligned}$$

Combining all terms together, the acceptance probability is

$$\alpha((\mu^*, \phi^*)_{new}, (\mu^*, \phi^*)_{old}) = \min(1, \exp[lpost_{new} - lpost_{old} - \log(\mu_{old}^* \phi_{old}^*) + \log(\mu_{new}^* \phi_{new}^*)]).$$

Then the covariance matrix is updated following the multivariate case ( $d = 2$ ) in step 4 of section A.3.3.

Note that due to label switching, the covariance matrix may have very large values. Therefore, to mitigate the multiplicative effect of the scale parameter  $s_d$  on the covariance, we fix  $s_d = 1$  instead of  $s_d = 2.4^2/2$ .

The above step is repeated for every  $j$  and  $g$ .

### A.9 Capture efficiencies $\beta_{c,d}$

From the posterior distribution (Eq (14)), we can separate each  $\beta_{c,d}$  and obtain its full conditional density as

$$\begin{aligned} \pi(\beta_{c,d} | \{y_{c,g,d}\}_{g=1}^G, z_{c,d} = j, \boldsymbol{\mu}_{1:J,1:G}^*, \boldsymbol{\phi}_{1:J,1:G}^*) &\propto \text{Beta}(\beta_{c,d} | a_d^\beta, b_d^\beta) \times \prod_{g=1}^G \text{NB}(y_{c,g,d} | \mu_{j,g}^* \beta_{c,d}, \phi_{j,g}^*) \\ &\propto (\beta_{c,d})^{a_d^\beta - 1} (1 - \beta_{c,d})^{b_d^\beta - 1} \\ &\quad \times \left[ \prod_{g=1}^G \left( \frac{1}{\phi_{j,g}^* + \mu_{j,g}^* \beta_{c,d}} \right)^{\phi_{j,g}^* + y_{c,g,d}} (\beta_{c,d})^{y_{c,g,d}} \right]. \end{aligned}$$

This does not have a closed form and we will apply AMH with the following variable transformation

$$X = \log \left( \frac{\beta_{c,d}}{1 - \beta_{c,d}} \right) \in \mathbb{R},$$

with Jacobian equal to

$$J_x = \frac{dX}{d\beta_{c,d}} = \frac{d}{d\beta_{c,d}} (\log(\beta_{c,d}) - \log(1 - \beta_{c,d})) = \frac{1}{\beta_{c,d}(1 - \beta_{c,d})}.$$

The inverse transformation is given by

$$\beta_{c,d} = \frac{1}{1 + \exp(-x)}.$$

Next, the logarithm of conditional distribution is

$$\begin{aligned} lpost &= (a_d^\beta - 1) \log(\beta_{c,d}) + (b_d^\beta - 1) \log(1 - \beta_{c,d}) \\ &\quad - \sum_{g=1}^G [(\phi_{j,g}^* + y_{c,g,d}) \log(\phi_{j,g}^* + \mu_{j,g}^* \beta_{c,d}) - y_{c,g,d} \log(\beta_{c,d})]. \end{aligned}$$

Therefore, the acceptance probability is given by

$$\begin{aligned} \alpha(\beta_{new}, \beta_{old}) &= \min \left( 1, \exp \left[ lpost_{new} - lpost_{old} \right. \right. \\ &\quad \left. \left. + \log(\beta_{new}) + \log(1 - \beta_{new}) - \log(\beta_{old}) - \log(1 - \beta_{old}) \right] \right). \end{aligned}$$

After the decision, we update the variance of the transformed variable  $X$ .

This step is repeated for every  $c$  and  $d$ .

### A.10 Hyper-parameters $r_j, s^2, h_j$ and $m^2$

#### A.10.1 PRIOR MEANS $r_j$

For each  $j$ , we have

$$\begin{aligned} \pi(r_j | \{t_{j,d}^*\}_{d=1}^D, \mu_r, \sigma_r^2, s^2) &\propto \prod_{d=1}^D N(t_{j,d}^* | r_j, s^2) \times N(r_j | \mu_r, \sigma_r^2) \\ &\propto \exp \left[ -\frac{1}{2s^2} \sum_{d=1}^D (r_j - t_{j,d}^*)^2 \right] \times \exp \left[ -\frac{1}{2\sigma_r^2} (r_j - \mu_r)^2 \right]. \end{aligned}$$

Recall our calculation for  $t_{j,d}^*$  in section A.3.2. It can be noticed that the full conditional distribution for  $r_j$  is a normal distribution

$$r_j | \dots \sim N(\hat{\mu}_r, \hat{\sigma}_r^2),$$

where

$$\begin{aligned} \hat{\sigma}_r^2 &= \left( \frac{1}{\sigma_r^2} + \frac{D}{s^2} \right)^{-1}, \\ \hat{\mu}_r &= \frac{\mu_r / \sigma_r^2 + \sum_{d=1}^D t_{j,d}^* / s^2}{1 / \sigma_r^2 + D / s^2}. \end{aligned}$$

#### A.10.2 PRIOR VARIANCE $s^2$

$$\begin{aligned} \pi(s^2 | \{t_{j,d}^*\}_{j=1, d=1}^{J,D}, \eta_1, \eta_2, \mathbf{r}) &\propto \prod_{j=1}^J \prod_{d=1}^D N(t_{j,d}^* | r_j, s^2) \times \text{IG}(s^2 | \eta_1, \eta_2) \\ &\propto (s^2)^{-\frac{JD}{2}} \exp \left[ -\frac{1}{s^2} \times \frac{1}{2} \sum_{j=1}^J \sum_{d=1}^D (t_{j,d}^* - r_j)^2 \right] \\ &\quad \times (s^2)^{-\eta_1 - 1} \exp \left[ -\frac{\eta_2}{s^2} \right], \end{aligned}$$

i.e.,

$$s^2 | \dots \sim \text{IG} \left( \frac{JD}{2} + \eta_1, \eta_2 + \frac{1}{2} \sum_{j=1}^J \sum_{d=1}^D (t_{j,d}^* - r_j)^2 \right).$$

#### A.10.3 PRIOR MEANS $h_j$

For each  $j$ ,

$$\begin{aligned} \pi(h_j | \{\sigma_{j,d}^{*2}\}_{d=1}^D, \mu_h, \sigma_h^2, m^2) &\propto \prod_{d=1}^D \text{log-N}(\sigma_{j,d}^{*2} | h_j, m^2) \times N(h_j | \mu_h, \sigma_h^2) \\ &\propto \exp \left[ -\frac{1}{2m^2} \sum_{d=1}^D \left( h_j - \log(\sigma_{j,d}^{*2}) \right)^2 \right] \times \exp \left[ -\frac{1}{2\sigma_h^2} (h_j - \mu_h)^2 \right]. \end{aligned}$$



Similar to  $r_j$ , its distribution is a normal distribution

$$h_j | \dots \sim \text{N}(\hat{\mu}_h, \hat{\sigma}_h^2),$$

where

$$\begin{aligned} \hat{\sigma}_h^2 &= \left( \frac{1}{\sigma_h^2} + \frac{D}{m^2} \right)^{-1}, \\ \hat{\mu}_r &= \frac{\mu_h / \sigma_h^2 + \sum_{d=1}^D \log(\sigma_{j,d}^{*2}) / m^2}{1 / \sigma_h^2 + D / m^2}. \end{aligned}$$

#### A.10.4 PRIOR VARIANCE $m^2$

$$\begin{aligned} \pi(m^2 | \{\sigma_{j,d}^{*2}\}_{j=1,d=1}^{J,D}, \kappa_1, \kappa_2, \mathbf{h}) &\propto \prod_{j=1}^J \prod_{d=1}^D \log\text{-N}(\sigma_{j,d}^{*2} | h_j, m^2) \times \text{IG}(m^2 | \kappa_1, \kappa_2) \\ &\propto (m^2)^{-\frac{JD}{2}} \exp \left[ -\frac{1}{m^2} \times \frac{1}{2} \sum_{j=1}^J \sum_{d=1}^D \left( \log(\sigma_{j,d}^{*2}) - h_j \right)^2 \right] \\ &\quad \times (m^2)^{-\kappa_1 - 1} \exp \left[ -\frac{\kappa_2}{m^2} \right], \end{aligned}$$

i.e.,

$$m^2 | \dots \sim \text{IG} \left( \frac{JD}{2} + \kappa_1, \kappa_2 + \frac{1}{2} \sum_{j=1}^J \sum_{d=1}^D \left( \log(\sigma_{j,d}^{*2}) - h_j \right)^2 \right).$$

### A.11 Variation of information

Let  $\mathbf{c}$  and  $\hat{\mathbf{c}}$  denote the true clustering and an estimate of the clustering, each consisting of  $k$  and  $k'$  clusters. Define  $C_i$  ( $i = 1, \dots, k$ ) to be the set of observation indices for cluster  $i$  under  $\mathbf{c}$ , and  $\hat{C}_j$  ( $j = 1, \dots, k'$ ) is for cluster  $j$  under  $\hat{\mathbf{c}}$ . The number of data points shared between  $C_i$  and  $\hat{C}_j$  is  $n_{ij} = |C_i \cap \hat{C}_j|$ , and the size of each cluster is  $n_{i+} = \sum_{j=1}^{k'} n_{ij}$  under  $\mathbf{c}$ , and  $n_{+j} = \sum_{i=1}^k n_{ij}$  under  $\hat{\mathbf{c}}$ .

The entropy  $H(\mathbf{c})$  of a clustering represents its uncertainty in assigning observations to clusters, and the mutual information  $I(\mathbf{c}, \hat{\mathbf{c}})$  between two clusterings measures the reduction in the uncertainty of the allocation of a data point in  $\mathbf{c}$  if we know clustering  $\hat{\mathbf{c}}$ . They are defined as

$$\begin{aligned} H(\mathbf{c}) &= - \sum_{i=1}^k \frac{n_{i+}}{N} \log \frac{n_{i+}}{N}, \\ I(\mathbf{c}, \hat{\mathbf{c}}) &= \sum_{i=1}^k \sum_{j=1}^{k'} \frac{n_{ij}}{N} \log \frac{n_{ij} N}{n_{i+} n_{+j}}, \end{aligned}$$

where  $N$  is the total number of data points. Variation of information is defined as

$$\text{VI}(\mathbf{c}, \hat{\mathbf{c}}) = H(\mathbf{c}) + H(\hat{\mathbf{c}}) - 2I(\mathbf{c}, \hat{\mathbf{c}}).$$

The optimal clustering  $\mathbf{c}^*$  is

$$\mathbf{c}^* = \arg \min_{\mathbf{c}} \mathbb{E} [\text{VI}(\mathbf{c}, \hat{\mathbf{c}}) | \mathcal{D}],$$

where  $\mathcal{D}$  is the data.

### A.12 Adjusted rand index

Following the notation in the last section, ARI between two clustering  $\mathbf{c}$  and  $\hat{\mathbf{c}}$  is

$$\text{ARI} = \frac{\sum_{ij} \binom{n_{ij}}{2} - \left[ \sum_i \binom{n_{i+}}{2} \sum_j \binom{n_{+j}}{2} \right] / \binom{N}{2}}{\frac{1}{2} \left[ \sum_i \binom{n_{i+}}{2} + \sum_j \binom{n_{+j}}{2} \right] - \left[ \sum_i \binom{n_{i+}}{2} \sum_j \binom{n_{+j}}{2} \right] / \frac{N}{2}}.$$

Values closer to 1 indicate better agreement between  $\mathbf{c}$  and  $\hat{\mathbf{c}}$ .

### A.13 Consensus clustering

The technique is fairly applicable to existing Bayesian clustering methods that does not require any subtle redevelopment of the original method. It has two important parameters, ensemble depth  $W$  (number of chains) and ensemble depth  $D$  (number iterations in each chain). Usually  $D$  is a relatively small number. For a given  $W$  and  $D$ , a Bayesian clustering method is applied to run  $W$  chains of  $D$  iterations in parallel. This can reduce a large amount of time compared with running few chains of long iterations. Then the  $D$ -th sample in each chain is combined to produce a consensus matrix  $M$ , just like a posterior similarity matrix, where the element in position  $(i, j)$  is the proportion of  $W$  samples where two observations  $i$  and  $j$  are grouped together. Using the consensus matrix  $M$ , a point estimate can be obtained such as from VI.

Coleman et al. (2022) propose a heuristic method to choose  $W$  and  $D$ . The rational is that, increasing  $W$  and  $D$  may improve the results to a large extent in the beginning, but the improvement will become smaller and smaller as their values increase, and finally converges. This is similar to PCA where more variance will always be captured for more principal components, but the gain in variance will be smaller and smaller, and eventually we will have few returns.

Given a set of candidate parameters  $D' = (d_1, \dots, d_I)$  and  $W' = (w_1, \dots, w_J)$ , for each  $w_j$ , we compute the consensus matrix based on the samples at the  $d_i$ -th iteration from  $w_j$  chains, and also compute  $M$  for the  $d_{(i-1)}$ -th iteration from  $w_j$  chains. The mean absolute difference (MAD) between the two matrices is a measurement of how stable the clustering partition is. Plotting these values as a function of  $D$ , we are likely to see an elbow-shaped curve, and we can choose a suitable  $D$  at which the curve plateaus. To choose  $W$ , we can fix  $D$  and compute MAD between  $w_{(j-1)}$  and  $w_j$ .

## Appendix B. Simulation study

In this section, we conduct simulation studies to assess the covariate-dependent HDP model, and inference is performed as stated in Section A. The main interest is the posterior inference of clusters, the time-dependent probabilities of belonging to each cluster, and cluster-specific parameters.

## B.1 Simulation setup

Each of the two datasets has 120 cells ( $C_1 = C_2 = 120$ ) with  $G = 10$  genes, and consists of  $J = 2$  clusters. For each observation,  $z_{c,d}$  is first simulated from its categorical distribution, given  $p_{j,d}^J(t_{c,d})$ , and then latent counts and observed counts are simulated from the model. Specifically,  $t_{c,d}$  are simulated from  $\text{Unif}(0, 1)$ ,

$$\begin{aligned} y_{c,g,d} | y_{c,g,d}^0, \beta_{c,d} &\stackrel{\text{ind}}{\sim} \text{Bin}(y_{c,g,d}^0, \beta_{c,d}), \\ y_{c,g,d}^0 | z_{c,d} = j, \mu_{j,g}^*, \phi_{j,g}^* &\stackrel{\text{ind}}{\sim} \text{NB}(\mu_{j,g}^*, \phi_{j,g}^*), \\ z_{c,d} | p_{1,d}^J(t_{c,d}), \dots, p_{J,d}^J(t_{c,d}) &\stackrel{\text{ind}}{\sim} \text{Cat}(p_{1,d}^J(t_{c,d}), \dots, p_{J,d}^J(t_{c,d})), \end{aligned}$$

where

$$\mu_{j,g}^* | j = 1 \stackrel{i.i.d.}{\sim} \log\text{-N}(1, \alpha_\mu^2), \quad \mu_{j,g}^* | j = 2 \stackrel{i.i.d.}{\sim} \log\text{-N}(3, \alpha_\mu^2),$$

and  $\phi_{j,g}^*$  is simulated from its prior. For each dataset, we set

$$\begin{aligned} d = 1 : \quad (t_{1,1}^*, t_{2,1}^*) &= (0.4, 0.9), \quad (\sigma_{1,1}^*, \sigma_{2,1}^*) = (0.08, 0.15), \quad (q_{1,1}, q_{2,1}) = (0.5, 0.5), \\ d = 2 : \quad (t_{1,2}^*, t_{2,2}^*) &= (0.8, 0.3), \quad (\sigma_{1,2}^*, \sigma_{2,2}^*) = (0.1, 0.1), \quad (q_{1,2}, q_{2,2}) = (0.3, 0.7). \end{aligned}$$

In addition, we assume  $\beta_{c,d} = 0.6$  for all cells,  $b_0 = 0.25$ ,  $b_1 = 0.5$ , and  $\alpha_\mu = \alpha_\phi = 0.1$ .

We visualize each dataset in two ways, either by clusters, or by latent time. Figure 11 shows the heatmaps of the simulated datasets on the log scale (after adding a value of 1). The clusters seem to be almost distinguishable from the latent time. Additionally, the time-dependent probabilities  $p_{j,d}^J$  against  $t$  for two datasets are given in Figure 12, indicating that the allocation is fairly decisive except for  $t$  around 0.6.

Note that due to the non-identifiability of  $\beta_{c,d}$ , we give an informative prior with mean equal to that of the simulated values (0.6). Otherwise, using 0.06 suggested by Tang et al. (2020) will lead to samples mainly around 0.06.

## B.2 Simulation results

With  $J = 4$ , we run the Gibbs sampling algorithm for 20000 iterations, and apply a burn-in of 10000 iterations, followed by a thinning of 5. Given posterior samples of allocations, the optimal clustering is computed by minimizing the posterior expectation of variation of information (Wade and Ghahramani, 2018). The optimal clustering from variation of information (VI) is compared to true clustering results by adjusted rand index (ARI). The details of VI and ARI are given in Section A.11 and A.12. The results are summarized below.

- **Optimal clustering:** the optimal clustering has an ARI of 0.9833, suggesting the result is very close to the truth. The posterior similarity matrix (PSM) is shown in Figure 13, where the uncertainty in allocations is quite low. Each entry in PSM represents the posterior probability that two cells are allocated to the same cluster.
- **Mean-dispersion relationship:** Figure 14 shows the result is reasonable with true relationship covered by the posterior samples.

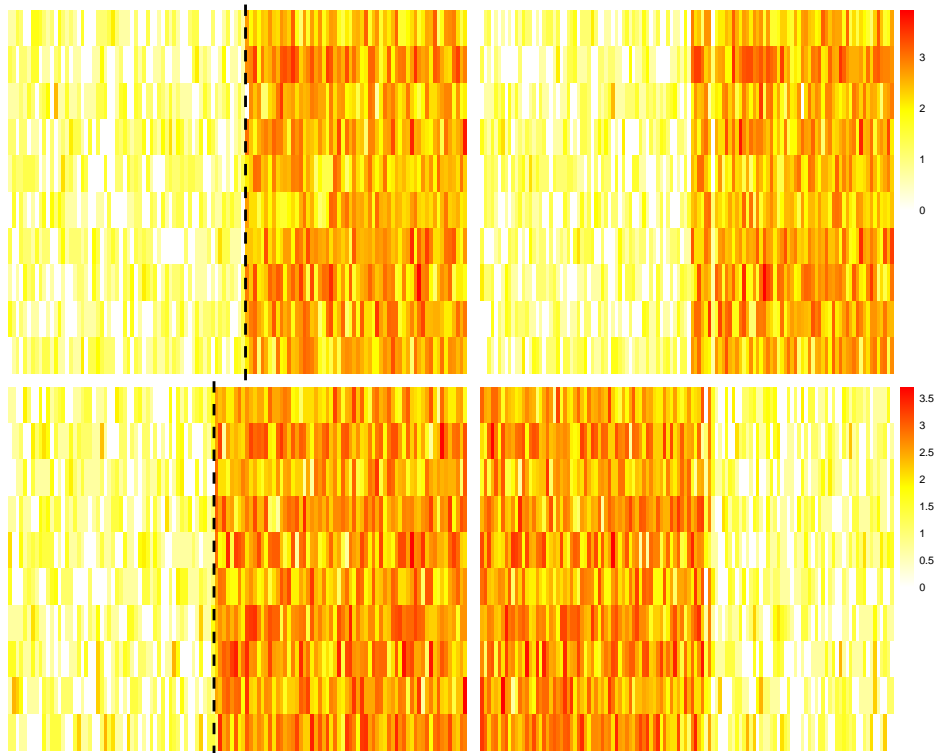


Figure 11: Simulation setting 1: Heatmaps of simulated datasets on the log scale (Top: dataset 1. Bottom: dataset 2). In each heatmap, each column is an observation and each row is a gene. The left two panels are the heatmaps for the data ordered by cluster labels (cluster 1 on the left). The dashed line is the separation. In the right two panels, cells are ordered by increasing time from left to right.

- Capture efficiency: Figure 15 shows that, for most cells, the 95% credible intervals (CIs) contain the true values, and we notice that the widths of CIs may be large for some observations, probably as a result of the identifiability issue.

As for the cluster-specific parameters and time-dependent probabilities, due to the label switching problem (Stephens, 2000), we cannot use the posterior samples for inference directly. Instead, we re-run our algorithm with the allocations  $z_{c,d}$  fixed at the optimal clustering from VI. The same length, burn-in and thinning are used in this post-processing step.

- Cluster-specific mean and dispersion parameters: Figure 16 compares the parameters for each gene. The sampled  $\mu_{j,g}^*$  are very distinct between two clusters. Although for  $g = 1, 5, 6$ , the true values for one cluster are not contained in the 95% CIs, probably because  $\mu_{j,g}^*$  is not identifiable from the likelihood, they all lie within the 99% CIs. As for  $\phi_{j,g}^*$  (Figure 17), the differences between clusters are less evident, with gene 5 having the largest overlaps. Unlike  $\mu_{j,g}^*$ , 95% CIs contain the true values for all  $\phi_{j,g}^*$ .

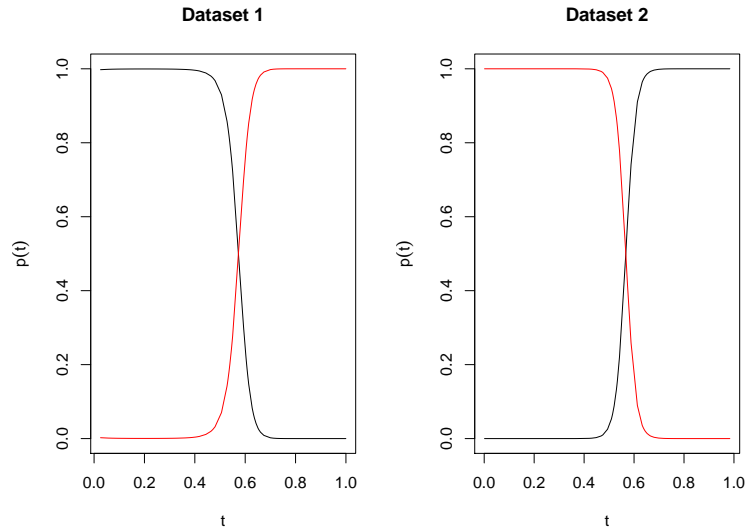


Figure 12: Simulation setting 1: Probability  $p_{j,d}^J$  as a function of  $t$  in each dataset. Black: cluster 1. Red: cluster 2.

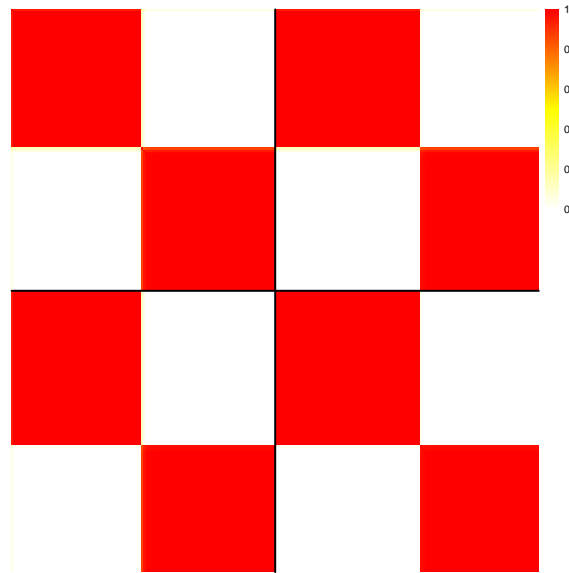


Figure 13: Simulation setting 1: Posterior similarity matrix. The black line separates the datasets. The diagonal block shows the posterior similarity matrix within each dataset.

- Time-dependent probabilities: Figure 18 shows the relationship between  $p_{j,d}^J$  and  $t_{c,d}$  is well recovered, except that the uncertainty may be too small around the boundary of two clusters ( $t \approx 0.6$ ). This is likely due to that the allocation variables are fixed and therefore the uncertainty can be smaller than expected. It is worth noting that, the samples for kernel parameters  $t_{j,d}^*$  and  $\sigma_{j,d}^{*2}$  exhibit clear trends in the traceplots,

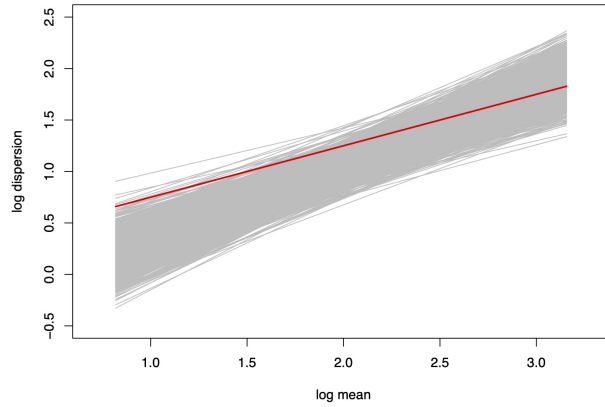


Figure 14: Simulation setting 1: Relationship between mean and dispersion parameters on the log scale. Grey: MCMC samples. Red: true relationship.

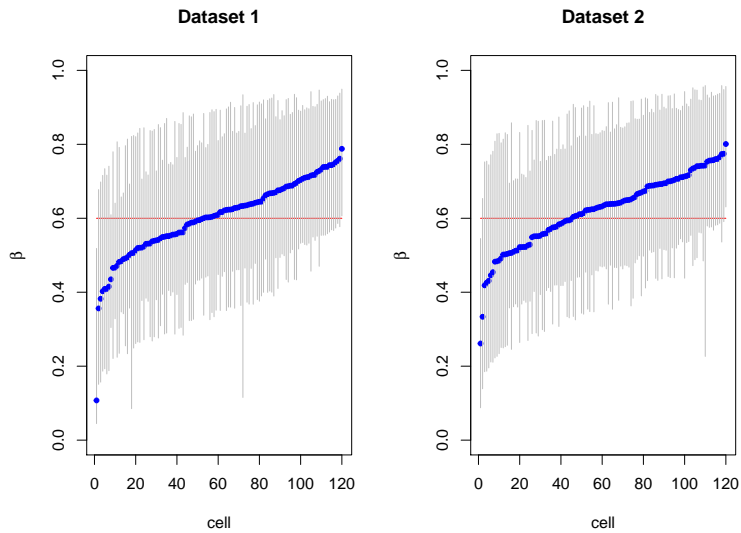


Figure 15: Simulation setting 1: MCMC samples for capture efficiencies  $\beta_{c,d}$ . In each dataset, the cells are ordered by increasing posterior means (blue). Red: truth. Grey: 95% credible interval.

and that the chain may not even visit the true values at all (Figure 19). Despite of this,  $p_{j,d}^J(t_{c,d})$  is well estimated, suggesting the kernel parameters may not be uniquely identifiable.

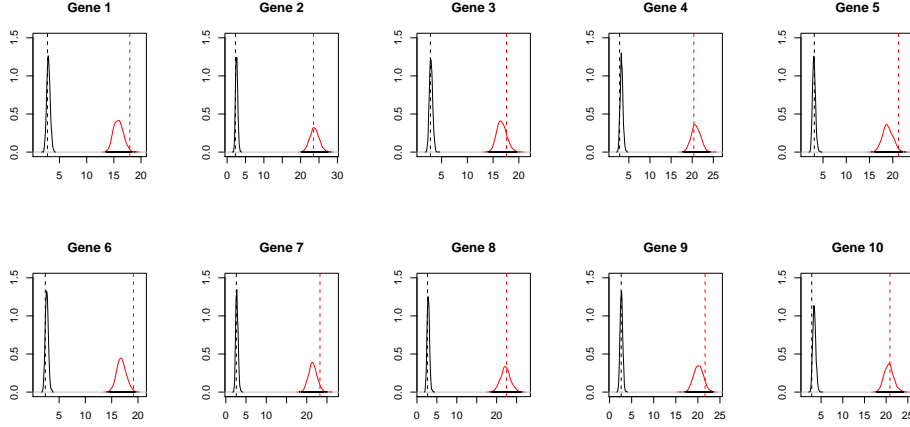


Figure 16: Simulation setting 1: Density plots for gene-wise mean parameter ( $\mu_{j,g}^*$ ). Black: cluster 1. Red: cluster 2. The vertical dashed lines are true values.

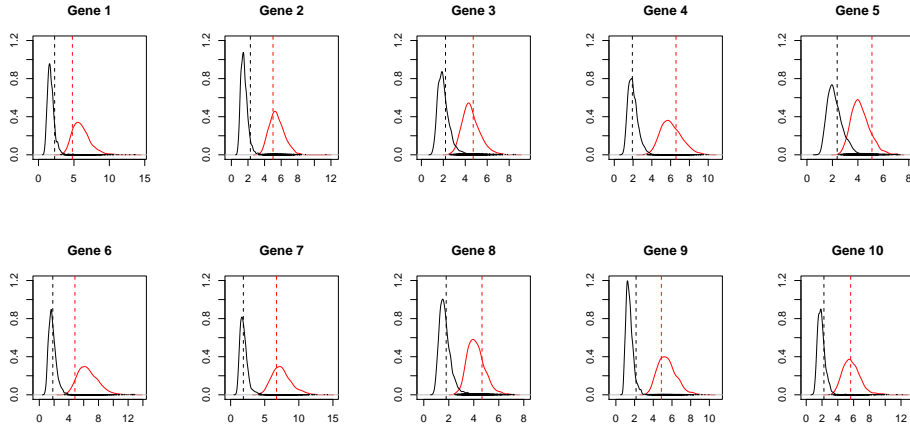


Figure 17: Simulation setting 1: Density plots for gene-wise dispersion parameter ( $\phi_{j,g}^*$ ). Black: cluster 1. Red: cluster 2. The vertical dashed lines are true values.

In addition to time-dependent probabilities, we also compute the mean of the latent count for a cell  $c$ , conditional on time, mean expressions,  $\mathbf{q}$  and kernel parameters:

$$\mathbb{E}(y_{c,g,d}^0 | t_{c,d} = t, \mathbf{q}, \boldsymbol{\mu}^*, \boldsymbol{\phi}^*) = \sum_{j=1}^J p_{j,d}^J(t) \mu_{j,g}^*. \quad (21)$$

Figure 20 shows the relationship between the mean of the latent count and time, under each gene in dataset 1. The true relationship is well recovered by the MCMC samples, and we can see a clear increase in the latent count as time increases. The result for dataset 2 is also adequate (Figure 21).

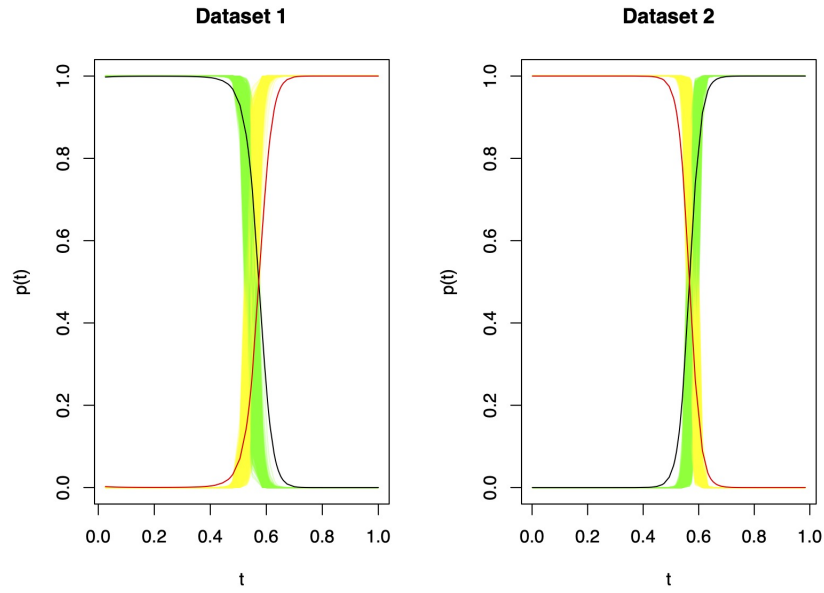


Figure 18: Simulation setting 1: Posterior samples for time-dependent probabilities in each dataset. Green: samples for cluster 1 overlaid by truth (black). Yellow: samples for cluster 2 overlaid by truth (red).

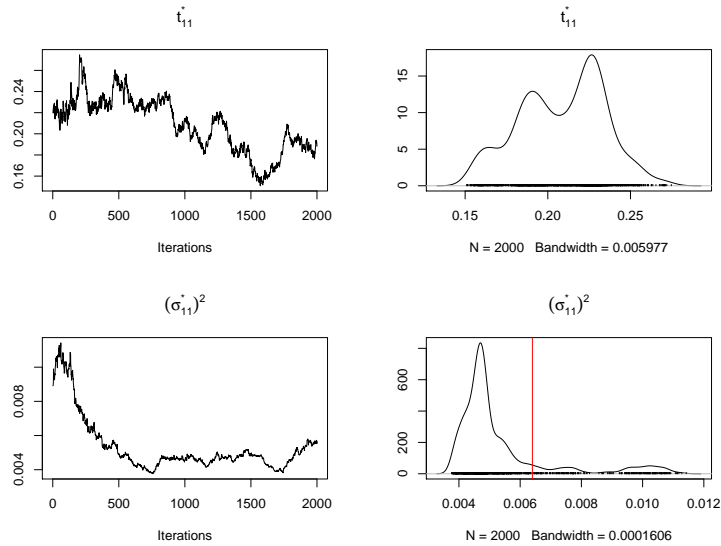


Figure 19: Simulation setting 1: Traceplots and density plots for kernel parameters  $t_{1,1}^*$  and  $\sigma_{1,1}^{*2}$ . The vertical red line is the truth.



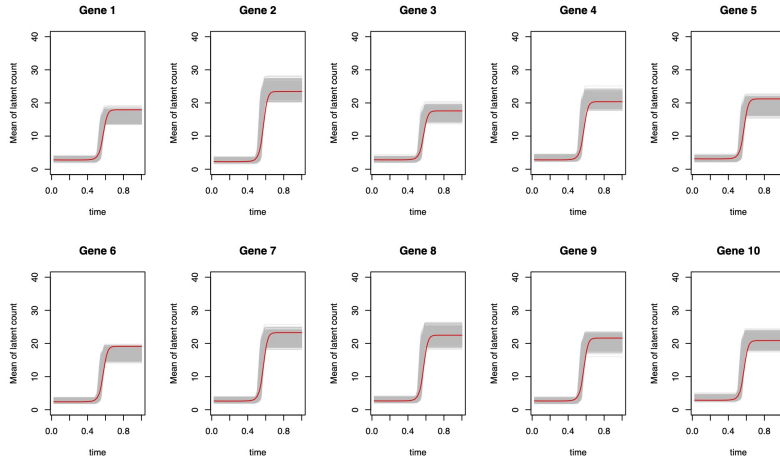


Figure 20: Simulation setting 1: Posterior mean of the latent count against latent time, for each gene in dataset 1. Red line denotes the truth.

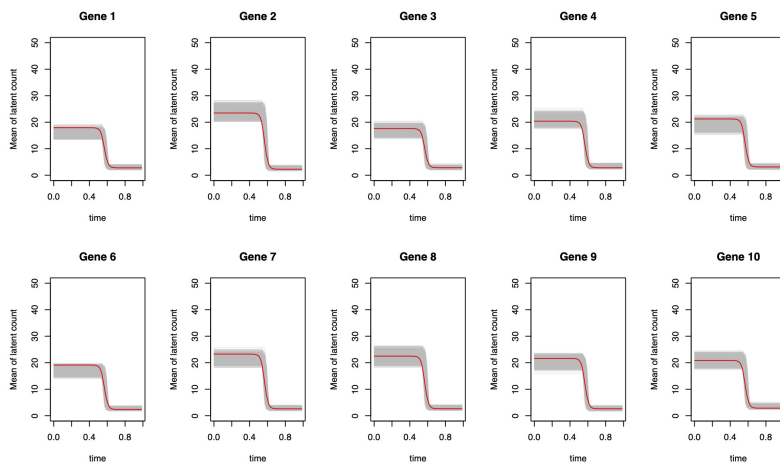


Figure 21: Simulation setting 1: Posterior mean of the latent count against latent time, for each gene in dataset 2. Red line denotes the truth.

## Appendix C. Additional results for Pax6

### C.1 Local marker genes

With regards to **local** DE genes, these genes are specific to each cluster only and are identified based on the minimum posterior tail probability. For cluster  $j$ , compute

$$P_{g,j}^* = \min_{j' \neq j} P_g(j, j'), \quad (22)$$

and genes with  $P_{g,j}^*$  greater than a threshold (calibrated according to EFDR) are identified as local DE genes. Intuitively, local DE genes can distinguish cluster  $j$  from any other cluster  $j'$ . Local DD genes are detected in a similar way, based on the dispersion parameters to compute minimum tail probabilities  $L_{g,j}^*$ .

In terms of local marker genes, the thresholds for local DE and DD genes are set to 1.2 and 1.6, respectively. Figure 22 shows the minimum posterior tail probabilities against the mean absolute LFCs for each cluster, along with the number of local genes in each cluster. Cluster 3 has the largest number of local DE genes, whereas the numbers of local DD genes are more evenly spread across 10 clusters.

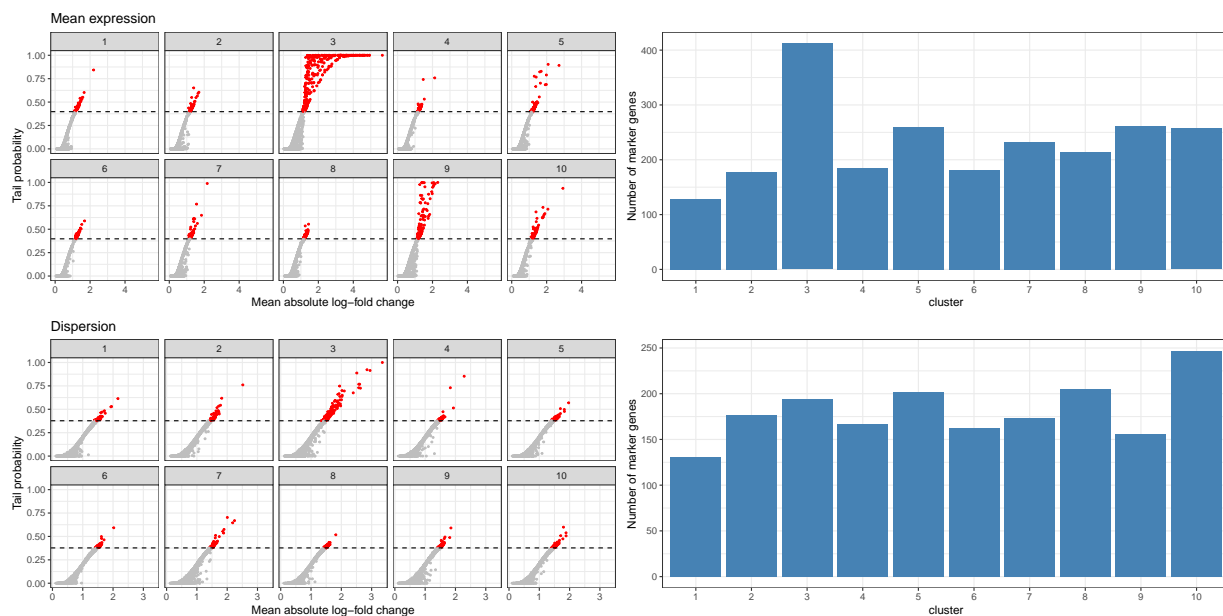


Figure 22: Left: Plot of minimum tail probabilities  $P_{g,j}^*$  and  $L_{g,j}^*$  against mean absolute LFCs for each cluster (top: mean expression, bottom: dispersion). The black dashed line indicates the threshold to determine local genes. Right: Number of local DE (top) and DD (bottom) genes in each cluster.

Figure 23 displays the estimated mean expressions and dispersions for local marker genes in each cluster. Similar to global DE genes, the local DE genes in cluster 3 exhibit higher mean expression levels. Moreover, for local DE genes in the other clusters, their mean expression levels are also higher in cluster 3. This trend is also observed for local DD genes in cluster 3.

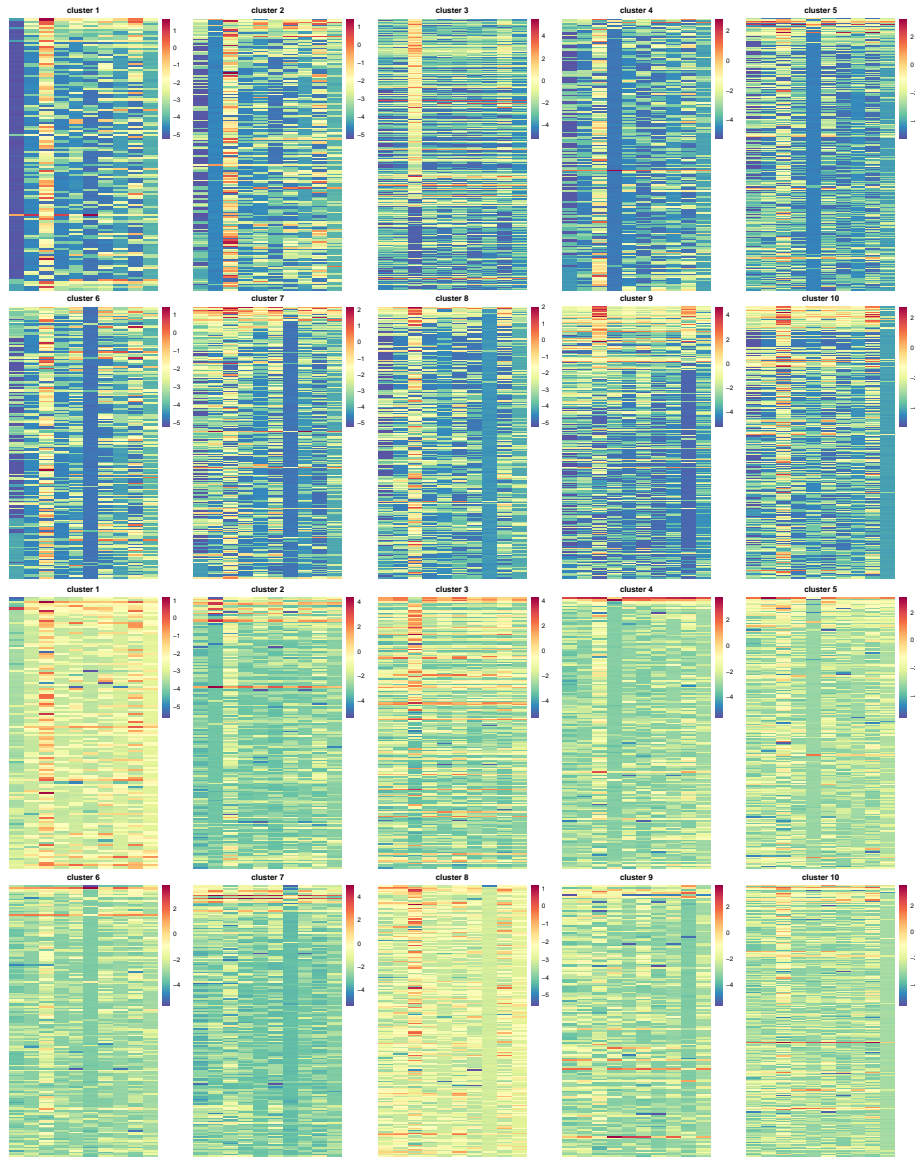


Figure 23: Local marker genes: Heatmaps of posterior mean of mean parameters  $\mu_{j,g}^*$  (top 2 rows) and dispersion parameters  $\phi_{j,g}^*$  (bottom 2 rows) on the log scale. Rows correspond to genes and columns correspond to clusters. Each panel corresponds to a specific cluster. Only the local DE (or DD) marker genes for this specific cluster are plotted and they are ordered by decreasing minimum posterior tail probabilities  $P_{g,j}^*$  and  $L_{g,j}^*$  from top to bottom.

## C.2 Posterior predictive checks

We follow Liu et al. (2024) and conduct posterior predictive checks based on a single replicate and then multiple replicates, given fixed optimal clustering.

## C.2.1 A SINGLE REPLICATE DATASET

For posterior predictive checks, we employ mixed predictive distribution (Lewin et al., 2007) based on the post-processing step. In particular, we simulate one replicate dataset using a single posterior sample of mean expression parameters  $\mu_{j,g}^*$ , capture efficiencies  $\beta_{c,d}$ , and generate dispersion parameters  $\phi_{j,g}^*$  from its hyper-priors given samples of  $\mathbf{b}, \alpha_\phi^2, \mu_{j,g}^*$ . For the observed and replicate data, we compute the following statistics for each gene in each dataset: the mean of log-shifted counts across cells, i.e.,  $\log(y+1)$ , the standard deviation of log-shifted counts, the logarithm of mean counts, and the dropout probabilities, i.e., proportion of cells with zero counts. The average in these statistics is taken across cells. We then compare the relationships for two pairs of statistics between the true and replicate datasets: 1. the mean and standard deviation of log-shifted counts; 2. the logarithm of mean counts and dropout probabilities.

Furthermore, we investigate the point-wise differences between the true and replicate datasets in terms of the mean of log-shifted counts, standard deviation of log-shifted counts and dropout probabilities. Figure 24 and Figure 25 demonstrate that the simulated replicate data exhibits similar relationships between pairwise statistics as observed in the true data. Additionally, the point-wise differences in statistics are nearly negligible, implying that the replicate data is reasonable and consistent with the observed one.

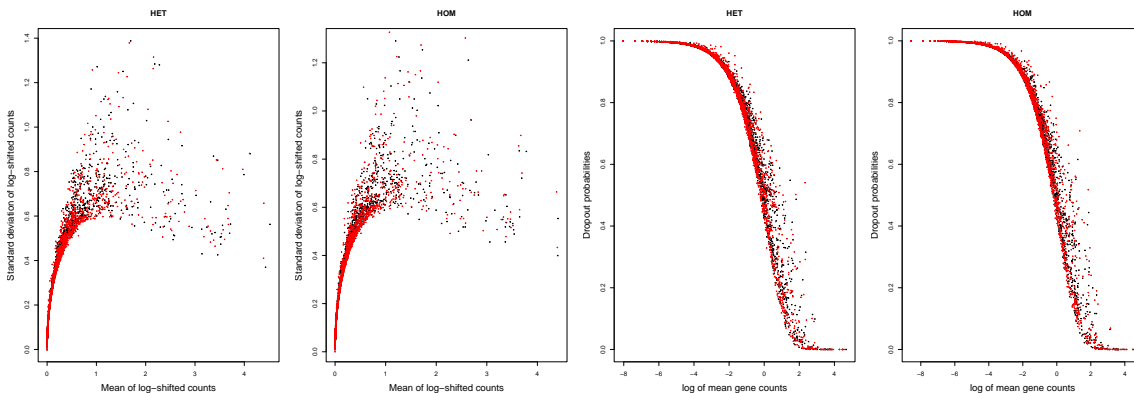


Figure 24: Posterior predictive checks with one single replicate dataset. Left two plots show the relationship between mean and standard deviation of log-shifted counts in true (red) and replicate data (black) for HET and HOM. Right two plots show the relationship between log of mean counts and dropout probabilities.

## C.2.2 MULTIPLE REPLICATES

For multiple replicates, we generate 200 datasets and compare the kernel density estimation of the statistics between the replicates and true data. From Figure 26, it is observed that estimated kernel is similar between the simulated 200 datasets and the true observed data.

Moreover, we compute the posterior predictive p-values (ppp) (Gelman et al., 1996) using three different discrepancy measures  $D_l(\cdot), l = 1, 2, 3$  for each gene  $g$  in each dataset

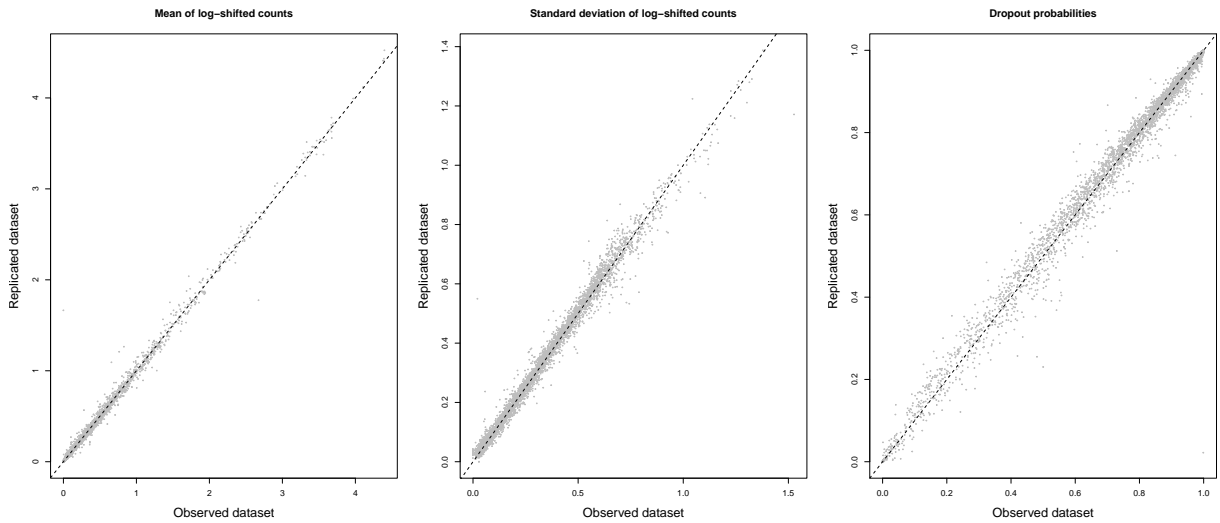


Figure 25: Posterior predictive checks with one single replicate dataset. Each panel shows pointwise differences in a statistic between true and replicate data (no separation of HET and HOM). Black dashed line corresponds to  $y = x$ .

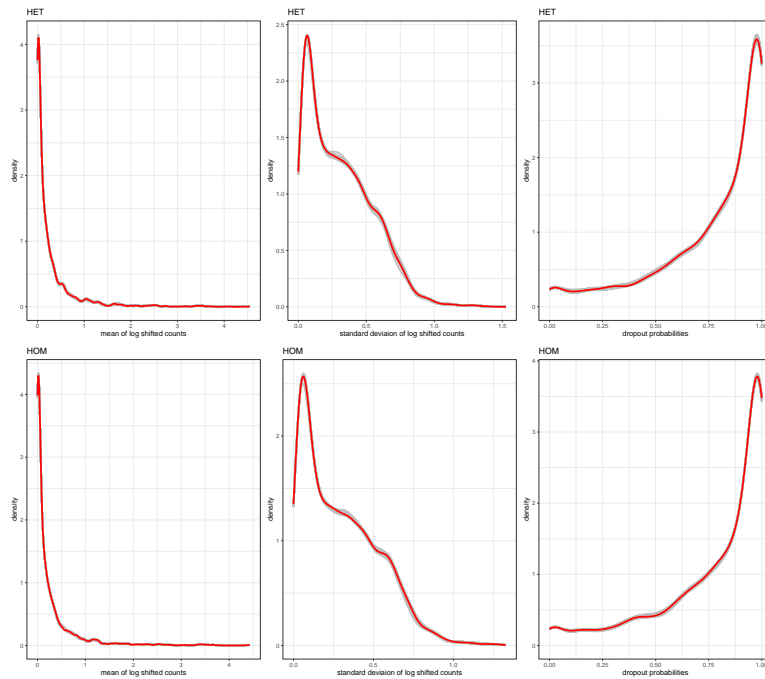


Figure 26: Posterior predictive checks with multiple replicates. Each panel shows the kernel density estimation of one statistics, with replicated and true datasets in grey and red, respectively. Left to right: mean of log shifted counts, standard deviation of log shifted counts and dropout probabilities.

$d$ :

$$\begin{aligned} \text{PPP}_l(\mathbf{y}_{\cdot,g,d}) &= \Pr\{D_l(\mathbf{y}_{\cdot,g,d}^{\text{rep}}, \boldsymbol{\theta}_{\text{post}}) \geq D_l(\mathbf{y}_{\cdot,g,d}, \boldsymbol{\theta}_{\text{post}}) \mid \mathbf{Y}\} \\ &\approx \frac{1}{T} \sum_{t=1}^T \mathbb{I}\{D_l(\mathbf{y}_{\cdot,g,d}^{\text{rep},(t)}, \boldsymbol{\theta}_{\text{post}}^{(t)}) \geq D_l(\mathbf{y}_{\cdot,g,d}, \boldsymbol{\theta}_{\text{post}}^{(t)})\}, \end{aligned}$$

where  $\boldsymbol{\theta}_{\text{post}}$  denotes the posterior samples for the mean parameters  $\mu_{j,g}^*$ , capture efficiencies  $\beta_{c,d}$ , hyper-parameters  $\mathbf{b}$  and  $\alpha_\phi^2$ . The superscript  $(t)$  indicates a particular sample, and  $\mathbf{y}_{\cdot,g,d}^{\text{rep},(t)}$  corresponds to the vector of counts for all cells in one replicate dataset  $d$  under gene  $g$ , generated using  $\boldsymbol{\theta}_{\text{post}}^{(t)}$ . The three discrepancy measures are defined below.

$$\begin{aligned} D_1(\mathbf{y}_{\cdot,d,g}, \boldsymbol{\theta}) &= \sum_{c=1}^{C_d} \frac{(y_{c,g,d} - \mathbb{E}[y_{c,g,d} | \boldsymbol{\theta}])^2}{\mathbb{E}[y_{c,g,d} | \boldsymbol{\theta}]}, \\ D_2(\mathbf{y}_{\cdot,d,g}, \boldsymbol{\theta}) &= \sum_{c=1}^{C_d} \left( \sqrt{y_{c,g,d}} - \sqrt{\mathbb{E}[y_{c,g,d} | \boldsymbol{\theta}]} \right)^2, \\ D_3(\mathbf{y}_{\cdot,d,g}, \boldsymbol{\theta}) &= \frac{1}{C_d} \sum_{c=1}^{C_d} |\mathbb{I}(y_{c,g,d} = 0) - \Pr(y_{c,g,d} = 0 | \boldsymbol{\theta})|. \end{aligned}$$

The first discrepancy measure is based on the  $\chi^2$  statistic (Gelman et al., 2013), and the second one is based on the Freeman-Tukey statistic (Kery and Royle, 2015) that is less sensitive to small expected values. Both measures have been used for count data. The third measure is relevant to the dropout probability. The computed ppp values are expected to be uniformly distributed when the model is true, but they have been shown to be conservative with a dome shape and concentrated around 0.5 (Conn et al., 2018; Sinharay and Stern, 2003). It is important to note that the data is used twice in the computation of ppp values: first to update the prior and obtain posterior distributions for the parameters, and then to assess the adequacy of the model based on these parameters (Hjort et al., 2006).

Nevertheless, p-values close to 0 or 1 still indicate a lack of fit to the data (Gelman et al., 2013) and Gelman (2013) emphasizes that deviations from a uniform distribution should not be a concern if the goal of model testing is to uncover discrepancies between the data and the fitted model.

From Figure 27, it is evident that all three discrepancy measures exhibit extremely small and large p-values, suggesting an inadequate fit for some of the genes, even though the distributions seems symmetric. The p-values obtained from the first and third discrepancy measure  $D_1$ , based on the  $\chi^2$  statistic and dropout probabilities, appear to be most similar to the uniform distribution, when restricted to the middle range. On the other hand, the p-values for  $D_2$  indicate a strong disagreement between the data and model.

Additionally, we also investigate the three discrepancy measures conditioned on each cluster (Lewin et al., 2007). For instance, the first discrepancy measure for a specific cluster  $j$  ( $j = 1, \dots, 10$ ) is given by

$$D_1^{(j)}(\mathbf{y}_{\cdot,d,g}, \boldsymbol{\theta}) = \sum_{c: \bar{z}_{c,d}=j} \frac{(y_{c,g,d} - \mathbb{E}[y_{c,g,d} | \boldsymbol{\theta}])^2}{\mathbb{E}[y_{c,g,d} | \boldsymbol{\theta}]},$$

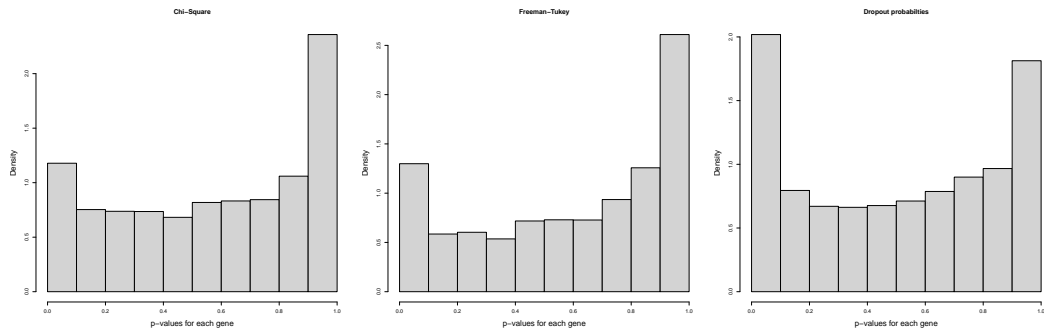


Figure 27: Posterior predictive checks with multiple replicates. Histograms for ppp values using three different discrepancy measures.

where  $\tilde{z}_{c,d}$  is the optimal clustering result from VI.

Figure 28, Figure 29 and Figure 30 display the histograms of ppp values for each discrepancy measure, conditioned on the optimal clustering and dataset. It is noteworthy that the extremely small ppp values disappear for all three measures, while values close to 1 still exist.

We also observe that the ppp values for cluster 3 are most similar to a uniform distribution, regardless of the discrepancy measure and dataset, suggesting a reasonable fit for this particular cluster. It should be emphasized that cluster 3 has been reported to have the highest number of local DE genes, and a higher mean expression level for global DE genes. Apart from that, compared to the ppp values without conditioning on the optimal clustering, the p-values for some clusters, e.g., cluster 6 in HOM, tend to concentrate around 0.5 (ignoring values close to 1), aligning with the arguments presented in Conn et al. (2018) and Sinharay and Stern (2003) (see discussion above).

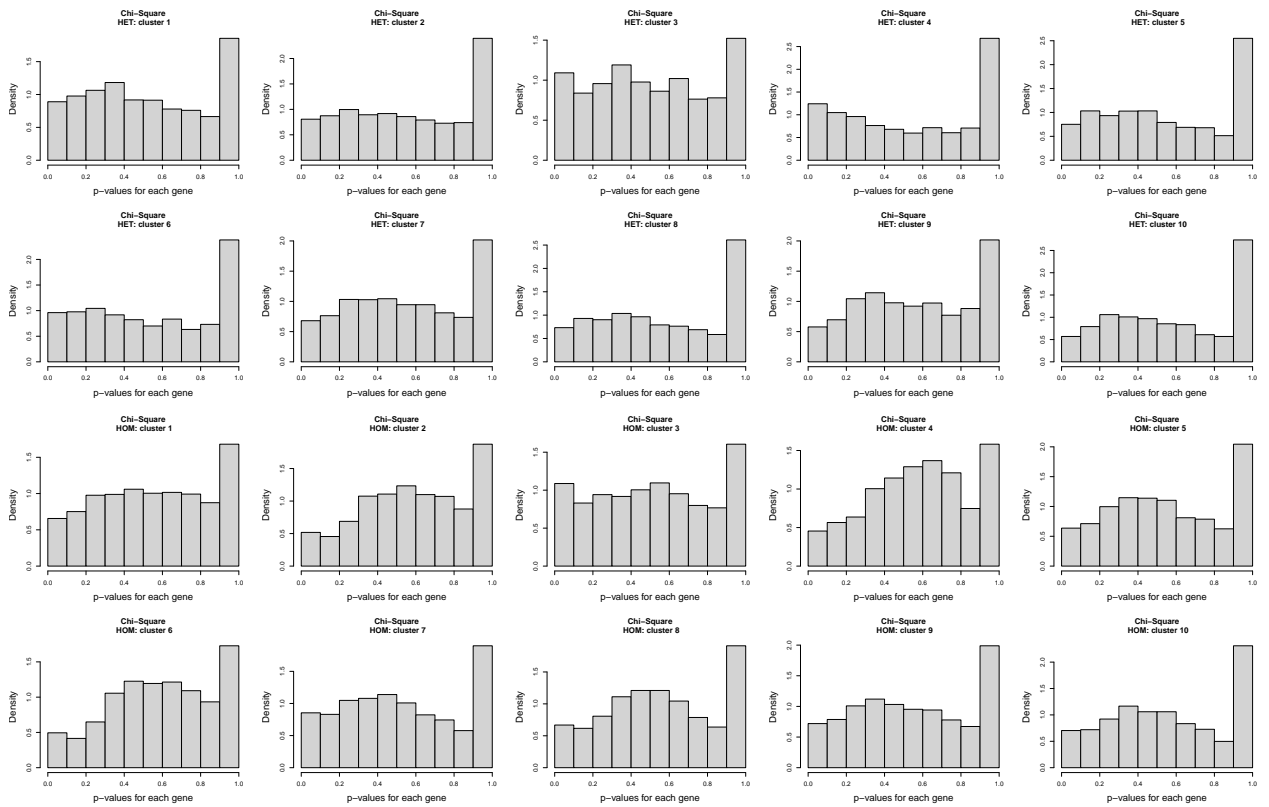


Figure 28: Posterior predictive checks with multiple replicates. Histograms for ppp values from  $D_1$ , conditional on the optimal clustering, for HET (upper two rows) and HOM (lower two rows),



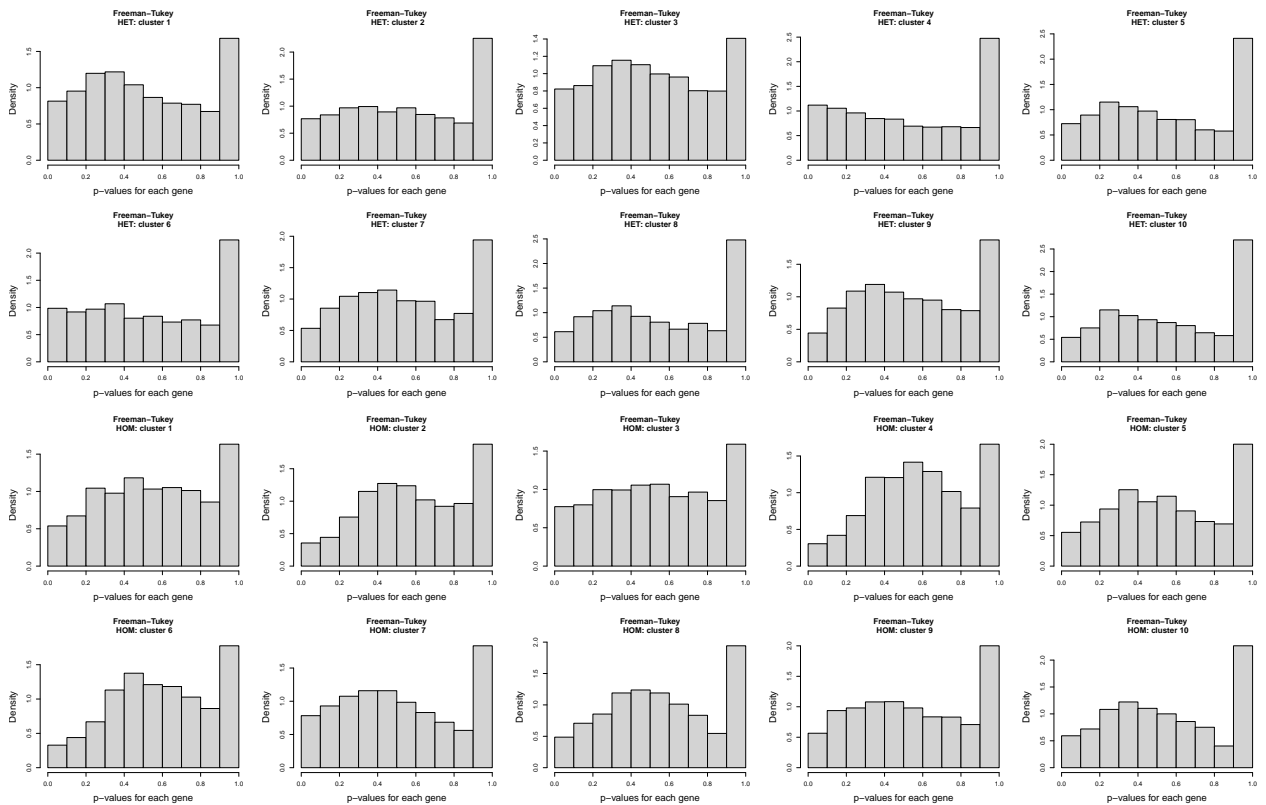


Figure 29: Posterior predictive checks with multiple replicates. Histograms for ppp values from  $D_2$ , conditional on the optimal clustering, for HET (upper two rows) and HOM (lower two rows),

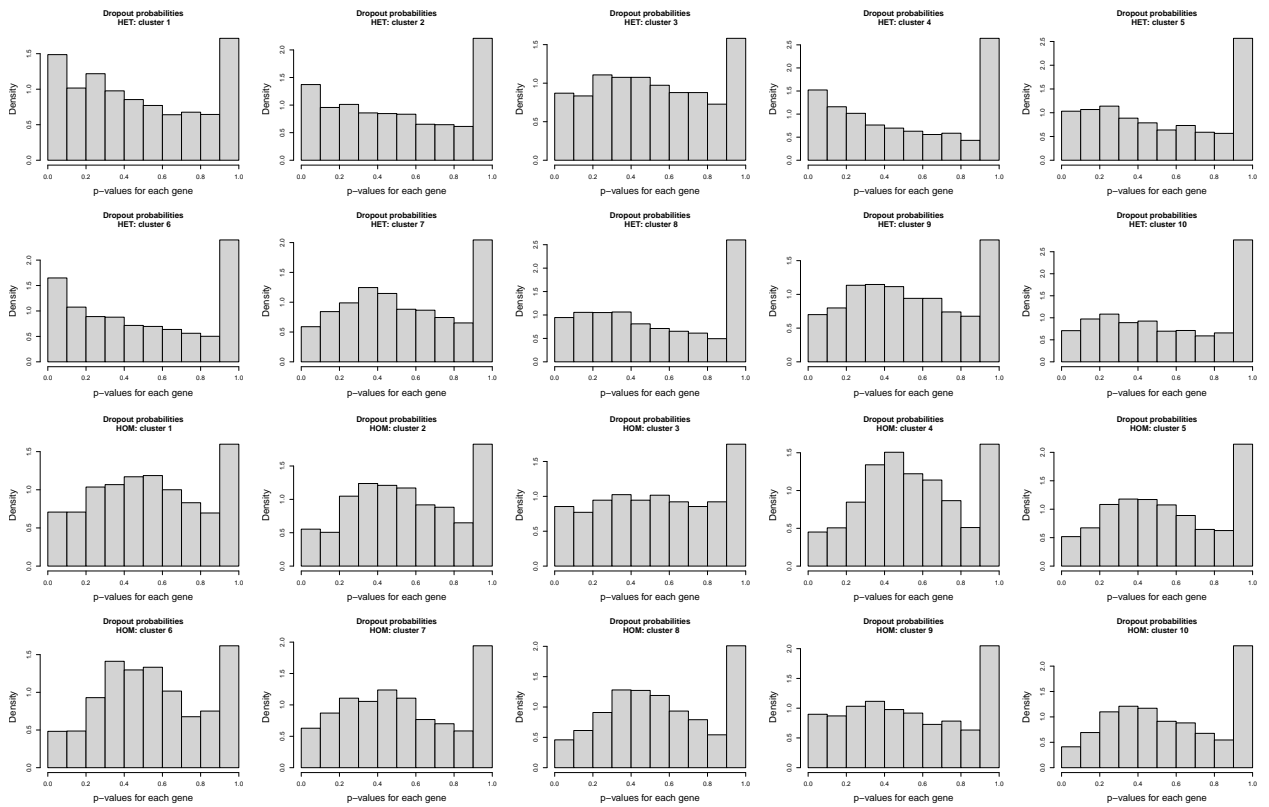


Figure 30: Posterior predictive checks with multiple replicates. Histograms for ppp values from  $D_3$ , conditional on the optimal clustering, for HET (upper two rows) and HOM (lower two rows),